UNIVERSITÉ DE MONTRÉAL

SIX-PORT DIGITAL RADIO COMMUNICATIONS AT VHF BAND

XIAO HU

DÉPARTEMENT DE GÉNIE ÉLECTRIQUE
ÉCOLE POLYTECHNIQUE DE MONTRÉAL

MÉMOIRE PRÉSENTÉ EN VUE DE L'OBTENTION
DU DIPLÔME DE MAÎTRISE ÈS SCIENCES APPLIQUÉES
(GÉNIE ÉLECTRIQUE)
DECEMBER 2006

Your file Votre référence
ISBN: 978-0-494-25548-3
Our file Notre référence
ISBN: 978-0-494-25548-3

UNIVERSITÉ DE MONTRÉAL

ÉCOLE POLYTECHNIQUE DE MONTRÉAL

Ce mémoire intitulé:

SIX-PORT DIGITAL RADIO COMMUNICATIONS AT VHF BAND

présenté par : XIAO Hu

en vue de l'obtention du diplôme de : Maîtrise ès sciences appliquées

a été dûment accepté par le jury d'examen constitué de :

M. Akyel Cevdet, D.Sc.A., président

M. Bosisio, Renato G., M. Sc. A, membre et directeur de recherche

M. Serioja O. Tatu, Ph.D., member et codirecteur de recherche

M. Nerguizian, Chahé, Ph.D., membre

DEDICATION

To the memory of my mother,
To my father, and
My family

ACKNOWLEDGEMENTS

This thesis summarizes the research works I have done in the Poly-Grames research centre during 2002 to 2006 period.

I would like to express my sincerest gratitude to my director, Prof. Renato G. Bosisio, for his dedication, guidance and support during the course of my project, and Prof. Serioja O. Tatu, for providing me with the opportunity to join this great research group, without his introduction, invaluable advice, and warm encouragement, I would not have achieved this accomplishment.

I am grateful to the members of the committee, Prof. Cevdet Akyel and Prof. Chahé Nerguizian for their review of this thesis.

Many thanks go to all the Poly-Grames research center staffs. Eric Marsan for his advice particularly; Roch Brassard, Steve Dubé, Jules Gauthier, Gagné Jean-Frederic and Antonescu Traian for their helps with fabrication and measurement of the circuit boards; René Archambault and Jean-Sebastien Décarie for their magic touches on my computer; Ginette Desparois for helping with ordering the parts.

I also would like to thank Rabih Barakat and Bilel Bensalem for reviewing my French translations.

Finally, I would like to thank my family and friends for their tremendous support throughout this project.

ABSTRACT

Digital communications in VHF band have been increasing over the recent years. The goal of this thesis is to develop a direct digital Six-Port QPSK modem(modulator and demodulator) at VHF band using discrete components, namely, surface mount devices (SMD) which are widely used in RF and microwave systems such as transceivers, up and down-converters. A new architecture of Six-Port modem is proposed which superior to the conventional direct conversion architecture in terms of circuit's simplicity, system performance and operating bandwidth.

To properly realize the system, circuit simulations using CAD tools such as Agilent advanced design system (ADS) and adequate models of the components are necessary. The modeling method of the power detectors is presented in this thesis.

Simulation results do not always agree to the measurement results all time. This work addresses this issue with analysis for the demodulator implementation results.

Another significant contribution of this research work is a new architecture for the direct Six-Port QPSK modulator. As the Six-Port modulator has wide-spread spectrum because of the lack of pulse shaping in the baseband data. A new spectrum shaping approach is proposed using half wavelength transmission line load.

The proposed digital Six-Port QPSK modem (modulator and demodulator) has been implemented and fabricated in the Poly-Grames research center. The performance tests are promising, indicating that they are the good candidate for VHF band digital communications.

RÉSUMÉ

Les communications numériques dans la bande VHF ont augmenté au cours des dernières années. Le but de cette thèse est de développer un modem numérique (modulateur et démodulateur) de Six-Port QPSK à la bande VHF en utilisant des composants discrets. On propose une nouvelle architecture de modem de Six-Port qui est supérieure à l'architecture de conversion directe conventionnelle en termes de simplicité du circuit, performance de système et largeur de bande utile.

Pour réaliser le système correctement, les simulations de circuit à l'aide des outils du logiciel ADS de Agilent et des modèles adéquats des composants sont nécessaires. La méthode modelant de détecteurs de puissance est présentée dans cette thèse.

Les résultats de simulation ne sont pas toujours en accord avec les résultats de mesure. Ce travail aborde cette question avec l'analyse pour les résultats d'exécution de démodulateur.

Une autre contribution significative de ce travail de recherche est la nouvelle architecture pour le modulateur direct du Six-Port QPSK. Comme le modulateur de Six-Port a le spectre étendu en raison du manque de `pulse shaping' dans les données de

bande de base, on propose une nouvelle approche de mise en forme du spectre transmission de charge de un demi longueur d'onde.

Le modem numérique proposé du Six-Port QPSK (modulateur et démodulateur) a été mis en application et fabriqué au centre de recherches Poly-Grames. L'essai de performance est prometteur, indiquant qu'ils sont le bon candidat pour des communications numériques de bande VHF.

CONDENSÉ EN FRANÇAIS

RADIOCOMMUNICATIONS DE SIX-PORT DIGITAL À LA BANDE DE VHF

0.1 Introduction

Une des parties principales dans une radio de télécommunication est le modem. Le mot modem provient de la modulation et de la démodulation. Ces mots se rapportent à la fonction d'un modem. Dans le contexte d'un terminal mobile, le démodulateur transforme les signaux venant du LNA en signaux numériques. Le modulateur convertit le flux de données numérique à la bande de base en signal RF, et ce signal est fourni à l'antenne par l'amplificateur de puissance.

La modulation et la démodulation numérique ont été présentes depuis les années 60, avec le besoin de communications par satellite numériques militaires [4]. Les bandes de fréquence se sont étendues de plusieurs mégahertz jusqu'à quelques 100 mégahertz. Le modem numérique pour la télécommunication mobile a commencé à apparaître dans les années 80, avec le développement des normes de DECT et de GSM. Celles-ci et d'autres normes de télécommunication pour la téléphonie mobile ont employé des radiofréquences entre 800 mégahertz et 3 gigahertz.

Des modems conventionnels sont classifiés dans deux catégories, hétérodynes et homodynes. L'homodyne s'appelle également à conversion directe ou zéro-IF. Ils se composent de filtres, de mélangeurs et d'oscillateurs. Dons les années récentes, l'architecture de homodyne est très populaire parce que ses dispositifs sont simples et à prix réduit. Cependant, elle souffre des inconvénients tels que l'excentrage de C.C, qui est provoqué par l'oscillateur local (LO) à la fuite de RF due à l'isolement limité du mélangeur entre le RF et le LO port.

En 1994, le Ji Li [14] a proposé une architecture numérique directe de nouveau récepteur Six-Port qui est composée de trois coupleurs et de diviseur de puissance. Parmi les six ports, deux ports sont employés comme RF (Porteuse modulé) et de LO (Oscillateur local) ports d'entrée, les quatre ports restants sont reliés à quatre détecteurs de puissance. En lisant les sorties de C.C des quatre détecteurs de puissance, le signal de RF modulé par phase peut être démodulé en rivalisant avec la phase du LO. En 2002, Eric Marsan [5] a proposé des modulateurs numériques directs du Six-Port QPSK prévus pour récupération de la porteuse à la bande S.

Comparé aux architectures conventionnelles homodyne, le modem numérique direct de Six-Port a plusieurs avantages en termes de largeur de bande, de simplicité d'architecture, de puissance d'énergie et de fonctionnement. L'objectif de cette thèse est de démontrer une nouvelle structure du modem numérique de Six-Port pour réaliser la

modulation directe et la démodulation de QPSK à la bande de VHF. Nous employons les composants discrets bon marché de SMD tels que des résistances, des inducteurs et des condensateurs pour établir nos circuits de modulateur et de démodulateur du Six-Port QPSK.

0.2 Concepts fondamentaux de modem de numérique de Six-Port

De la définition de matrice de S-paramètre, il est facile de déduire le les paramètres de dispersion S (paramètre-S) du Six-Port

$$[S]=\begin{pmatrix} 0 & j/2 & -1/2 & -1/2 & j/2 & 0 \\ j/2 & 0 & 0 & 0 & 0 & -1/2 \\ -1/2 & 0 & 0 & 0 & 0 & j/2 \\ -1/2 & 0 & 0 & 0 & 0 & 1/2 \\ j/2 & 1/2 & 0 & 0 & 0 & j/2 \\ 0 & -1/2 & j/2 & 1/2 & j/2 & 0 \end{pmatrix} \tag{0.1}$$

Définissons $\Gamma_{23}, \Gamma_{23} = \Gamma_2 = \Gamma_3$, Γ_2 et Γ_3 sont les coefficients de réflexion du port 2 et du port 3, respectivement. De même, nous définissons le coefficient de réflexion $\Gamma_{45} = \Gamma_4 = \Gamma_5$ au port 4 et le port 5, donc, nous avons la formule fondamentale pour notre modulation du Six-Port QPSK,

$$(S_{61})_{SP} = -(\Gamma_{23} + j\Gamma_{45})/2 \tag{0.2}$$

D'après (0.2) les valeurs de la constellation de modulation du Six-Port QPSK peuvent être calculées.

Selon la matrice de S-paramètre de Six-Port de (0.1), nous avons les équations d'ondes de réflexion de quatre ports:

$$\begin{aligned} b_2 &= (ja_1 - a_6)/2 \\ b_3 &= (-a_1 + ja_6)/2 \\ b_4 &= (-a_1 + a_6)/2 \\ b_5 &= (ja_1 + ja_6)/2 \end{aligned} \tag{0.3}$$

où b2, b3, b4, et b5 sont les signaux reflétées de quatre port2 à port5 respectivement, a1 et a6 sont les signaux incident aux port1 et port6 respectivement. Les deux signaux d'entrée sont décrits par :

$$\begin{aligned} a_1 &= |a_1| \cdot \exp(j\varphi_1) \\ a_6 &= |a_6| \cdot \exp(j\varphi_6) \end{aligned} \tag{0.4}$$

Les angles représentent l'état de phase des signaux aux ports du Six-Port. Supposons que les deux signaux d'entrée ont la même fréquence, la même amplitude |a1| = |a6| = A, et ont chaque port adapté, les équations d'ondes de (0.3) aux quatre ports deviennent :

$$\begin{aligned} b_2 &= A \cdot (\exp(j(\varphi_1 - \varphi_6 - \pi/2) + 1)/2 \\ b_3 &= A \cdot (\exp(j(\varphi_1 - \varphi_6 + \pi/2) + 1)/2 \\ b_4 &= A \cdot (\exp(j(\varphi_1 - \varphi_6 + \pi) + 1)/2 \\ b_5 &= A \cdot (\exp(j(\varphi_1 - \varphi_6) + 1)/2 \end{aligned} \tag{0.5}$$

La puissance de chaque port est proportionnelle à une charge assortie. Nous notons que pour chaque port il y a un déphasage entre les deux signaux d'entrée. La puissance correspondant à chaque port peut être exprimée comme suit :

$$P_i = | b_i |^2, i = 2,3,4,5 \tag{0.6}$$

Si $\varphi_1 - \varphi_6 = 0,\ \pi/2,\ \pi$ et $-\pi/2$ respectivement, on peut calculer la puissance pour chaque port avec la différence de phase correspondante, qui représente la constellation de modulation du Six-Port QPSK. Il y a un minimum et un maximum à chaque phase. Il est possible de démoduler un signal QPSK par une lecture simple de puissance, détectant un minimum ou un maximum à celui des quatre ports.

0.3 Six-Port de Lumped-Élément

La conception du Six-Port de lumped-élément commence par l'architecture du Six-Port de lumped-élément. Elle se compose de trois coupleurs de quadrature du lumped-élément et de diviseur de puissance de Wilkinson. Ils sont souvent faits dans la ligne de microruban ou la ligne de ruban [3]. Dans la bande de fréquence de VHF, nous employons lumped éléments au lieu de la ligne de microruban pour établir le diviseur hybride de coupleur et de puissance de Wilkinson en raison de la restriction de taille.

Les simulations utilisant le logiciel ADS de Agilent ont été conduites pour le diviseur hybride de coupleur et de puissance de Wilkinson. Des 0805 et 0603 modèles de S-paramètre de composants de SMD pour le coupleur de quadrature du coilcraft et du TDK ont été employés dans des simulations de circuit. Tous les composants comportaient 5 pour cent de tolérance dans les caractéristiques. La simulation et la mesure des résultats de différence de phase ont été présentées. Elles prouvent qu'il y a une différence de phase de 90° désirée à 230 mégahertz. Elles montrent également la

simulation et la mesure des résultats de pertes de retour, mesurant le 34 dB au port 1, le 33 dB aux ports 2 et 25 au port 3. La perte d'insertion à la fréquence centrale est environ 4 dB pour la mesure. Toutes les simulations et les résultats de mesure sont très proches d'une certaine fréquence décalés vers le bas en raison des tolérances de composants et des dispositifs parasites qui ont été négligés dans les simulations. Un meilleur accord a pu être réalisé en considérant un modèle proportionnel aux dispositifs parasites.

Basé sur l'architecture de Six-Port et l'Agilent ADS, la simulation de carte de Six-Port de lumped-élément à la bande VHF a été conduite pour produire des paramètres-S du Six-Port. Alors la simulation harmonique d'équilibre a été effectuée. Les résultats prouvent qu'à la plus basse ou la plus élevée position de la tension, il y a une différence de phase de 90 degrés entre les quatre sorties.

Le circuit de Six-Port a été fabriqué dans notre laboratoire en utilisant Rogers RO4003. Nous avons mesuré les paramètres-S du Six-Port fabriqué en utilisant l'analyseur de réseau de HP8753D. Les résultats de mesure prouvent que les pertes d'insertion à la fréquence centrale sont environ 6.8 dB, le 20 dB du résultat de pertes de retour au port de RF, le 30 dB au LO port, et l'isolement entre LO et le RF atteint le 35 dB. Les résultats de mesure sont très près des simulés avec un décalage mineur de fréquence de centre à f_0 = 230 MHz dus aux tolérances d'inducteurs et de condensateurs et aux dispositifs parasites.

0.4 Démodulateur direct du Six-Port QPSK de Lumped-élément

Le principe de la démodulation de Six-Port est que, en lisant la puissance des quatre sorties des Six-Ports, la différence de phase entre le rf et le LO peuvent être déterminés. Par conséquence dans la démodulation du Six-Port QPSK, les détecteurs de puissance sont les composants les plus cruciaux. Théoriquement, la loi carrée pour les quatre détecteurs de puissance est assumée. Dans ce travail, nous employons quatre détecteurs de puissance de loi carrée de Wiltron pour traduire la puissance RF à la tension de CC. Par conséquent, la conception du sous-ensemble direct de démodulateur du Six-Port QPSK de lumped-élément est concentrée sur le modèle du détecteur de puissance de Wiltron en utilisant les données de mesure. Trois charges différentes de charges, OUVERT, 11KΩ, et 330kΩ de charge, ont été employées pour évaluer l'effet de la charge à la sensibilité du détecteur de puissance. Les résultats prouvent que dans la région entre le -30 dBm au -10 dBm, la réponse change d'une loi plus élevée pour la loi carrée. Elle prouvent également que le meilleur ajustement est la charge 330KΩ, dont la gamme carrée de loi est du -10 dBm - le 25 dBm. La charge 11Kohm a un meilleur ajustement en-dessous de la gamme du -15 dBm. Pour la charge ouverte, l'exécution commence à détériorer en-dessous du -25 dBm. Afin de produire du modèle pour simuler des circuits de détecteur de puissance de Wiltron dans l'ADS, des données de la mesure ci-dessus et le Matlab de Mathwork en tant qu'outil d'ajustement de courbe ont été employé, et nous avons l'équation adaptée.

Une mesure a été conduite pour mesurer les sorties du C.C des quatre détecteurs de puissance pendant que le RF entrait des changements de phase selon la phase du LO. Le résultat montré à chaque différence de phase de 90 degrés entre le RF et LO, un des quatre détecteurs au rendement de tension CC de maximum. Ainsi nous pouvons employer ce dispositif pour comparer quatre statuts différents en utilisant l'étape de comparaison des circuits. Les tensions de rendement des quatre détecteurs de puissance sont très basses, sont habituellement de 30 mV. Ainsi l'amplificateur des quatres canaux a été utilisé pour amplifier les sorties de C.C des détecteurs de puissance afin de faire une bonne mesure de BER. Nous empruntons également le travail de la conception de décodeur à un autre projet principal [13], et fabriqué par Dr. Serioja [21] qui sont un décodeur parfait pour notre projet.

La mesure de taux d'erreur binaire (BER) a été effectuée à l'aide des instruments d'Anritsu ME522A avec l'état de la fréquence RF = 230 mégahertz, fréquence de LO = 230 mégahertz, puissance de rf = -10 dBm, puissance de LO = -10 dBm, Rs=2MHz. La simulation de BER a été conduite en utilisant l'ADS. Le résultat de simulation a la bonne concordance avec la première mesure une. La mesure de BER a exécutés avec la variation de phase entre le porteur de l'entrée RF et le signal du LO aux états de fréquence de RF = 230 mégahertz, de puissance RF = -10 dBm, puissance de LO = -10dBm, Rs=2MHz. Elle prouve que quoique la phase du porteur ait des changements relativement au signal du LO aussi grand que 46 degrés, nous pouvons obtenir le bon

résultat de BER de 10^{-9}, qui signifie que la tolérance pour le changement de phase du RF ou du LO est excellente. L'essai de BER est également exécuté avec la variation de fréquence de RF et le LO fréquence = 230 mégahertz, de puissance RF = -10 dBm, puissance de LO = -10 dBm, Rs=2MHz. Nous pouvons voir que la largeur de bande de la démodulation peut être de 34 mégahertz, environ 14.78%, qui signifie que le Six-Port proposé convient à l'application à large bande.

0.5 Modulateur direct du Six-Port QPSK de Lumped-élément

Le principe de la théorie de modulation directe du Six-Port QPSK est en appliquant le signal de données d'I/Q à quatre ports afin de commuter le coefficient de réflexion des deux ports entre le 2 statut (+1 et -1), de cette manière, quatre états de QPSK peut être produite. Ces quatre états directs manœuvrent le signal de l'entrée rf pour former le signal modulé de QPSK. Dans la conception directe de modulateur du Six-Port QPSK, quatre commutateurs ont été utilisés pour exécuter les ouverts et courts qui correspondent aux +1 et au -1 du coefficient de réflexion respectivement. Par conséquent, la réalisation réussie des commutateurs forme les parties du projet global de modulateur de QPSK. Un bon commutateur assorti donne une bonne réflexion courte (Γ = -1) et la réflexion ouverte (Γ = +1). Reflété dans le diagramme de constellation, il devrait y avoir déséquilibre d'aucune phase et d'amplitude. Les commutateurs devraient également avoir la bonne vitesse de commutation et le bon isolement entre le port d'entrée, le port de sortie et le port de contrôle.

Dans la pratique, les commutateurs commerciaux de (RF Micro devices) ont été adoptés. Le RF2436 est un commutateur peu coûteux de la transmission/réception GaAs MESFET à l'origine conçu pour des applications sans fil de téléphones RX/TX. Il comporte la capacité de puissance élevée (dBm 28) et la consommation à faible courant dans une gamme de fréquence de fonctionnement de C.C à 2500MHz. Afin de valider la praticabilité d'employer RF2436 comme commutateurs, des essais de phase et d'amplitude du modulateur du Six-Port QPSK de lumped-élément avec quatre commutateurs ont été effectués. Le processus est celui par l'application basse et les tensions élevées à quatre commutateurs de ports le contrôle, quatre statuts de constellation à quatre ports RF reflétant peuvent être produites. Les résultats ont montrés que de 220 mégahertz à 260 mégahertz de gamme de fréquence, les différences de phase entre l'entrée de rf et le rf produit pour quatre statuts différents de commutation ont été également 90°, et les différences d'amplitude pour quatre statuts sont à moins de 5 dB.

Une simulation de niveau de système a été conduite en utilisant l'ADS avec quatre commutateurs idéaux avec des résultats prometteurs. Alors des commutateurs idéaux ont été remplacés par le fichier de données de S-paramètre de la mesure S1P pour ouvert et court circuit des commutateurs RF2436. Les données ont été prises en utilisant l'analyseur de réseau de HP8753D. La simulation d'enveloppe dans l'ADS a été conduite pour vérifier le diagramme de constellation et le diagramme de spectre de puissance du modulateur du Six-Port QPSK. Un panneau de circuit imprimé a été établi dans notre

laboratoire en utilisant le matériel de Rogers RO4003C avec Er=3.38 et l'épaisseur est de 32 mil.

L'installation de mesure a été faite. Un analyseur de signal de vecteur d'Agilent VSA 89600 a été utilisé comme un récepteur pour démoduler le signal de QPSK du modulateur du Six-Port QPSK. L'analyseur VSA de signal de vecteur d'Agilent 89600 est un instrument puissant d'analyse qui vient avec le logiciel d'analyseur de signal de 89600 vecteurs et le matériel d'unité centrale et est idéal pour évaluer des signaux de communication numérique. Les mesures pour le spectre, la constellation, et le diagramme d'EVM ont été faites aux niveaux de puissance de rf s'étendant du -15 dBm au 13 dBm. Le débit est 1 MHz/s, le f_{RF}= 230MHz fixé. Des résultats de mesure et les exécutions du modulateur du Six-Port QPSK sont montrés que dans le meilleur cas avec les S/N = 21.79 dB et de puissance de rf égales 13 dBm ce qui est le maximum de puissance de sortie du générateur de signal, l'EVM (RMS) est 8.13%. Le pire cas avec le S/N= 14.67 dB, puissance de rf égale -15dBm et EVM (RMS) est 29.56%.

Les spectres du modulateur du Six-Port QPSK de lumped-élément sont au loin écartés en dehors de la bande due aux changements brusques entre les statuts de symbole qui correspondent au court et ouvrent circuit dans le modulateur de Six-port. Nous proposons une approche de ligne de transmission de charge qui emploie la ligne de transmission de charge quatre $\lambda/2$ qui est insérée entre les ports de rendement du Six-

port quatre et les commutateurs se reliant au court ou ouvert des charges. La ligne proposée de transmission charge ralentit les changements entre le statut de symboles, évitant le changement soudain de phase du modulateur du Six-port QPSK. Dans le meilleur des cas, un changement linéaire se produit dans un temps de symbole. Des simulations employant Agilent ADS ont été faites et les résultats de spectre ont montrés qu'une réduction extérieure de bande du 10 dB a été réalisée avec méthode proposée de ligne de transmission.

0.6 Conclusions et travaux futures

Ce travail a été concentré pour démontrer la technologie de Six-port dans le modem numérique fonctionnant aux fréquences de VHF. Ceci a comporté l'utilisation des simulations et de l'exécution physique d'un modulateur et du démodulateur de QPSK dans le matériel. Pour la démodulation de QPSK, l'exécution de BER est le paramètre le plus important qui doit être maintenu. Pour le modulateur de QPSK, la constellation et la formation du spectre sont la critique.

La théorie de la radio de Six-Port a prouvé qu'en combinant simplement les composants passifs tels que des coupleurs, le diviseur de puissance et la diode de puissance détecteurs, le Six-Port peut réaliser la discrimination de phase du signal de RF modulé par entrée. En reliant la charge courte et ouverte à l'aide des commutateurs, le Six-Port peut être un modulateur de QPSK aussi bien. Pour prouver les concepts, un Six-Port

employant les composants discrets a été mis en application à la bande de VHF. Les différentes simulations et résultats de mesure prouvent que le Six-Port proposé avait fonctionné correctement. Car nous avons déjà vu que même à de basse fréquence la bande de VUF, l'effet de ligne de transmission ne peut pas être donnée supassé. L'exécution du démodulateur de QPSK a été effectuée dans deux étapes. Car des détecteurs de puissance de Wiltron ont été employés, pour caractériser ces dispositifs, un modèle approprié est nécessaire et a été fait en mesurant de puissance d'entrée et de sortie des détecteurs. La performance de BER est le critère critique pour le démodulateur de QPSK. Afin de faire la mesure appropriée de BER, un amplificateur de quatre canaux a été fabriqué pour aborder la question liée à la gamme dynamique du récepteur de Six-Port. Pour sauver notre temps, un décodeur des travaux précédents a été adopté dans notre installation de mesure de BER. Un modulateur du Six-Port QPSK à la bande de VHF a été décrit, conçu et enfin mis en application. Des commutateurs commerciaux ont été utilisés pour réaliser les charges courtes et ouvertes. Pour réduire l'interférence extérieure de bande, un bon modulateur devrait avoir une formation appropriée de spectre. On a proposé une approche de ligne de transmission de charge pour améliorer la forme de spectre du modulateur du Six-Port QPSK. Le modem du Six-Port QPSK mis en application dans cette thèse a réalisé simultanément le débit le plus élevé, la meilleure exécution de BER et l'excellente constellation de modulation de toutes des réalisations par radio éditées précédemment connues de QPSK à la bande de VHF.

Pour les travaux futurs, il y a plusieurs recommandations. Premièrement, une recommandation est donnée pour la mesure de BER d'émetteur et de récepteur en intégrant les antennes, LNA, amplificateur de puissance dans le système radio entier. Pour plus de simplicité de circuit et coût du démodulateur, la prochaine recommandation est d'employer des détecteurs de puissance de SMD au lieu des détecteurs coûteux de puissance de Wiltron dans le démodulateur du Six-Port QPSK. La troisième recommandation pour les travaux futurs est le modulateur de spectre simulant les différentes charges et établissant les circuits pour examiner la théorie.

TABLE OF CONTENTS

LIST OF FIGURES

LIST OF TABLES

LIST OF ABBREVIATIONS AND ACRONYMS

ADS	Advanced Design System
ADC	Analog to Digital Converter
BER	Bit to error ratio
EC	Equivalent Circuit
EVM	Error Vector Magnitude
DAC	Digital to Analog Converter
DECT	Digital Enhanced Cordless Telecommunications
GMSK	Gaussian Minimum Shift Keying
GSM	Global System for Mobile communications
IF	Intermediates Frequencies
LE	Lumped Element
LO	Local Oscillator
PRBS	Pseudo-random binary sequence
PLL	Phase Locked Loops
QAM	Quadrature Amplitude Modulation
QPSK	Quadrature Phase Shift Keying
RF	Radio Frequency
SMD	Surface Mount Device
SNR	Signal to Noise Ratio

VHF	Very High Frequency
UHF	Ultra High Frequency
WLAN	Wireless LAN

Chapter 1

Introduction

One of the key parts in a telecommunication radio is the modem. The term modem stems from the words modulation and demodulation. These words refer to the main task of a modem. In the context of a mobile telecommunication terminal, the demodulator transforms the signals coming from the LNA into the digital domain signals. The modulator converts the digital data stream at baseband into a signal at radio frequencies, and this signal is delivered to the antenna by power amplifier.

Digital modulation and demodulation have been around since the 1950s, with the need for military digital satellites communications [4]. The frequency bands ranged from a few 100 MHz up to several GHz. Digital modem for mobile telecommunication started to appear in the 1980s, with the development of DECT and GSM standards. These and other telecommunication standards for mobile telephony used radio frequencies between 800 MHz and 3 GHz.

Conventional modems are built up around a few basic building blocks, namely filters, mixers and oscillators. A frequency synthesizer is often used to generate the local oscillator frequency with required phase noise. With these building blocks several architectures can be realized.

In a heterodyne architecture, a single local oscillator frequency is used for down-conversion of the RF signals. To circumvent the image rejection problem a dual-conversion architecture can be employed. Two local oscillators are then used; the first one to take care of the image rejection issue and the second one to ease the channel selection problem.

With the use of Digital Signal Processing (DSP), complex modulation and demodulation in the mobile terminal became reality, leading to quadrature up- and down-conversion architectures. A commonly used modem architecture is the homodyne architecture, also called direct-conversion or zero-IF architecture, which means the intermediate frequency (IF) is set to zero. The zero-IF architecture can be found in, for example, GSM, DECT and WLAN front ends.

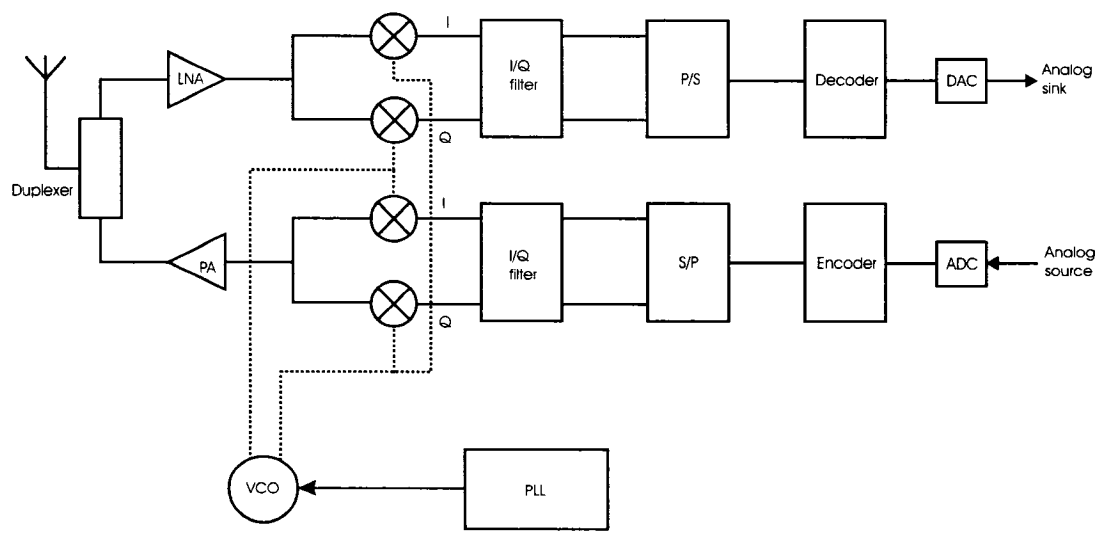

Figure 1-1 An example of a zero-IF modem within a transceiver

Figure 1.1 depicts an example of a zero-IF modem within a transceiver. After the duplexer, a low noise amplifier (LNA) first amplifies the signals in the receiver path. Then quadrature mixing is performed to down-convert the RF signals to an IF frequency at zero Hertz. Two quadrature (90° out-of-phase) signals from the local oscillator (LO) are needed, for the realization of an effective mixing operation with a single positive frequency. Intermediate frequency filtering can be performed to attenuate adjacent and non-adjacent channels. The resulting paired I/Q baseband signals are combined by a parallel to serial converter, and then feed to a decoder before digital-to-analog converter (DAC) can be performed. At the transmit side, the signals are transformed into the digital domain by an analog-to-digital converter (ADC). The resulting baseband signals are by means of quadrature up-conversion converted to a real signal at the radio frequency. Then the power amplifier (PA) boosts the signals towards the antenna at the required power transmit level. A phase-locked loop (PLL) is needed to generate a stable and correct RF frequency from a reference oscillator, usually a crystal oscillator. This work will discuss the design of the digital QPSK (de-)modulation circuits needed to built a RF transceiver like the one in Figure 1.1, Filters, data converters, and amplifier are however outside the scope of this work.

The homodyne architecture offers two advantages over the heterodyne one. First, the image rejection problem is eliminated, as a result, no image filters is required. Second, the IF SAW filter and subsequent down-conversion stages are replaced with low pass

filter and baseband amplifiers. However, there are several drawbacks of this architecture. First, there is a DC offset problem, which is caused by LO to RF leakage due to the limited mixer isolation between RF and LO port. Second I/Q mismatch which is caused by the phase and amplitude imbalances in I and Q signal paths. Third, flick noise problem, which can corrupt the baseband signal.

In 1994, Li[14] proposed a new Six-Port direct digital receiver architecture which depicts in Figure1.2. Six-Port circuit is composed of passive components, three couplers and a power divider. Among the six ports, two ports are used as RF and LO input ports, the remaining four ports are connected to four power detectors. The four power detectors' DC outputs contain all information about the phase and amplitude between RF and LO signals. In other words, by reading the DC outputs of the four power detectors, phase modulated RF signal can be demodulated by comparing with the phase of LO signal.

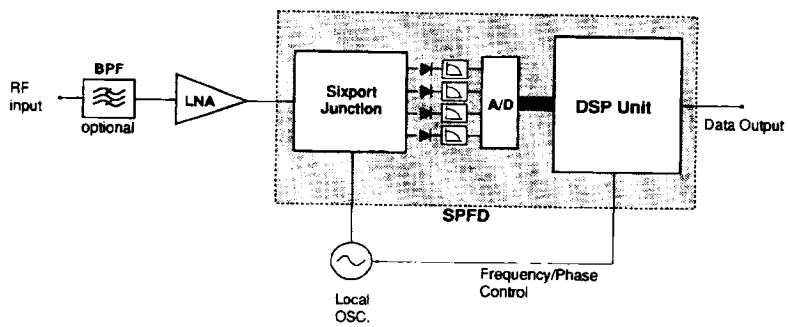

Figure 1-2 Six-Port QPSK demodulator proposed by Li

In 2001, Serioja [19] has proposed another Six-Port receiver based on MHMIC technique at Ka band frequency using analog decoder (see figure 1-3).

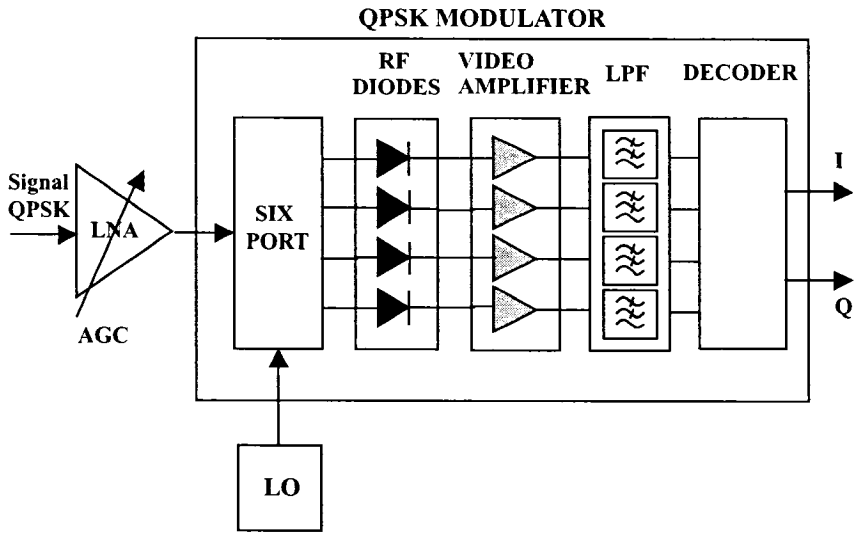

Figure 1-3 Serioja's Six-Port receiver

In 2001, Eric [5] proposed a Six-Port direct digital QPSK modulator at S band which was used to do the carrier recovery. In this architecture, four switches were employed to control the reflections of the four ports among the six ports in order to realize the QPSK modulation.

Six-Port direct digital demodulator and modulator have several advantages over conventional direct conversion counterpart. First, in this architecture, a Six-Port which contains only passive components, such as couplers and power divider, does not use mixer as frequency translating component, therefore circumventing the image rejection and spurious problems associated with mixers. Second, cheap power detectors are used

to generate the DC output which can be used either to do the analog demodulation or DSP demodulation for more complex modulation schemes, the requirement for the speed of ADC can be lower as well. Third, Six-Port modulation and demodulation are not "analog" like its conventional counterpart, its digital modulation and demodulation are direct or "digital". In another word, it maneuver RF signal directly in phase and amplitude. Forth, because no filter for BPF is needed, just using passive components such power divider and hybrid couplers, it results a significant reduction of parts and consequently, cost. Power consumption of whole circuit can be lower as well. Fifth, Six-Port can be made at high frequency which is particularly beneficial at high frequency digital modulation. Last but not least, theoretically and experimentally, Six-Port can be made wideband, which is a good candidate for today's wideband applications.

This work is based on our research activities in the Poly-Grames Research Center. Our objective is to demonstrate a new structure of lumped elements Six-Port digital modem in order to realize QPSK modulation and demodulation at VHF band. We use cheap SMD discrete components such as resistors, inductors and capacitors to build our Six-Port QPSK modulator and demodulator circuits.

In addition to the introductory chapter, this thesis contains five chapters. In Chapter 2, fundamental knowledge and design concepts for a digital Six-Port modem are

developed. The focus is to introduce mathematical formulas in order to realize digital Six-Port modulation and demodulation.

In Chapter 3, a Six-Port using discrete components is designed and implemented. S-parameters are shown and compared with simulation results. A discussion for the frequency shift phenomenon is given for further assistance of our design.

In Chapter 4, direct QPSK demodulator is investigated. Modeling power detectors, which optimize the power detectors utilization is described. This requires an analytical model to characterize the power detectors for power detection operation. Following is four channel DC amplifier design and implementation. BER measurement, which is to characterize the key parameter of the demodulator, is performed and different results are given.

Techniques for implementation of a new direct QPSK modulator architecture are introduced in Chapter 5. An analytical method is developed to investigate the operation of direct QPSK modulators using switches. PIN diodes and commercial switches are compared and selected. Further discussions are given to address the modulation spectrum and the power conversion efficiency.

Finally, conclusions and future works are presented in Chapter 6.

Chapter 2

Fundamental Concepts of Six-Port Digital Modem

2.1 Six-Port technology review

A Six-Port is a passive circuit originally designed for the measurement of the microwaves circuits. A example of the early application of the Six-Port was the reflectometer[18]. The Six-Port system which has six ports, two inputs and four outputs, consist of three hybrid couplers and a Wilkinson power divider as shown in figure 2.1. The outputs are connected to four power detectors. When the six port behavior is linear, the input-output relations can be analytically derived, and phase and amplitude measurements can be accurately performed.

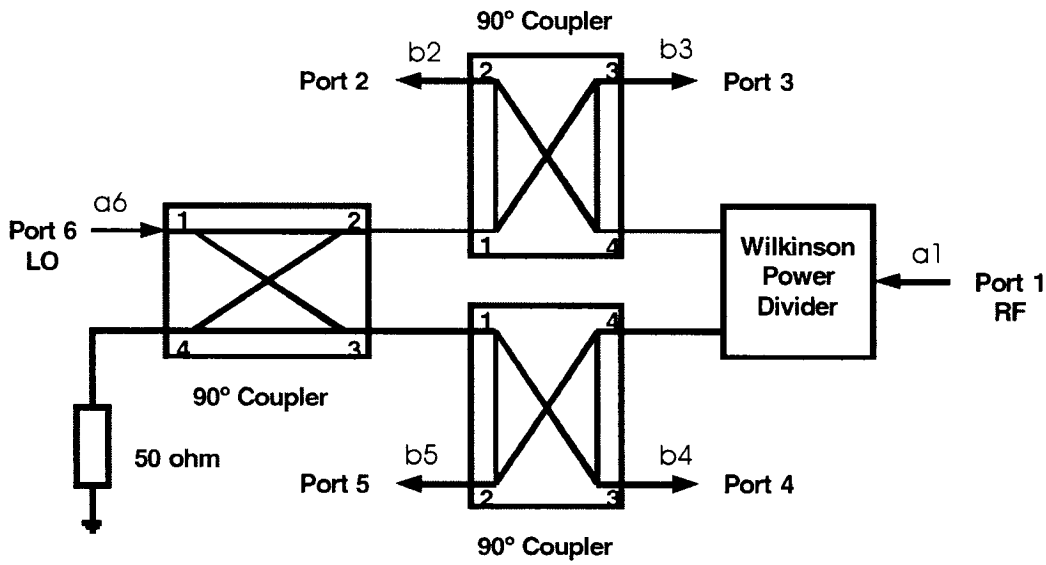

Figure 2-1 **Block Diagram of Six-Port**

Since 1994, after Li's discovery[14] of the application of six-port in direct conversion receiver, many other researches [19] [6] [11] [8] [6] which based on the similar architecture show that the Six-Port architecture is a promising candidate to be used in various direct PSK and QAM modulation and demodulation.

2.2 The principle of operation of the Six-Port QPSK modulation

Figure 2.2 depicts the structure of the 90° Hybrid Coupler, and the S-parameters [3] is shown in (2.1)

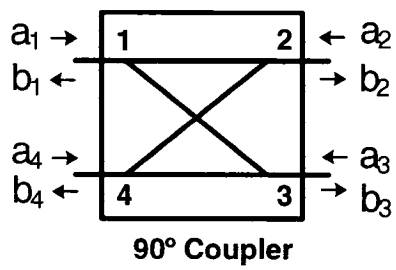

Figure 2-2 **block diagram of a 90° Hybrid Coupler**

$$[S]_{coupler} = \frac{-1}{\sqrt{2}} \begin{pmatrix} 0 & j & 1 & 0 \\ j & 0 & 0 & 1 \\ 1 & 0 & 0 & j \\ 0 & 1 & j & 0 \end{pmatrix} \tag{2.1}$$

From (2.1), by matrix definition of S-parameter, we have (2.2) and (2.3)

$$\begin{pmatrix} b_1 \\ b_2 \\ b_3 \\ b_4 \end{pmatrix} = [S]_{coupler}[a] = \frac{-1}{\sqrt{2}} \begin{pmatrix} 0 & j & 1 & 0 \\ j & 0 & 0 & 1 \\ 1 & 0 & 0 & j \\ 0 & 1 & j & 0 \end{pmatrix} \begin{pmatrix} a_1 \\ a_2 \\ a_3 \\ a_4 \end{pmatrix} \tag{2.2}$$

$$\begin{pmatrix} b_1 \\ b_2 \\ b_3 \\ b_4 \end{pmatrix} = \frac{-1}{\sqrt{2}} \begin{pmatrix} a_2 j + a_3 \\ a_1 j + a_4 \\ a_1 + a_4 j \\ a_2 + a_3 j \end{pmatrix} \tag{2.3}$$

By definition of reflection coefficient Γ, and let

$$\Gamma = \frac{a_2}{b_2} = \frac{a_3}{b_3} \tag{2.4}$$

We have

$$b_1 = \frac{-1}{\sqrt{2}}(j\Gamma b_2 + \Gamma b_3) \tag{2.5}$$

$$b_4 = \frac{-1}{\sqrt{2}}(\Gamma b_2 + j\Gamma b_3) \tag{2.6}$$

Now we go back to the detailed block diagram of Six-Port shown in figure 2.3.

Let us define

$$\Gamma_1 = \Gamma \tag{2.7}$$

(2.7) is the reflection coefficient of port 2 and port 3. Since there is no reflection at port 4 (adapted to 50 ohm) of the coupler connecting to port 6, and after some mathematical reductions, we have

$$b''_4 = \frac{1}{\sqrt{2}} a'_1 \Gamma_1 \tag{2.8}$$

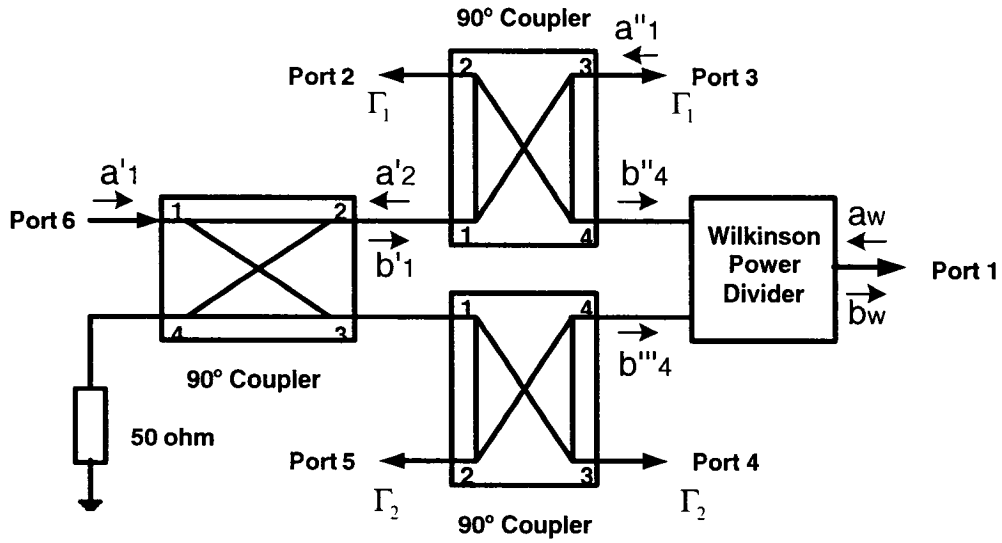

Figure 2-3 **Block diagram of Six-Port**

Similarly, defining $\Gamma_2 = \Gamma$ at port 4 and port 5, we have

$$b'''_4 = \frac{-1}{\sqrt{2}} j a'_1 \Gamma_2 \tag{2.9}$$

Let us look at the Wilkinson power divider shown in figure 2-4

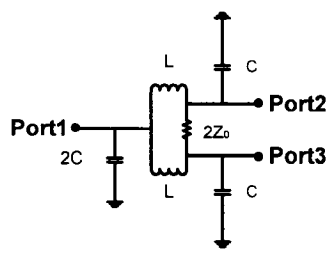

Figure 2-4 **Block diagram Wilkinson**

(2.10) shows the S-parameter of Wilkinson power divider [3],

$$[S]_W = \frac{-j}{\sqrt{2}}\begin{pmatrix} 0 & 1 & 1 \\ 1 & 0 & 0 \\ 1 & 0 & 0 \end{pmatrix} \tag{2.10}$$

Using the S-parameter definition, we have

$$b_w = \frac{-j}{\sqrt{2}}(a_2 + a_3) \tag{2.11}$$

Substitute (2.8) and (2.9) into (2.11), we have

$$b_w = \frac{-1}{2}(\Gamma_2 + j\Gamma_1)a'_1 \tag{2.12}$$

Finally, we have the fundamental formula for our Six-Port QPSK modulation,

$$(S_{61})_{SP} = \frac{b_w}{a'_1} = \frac{-1}{2}(\Gamma_2 + j\Gamma_1) \tag{2.13}$$

For short circuit of Six-Port, Γ=-1 and for open circuit Γ=1. From (2.13), we can calculate the values of constellation of Six-Port QPSK modulation shown in figure 2-5, Table 2-1 and Table 2-2.

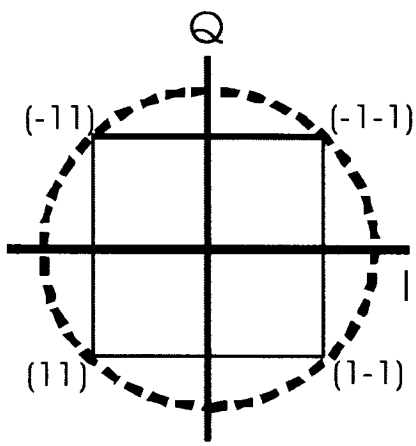

Figure 2-5 Constellation of Six-Port QPSK modulation

If we extend (2.13), say, Γ1 and Γ2 has arbitrary phase θ, we have

$$(S_{61})_{SP'} = \frac{1}{\sqrt{2}} e^{j\theta} \tag{2.14}$$

If during a symbol period, we change (shift or circle) phase θ in constellation diagram a few steps, we can have MSK-like modulation as shown in figure 2-5.

Table 2-1 Constellation value of Six-Port QPSK modulation

	Γ_2 (Short)	Γ_2 (Open)
Γ_1 (Short)	$\frac{1}{2}+\frac{1}{2}j$	$-\frac{1}{2}+\frac{1}{2}j$
Γ_1 (Open)	$\frac{1}{2}-\frac{1}{2}j$	$-\frac{1}{2}-\frac{1}{2}j$

Table 2-2 Phase representation of constellation value of Six-Port QPSK modulation

	Γ_2 (Short)	Γ_2 (Open)
Γ_1 (Short)	$\frac{1}{\sqrt{2}} e^{j\frac{\pi}{4}}$	$\frac{1}{\sqrt{2}} e^{j\frac{3\pi}{4}}$
Γ_1 (Open)	$\frac{1}{\sqrt{2}} e^{-j\frac{\pi}{4}}$	$\frac{1}{\sqrt{2}} e^{-j\frac{3\pi}{4}}$

Table 2-3 Symbol representation of constellation of Six-Port QPSK modulation

Symbol	Phase (degree)
-1,-1	45
-1,1	135
1,-1	-45
1,1	-135

Table 2-3 shows the phase and Symbol representation of constellation of Six-Port QPSK modulation. In general, if we use switches to generate the value of -1 and 1 (corresponding to the data symbols), which is equivalent to connect the switches to ground and to open terminals, we can change the phase (even amplitude) of incoming RF signal, therefore we have QPSK modulation.

2.3 The principle of operation of the Six-Port QPSK demodulation

Figure2.6 illustrates the proposed Six-Port QPSK demodulator.

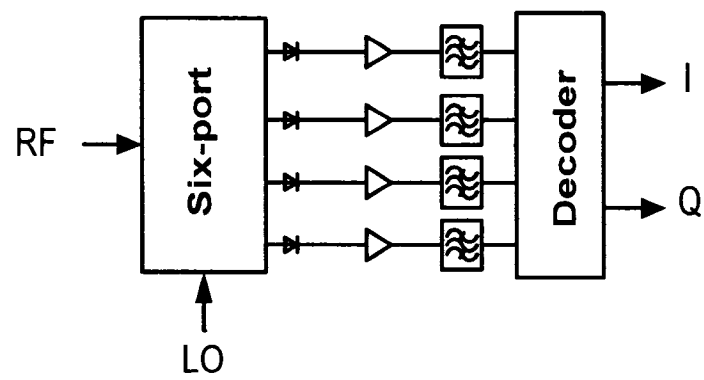

Figure 2-6 Six-Port QPSK demodulator

We will evaluate the S-parameters of the Six-Port starting from the general relation which gives the vector of the reflected waves b, to the vector of incident waves a:

$$[b]=[S]\cdot[a] \tag{2.15}$$

By supposing that hybrid couplers and the power divider are lossless, we can calculate the S parameters of the Six-Port and obtain:

$$[S]=\begin{pmatrix} 0 & j/2 & -1/2 & -1/2 & j/2 & 0 \\ j/2 & 0 & 0 & 0 & 0 & -1/2 \\ -1/2 & 0 & 0 & 0 & 0 & j/2 \\ -1/2 & 0 & 0 & 0 & 0 & 1/2 \\ j/2 & 1/2 & 0 & 0 & 0 & j/2 \\ 0 & -1/2 & j/2 & 1/2 & j/2 & 0 \end{pmatrix}$$

The Six-Port presented in figure 2.1 is linear and we can deduce the expressions from the forms of the four incident waves b2, b3, b4, b5, according to the two incidental waves a1 and a6.

$$b_2=\frac{1}{2}(ja_1-a_6) \tag{2.16}$$

$$b_3=\frac{1}{2}(-a_1+ja_6) \tag{2.17}$$

$$b_4=\frac{1}{2}(-a_1+a_6) \tag{2.18}$$

$$b_5=\frac{1}{2}(ja_1+ja_6) \tag{2.19}$$

The two input signals are described by:

$$a_1 = |a_1| \cdot \exp(j\varphi_1)$$
$$a_6 = |a_6| \cdot \exp(j\varphi_6) \tag{2.20}$$

The angles represent the state of phase of the signals at the ports of the Six-Port. Ports LO and RF are insulated, the input signals are propagated only at the ports of the six-port where they are superimposed according to single relations of phase. Let us suppose two input signals of the same frequency, of the same amplitude |a1| = |a6| = A, and suppose that each port is adapted, the equations of the waves (2.16) to (2.19) at the four ports become:

$$b_2 = \frac{A}{2} \cdot (\exp(j(\varphi_1 - \varphi_6 - \frac{\pi}{2}) + 1)$$
$$b_3 = \frac{A}{2} \cdot (\exp(j(\varphi_1 - \varphi_6 + \frac{\pi}{2}) + 1)$$
$$b_4 = \frac{A}{2} \cdot (\exp(j(\varphi_1 - \varphi_6 + \pi) + 1)$$
$$b_5 = \frac{A}{2} \cdot (\exp(j(\varphi_1 - \varphi_6) + 1)$$

The power of each port is proportional on a matched load. We note that for each port there is a phase shift between the two input signals. The power corresponding to each port can be expressed as follows:

$$P_i = | b_i |^2, i = 2,3,4,5$$

If $\varphi_1 - \varphi_6 = 0$, $\frac{\pi}{2}$, π and $-\frac{\pi}{2}$ respectively, we can calculate the power for each port with corresponding phase difference value as shown in Table 2-4.

Table 2-4 Powers at the four ports of the Six-Port at QPSK modulation

$\varphi_1 - \varphi_6$	P_2	P_3	P_4	P_5
0	$A^2/2$	$A^2/2$	0	A^2
$\pi/2$	A^2	0	$A^2/2$	$A^2/2$
π	$A^2/2$	$A^2/2$	A^2	0
$-\pi/2$	0	A^2	$A^2/2$	$A^2/2$

The Table 2.4 expresses then the powers at the four ports of the Six-Port at QPSK modulation. There is a minimum and a maximum at each phase status. It is possible to demodulate a QPSK signal by a simple reading of power, detecting a minimum or a maximum at the one of the four ports. In QPSK modulation, we have two bits corresponding to one symbol 0 or 1 as shown in figure 2.7

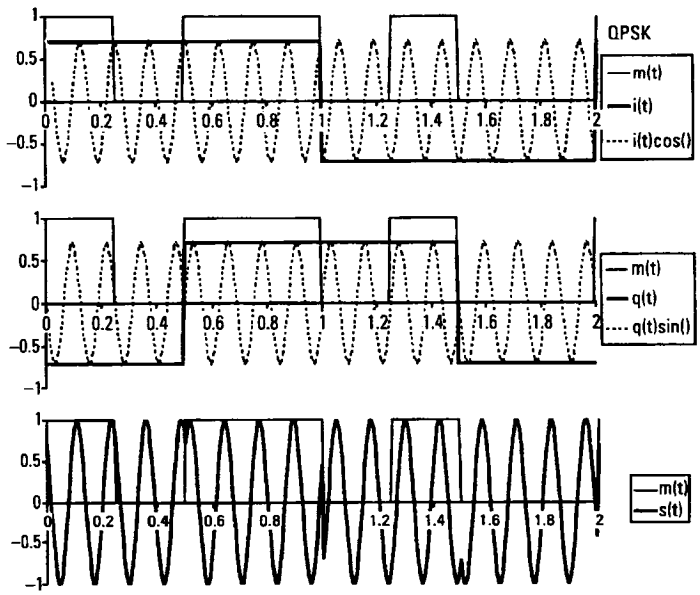

Figure 2-7 QPSK carrier, bits and symbol waveforms [9]

The modulator takes the input bits two by two and sends modulated carrier whose phase is one of the four possibilities as the summary given in Table 2.5:

Table 2-5 Phases corresponding to the pairs of bits sent

Bits information	Phase
0 0	0
0 1	$\pi/2$
1 1	π
1 0	$-\pi/2$

If we use the six-port as demodulator of phase for a QPSK signal, we can differentiate the four states of modulation. Figure 2.8 shows the constellation of QPSK demodulation.

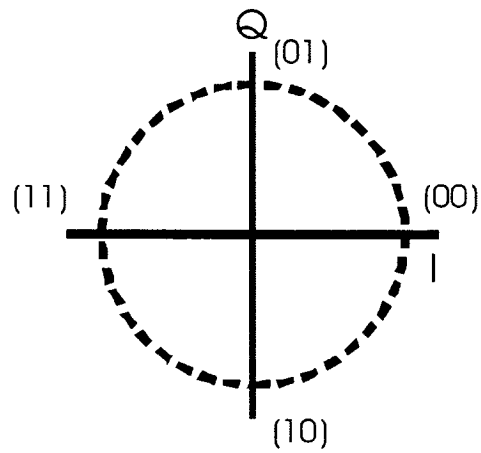

Figure 2-8 Constellation of QPSK demodulation

Chapter 3

Lumped-Element Six-Port

In this chapter, we will build a lumped-element Six-Port using discrete components. First we fabricate a coupler, and a Wilkinson power divider, and then we construct the Six-Port using three couplers and a Wilkinson power divider. In all of this process, Agilent Advanced Design System (ADS) was used to simulate the circuits. Simulation and measurement results are given. Finally detailed evaluation of the frequency shift phenomenon has been conducted.

3.1 Introduction

Lumped elements six-port is composed of lumped elements, namely, inductors, capacitors, resistors. At VHF band, parasite effects associated with these elements can not be overlooked. These effects are attributable to the physical size of the component and are described by parameters such as the effective series inductance (ESL) and effective series resistance (ESR). Generally speaking, a smaller size of the components results less parasite effects. In practice, we chose SMD components instead of through-hole components, and smaller physical size like 0805 or 0603 in our design. Working frequency range must be also considered. If proper models are not readily available, then S-parameter must be used in the circuits. The transmission line connection between

those components must also be carefully designed at VHF frequency in order to get desired results.

3.2 System description

The design of the lumped-element Six-Port begins with the architecture of lumped-element Six-Port. Figure 3-1 is the block diagram which is used to construct the Six-Port. It composes of three lumped-element quadrature couplers and a Wilkinson power divider.

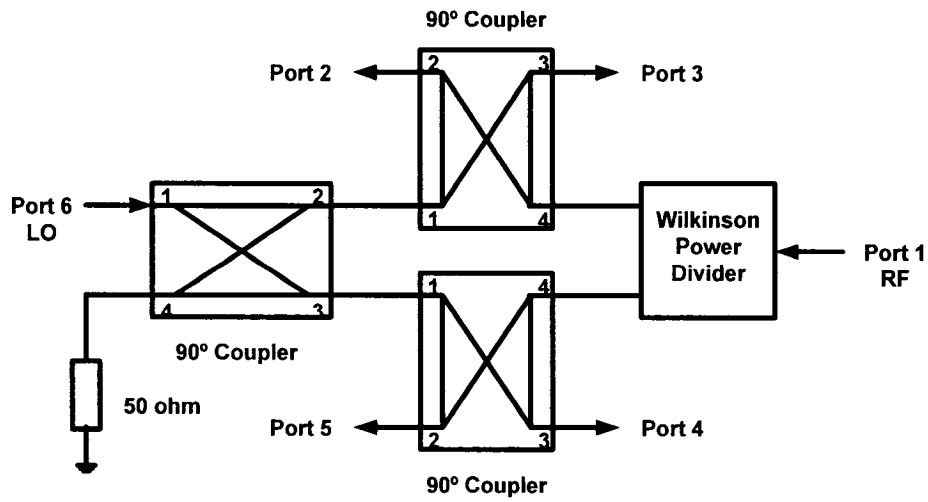

Figure 3-1 The Architecture of Lumped-Element Six-port

An ideal lumped element is not realizable even at VHF frequencies because of the associated parasitic reactances due to fringing fields. At RF and microwave frequencies, each component has associated electric and magnetic fields and finite dissipative loss. Thus, such components store or release electric and magnetic energies across them and

their resistance accounts for the dissipated power. The relative values of the *C, L,* and *R* components in these elements depend on the intended use of the lumped-elements. To describe their electrical behavior, equivalent circuit models for such components are commonly used. Lumped-element equivalent circuit models consist of basic circuit elements (*L, C,* or *R*) with the associated parasitics denoted by subscripts. Accurate computer aided design requires a complete and accurate characterization of these components. This requires comprehensive models including the effect of ground plane, fringing fields, proximity effects, substrate material and thickness, conductor thickness, and associated mounting techniques and applications. Thus, an equivalent circuit representation of a lumped element with its parasitics and their frequency-dependent characteristics is essential for accurate element modeling. An equivalent circuit model consists of the circuit elements necessary to fully describe its response, including resonances, if any. Models can be developed using analytical, electromagnetic simulation, and measurement based methods.

3.2.1 Inductors

An equivalent circuit [16] of SMD inductors is shown in figure 3-2.

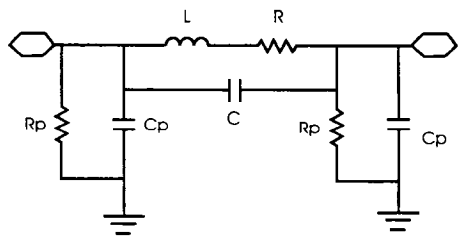

Figure 3-2 An equivalent circuit of SMD inductor

where resistance R includes the SMD package and inductor losses. Likewise, the capacitance C represents the self-capacitance of the inductor package. Since there are no leads, L is simply equivalent inductance of the element.

Since Coilcraft [2] provides S-parameters for all inductors, we chose surface mount (SMD) inductors from Coilcraft instead of modeling inductors by ourselves.

3.2.2 Capacitors

An equivalent circuit for capacitors is shown in figure 3-3.

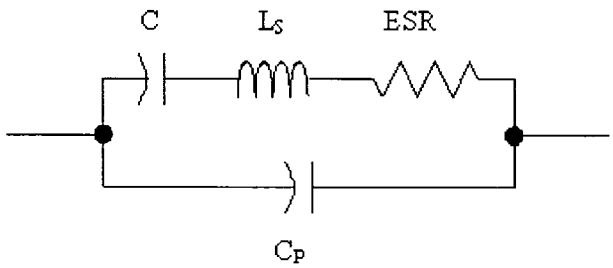

Figure 3-3 A equivalent circuit for capacitors

The element denoted "C" in the model is the nominal capacitance value, the rest of the elements are considered parasitics. Ls is the self-inductance of the structure. The equivalent series resistance (ESR) is the real part of the series impedance of a capacitor, and is the element that causes loss due to heat. The parallel capacitance Cp also causes some troubles, but can often be ignored because we try to operate below the frequency where this causes a resonance.

Same as with inductors, modeling capacitors can be tedious and require particular equipments which are not available for us currently. For simplicity, we chose surface mount (SMD) multilayer ceramic capacitors from TDK since it provides S-parameters for all capacitors.

3.2.3 90° Directional Coupler

90° directional coupler is also called quadrature hybrid coupler, which is a 3dB directional coupler with a 90° phase difference in the outputs of the through and coupled arms. It is often made in microstrip line or stripe line as shown in figure 3-4 [3]. In VHF frequency band, we use lumped elements instead of microstrip line to build 90° directional coupler because of the size restriction.

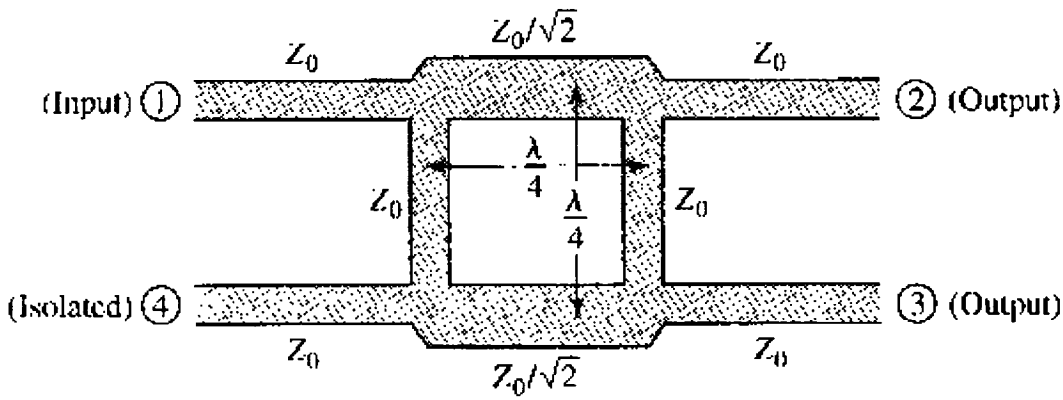

Figure 3-4 90° directional coupler made in microstrip line [3]

Figure 3.5 illustrates the equivalent circuits of a 90° directional coupler using lumped

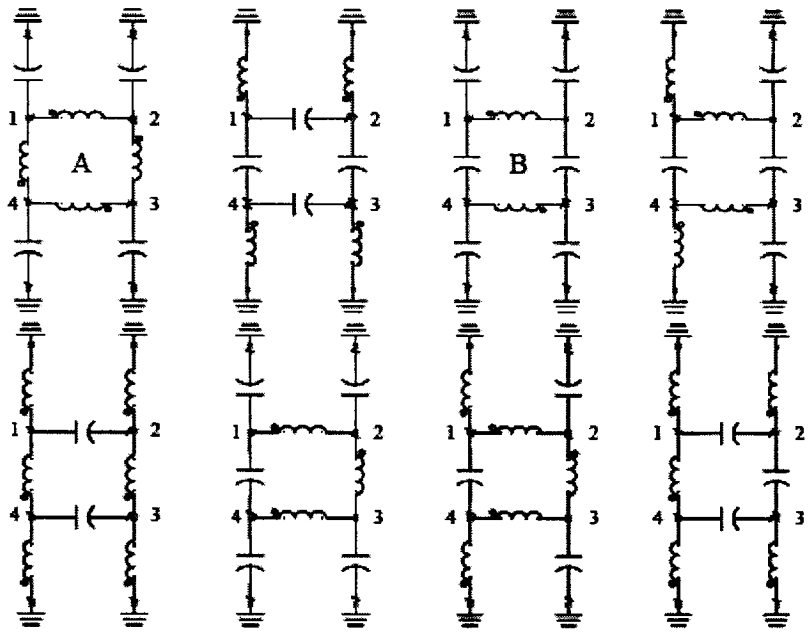

Figure 3-5 Equivalent circuit of a lumped elements 90° directional coupler

elements [17] [7]. They are composed of inductors and capacitors. As we can see, there are eight varieties of construction forms. We chose symmetric one (type A which is shown in figure 3-6) in our project because it has symmetric S-parameters frequency response.

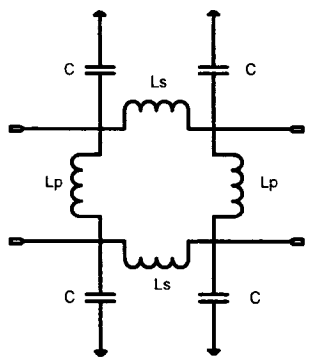

Figure 3-6 Equivalent circuit of coupler

3.2.4 Wilkinson power divider

Microwave power splitters (combiners), such as Wilkinson dividers and hybrid rings, generally employ quarterwave transmission line sections at the design center frequency, which can have unrealistic dimensions at frequencies in VHF bands, where the wavelength is large. It would be preferable to use lumped-element equivalent networks to replace the λ/4 transmission lines as shown in figure 3-7. Moreover, the Pi LC equivalent networks exhibit a low-pass behavior, rejecting high frequencies, while the response of the classical Wilkinson divider repeats at odd multiples of center frequency ($3f_0$ and $5f_0$, mainly). This behavior is desirable in the Six-Port QPSK modulator and demodulator to suppress unwanted high frequency interference and spurious.

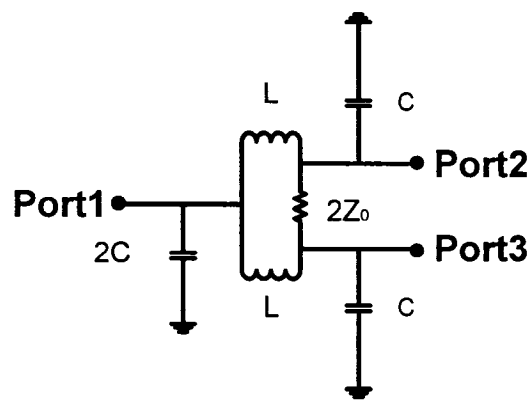

Figure 3-7 Equivalent circuit of Wilkinson power divider

3.3 The system design and simulation in ADS

System design of the Six-Port is composed of designing of couplers and Wilkinson power divider.

3.3.1 Design consideration of the coupler

The S-parameter of lumped elements 90° directional coupler is shown in figure 3-8 [3].

$$\begin{pmatrix} 0 & -j/\sqrt{2} & -1/\sqrt{2} & 0 \\ -j/\sqrt{2} & 0 & 0 & -1/\sqrt{2} \\ -1/\sqrt{2} & 0 & 0 & -j/\sqrt{2} \\ 0 & -1/\sqrt{2} & -j/\sqrt{2} & 0 \end{pmatrix}$$

Figure 3-8 S-parameter of lumped elements 90° directional coupler

Elements values of lumped-element 90° directional coupler can be derived from [17]. At 250 MHz frequency, using calculation formulas from [7] we have

$$\begin{aligned} Ls &= \frac{Z_0}{\omega\sqrt{2}} = \frac{Z_0}{2\pi f\sqrt{2}} 22.5nH \\ Lp &= \sqrt{2}Ls = 31.8nH \\ C &= \frac{\sqrt{2}+1}{\sqrt{2}\omega^2 Ls} = 30pF \end{aligned} \tag{3.1}$$

3.3.2 The simulation and the measurement of the coupler

Standard low-cost 0805 and 0603 SMD components S-parameter models for the

quadrature coupler from Coilcraft and TDK were used in circuit simulations. All components were featuring 5 percent tolerance in specifications. The simulation schematic is shown in figure 3-9 (a half of the coupler is shown because of the symmetry of the circuit).

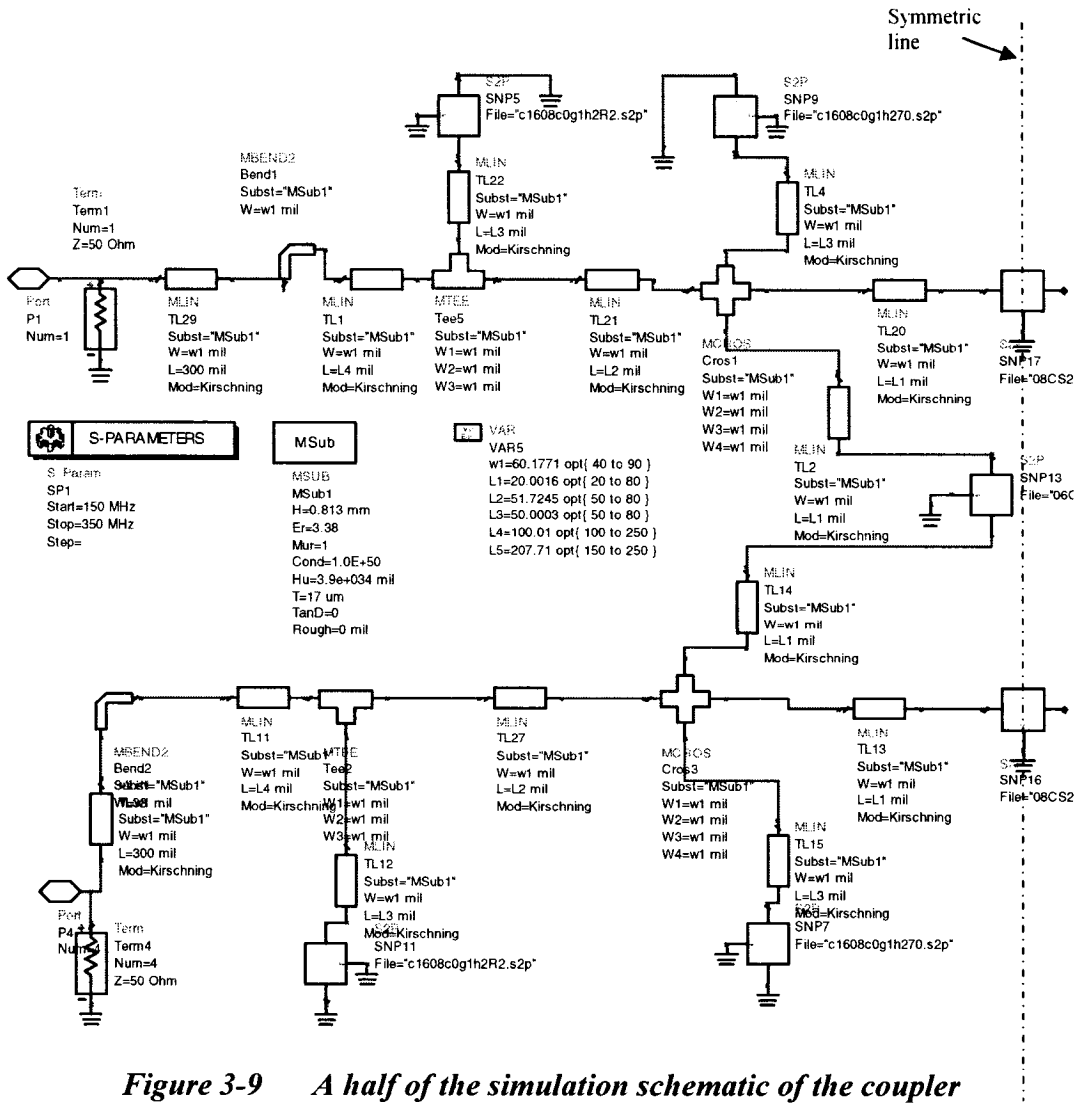

Figure 3-9 A half of the simulation schematic of the coupler

The simulation and the measurement of the phase difference results are presented in figure3-10 and 3-11 respectively. It can be seen that there is a desired 90° phase

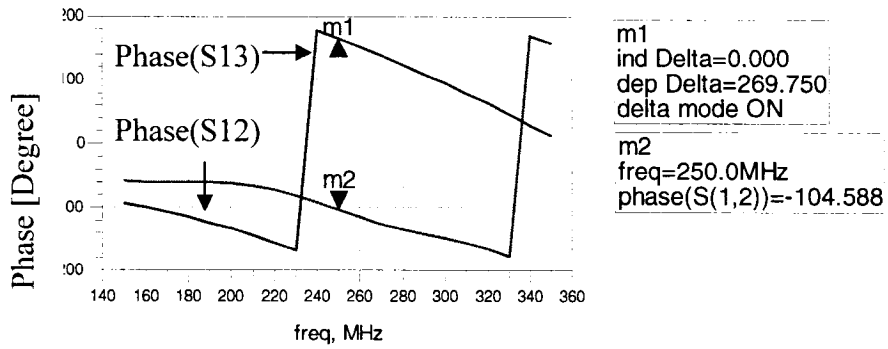

Figure 3-10 Simulation of phase difference between port 2 and port 3 of lumped-element coupler

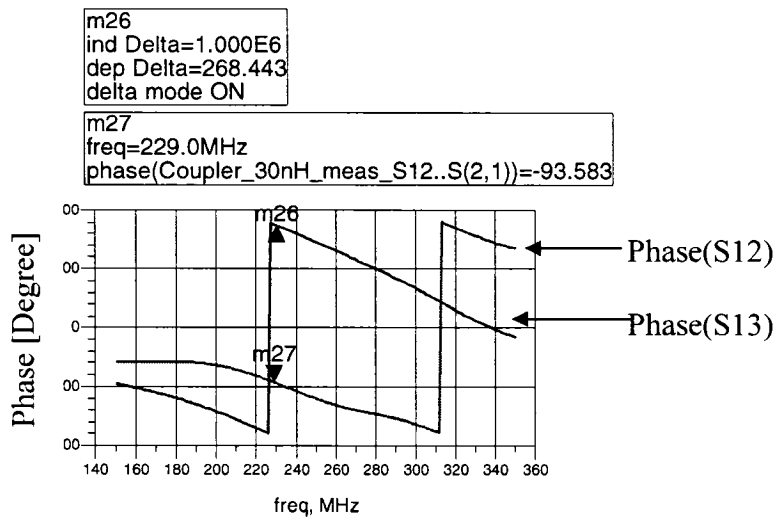

Figure 3-11 Measurement of phase difference between port 2 and port 3 of lumped-element coupler

difference at 230 MHz in the measurement result. Figure 3-12 and 3-13 show simulation and the measurement return losses results, measuring 34 dB at port 1, 33 dB at port 2 and 25 dB at port 3. Insertion loss at center frequency is about 4 dB for the measurement as shown in figures 3-14 and 3-15. Isolation between port 1 and port 4 at center frequency is about 25 dB for the measurement as shown in figure 3-16. As we can see that all the simulation and the measurement results are very close despite of some frequency down shift which will be explained in later session. The results also show that the designed coupler was working at f_0=230 MHz. The actual performance at higher frequencies differs from the expected values because the device parasitics were neglected in the simulations. Better agreement could be achieved by considering an adequate modeling of device parasitics.

The board layout was generated using Agilent ADS, which is depicted in figure 3-17 and 3-18. RO4003C (Er=3.38 thickness=32 mil) from Rogers was used to fabricate the PCB board. The size of the circuit board is less than two square centimeter.

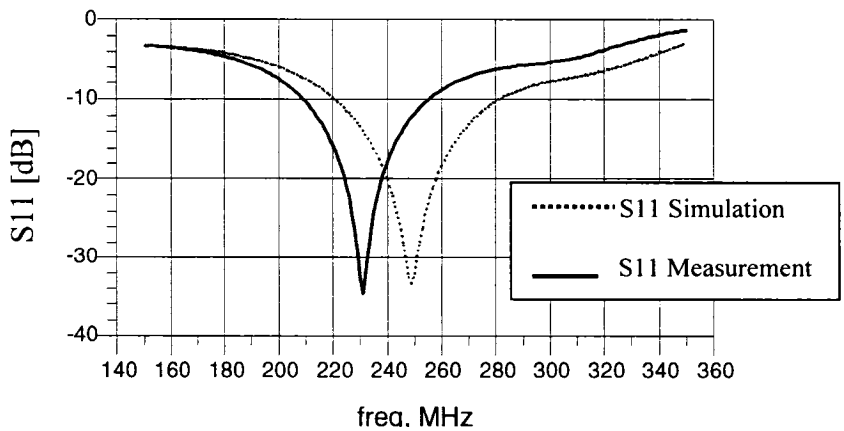

Figure 3-12 Measurement and simulation return loss at port 1

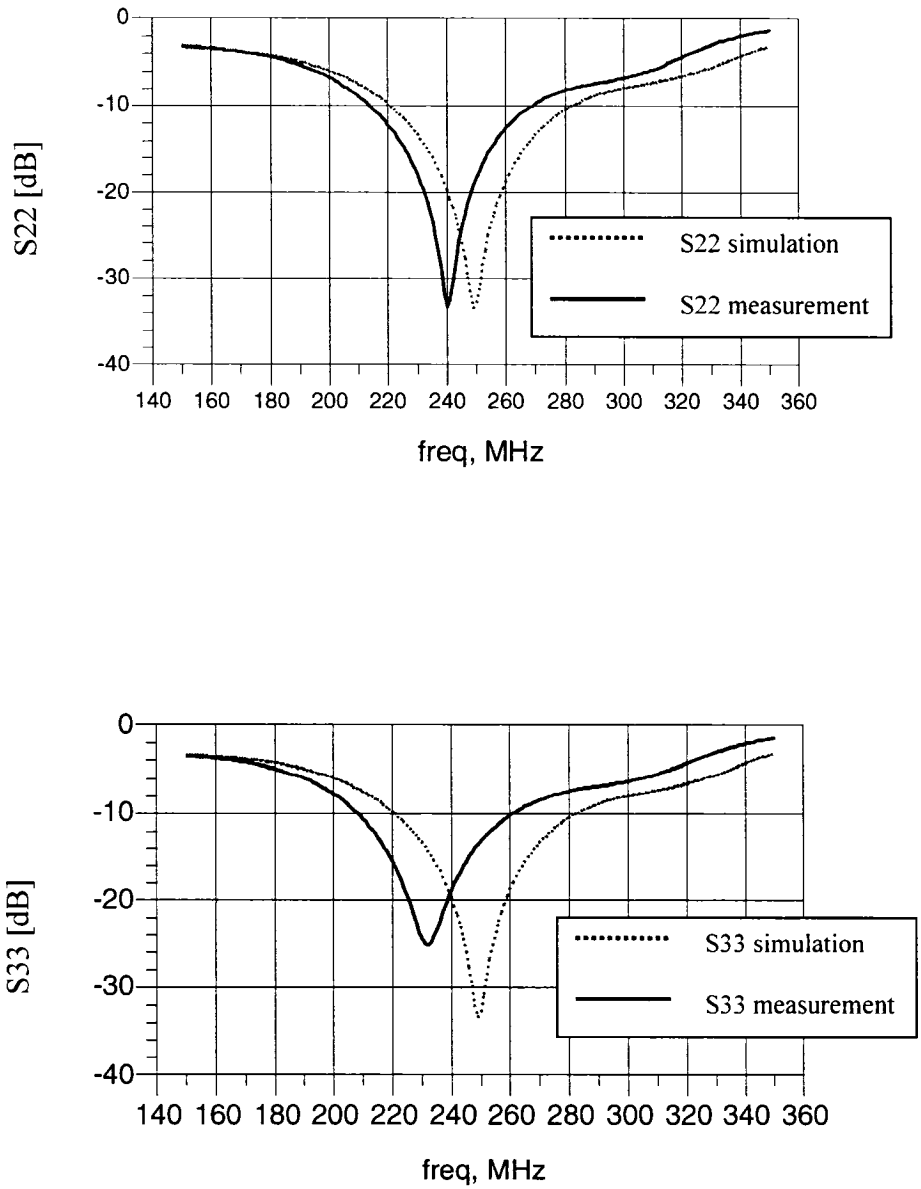

Figure 3-13 Measurement and simulation return loss at port2 and port3

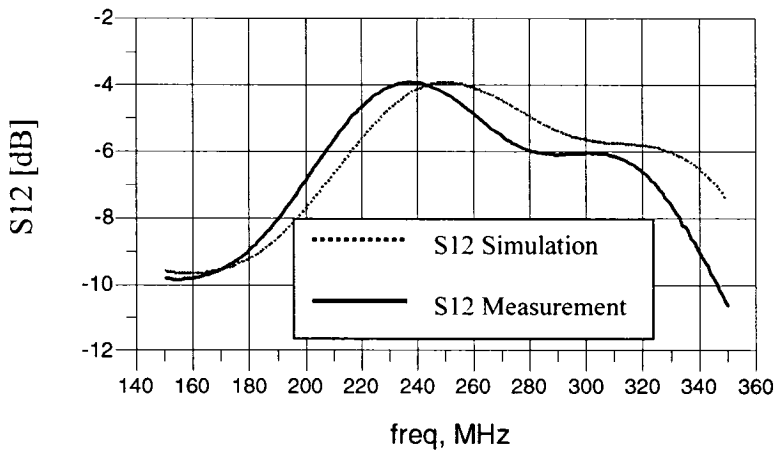

Figure 3-14 Insertion loss between port 1 and port 2

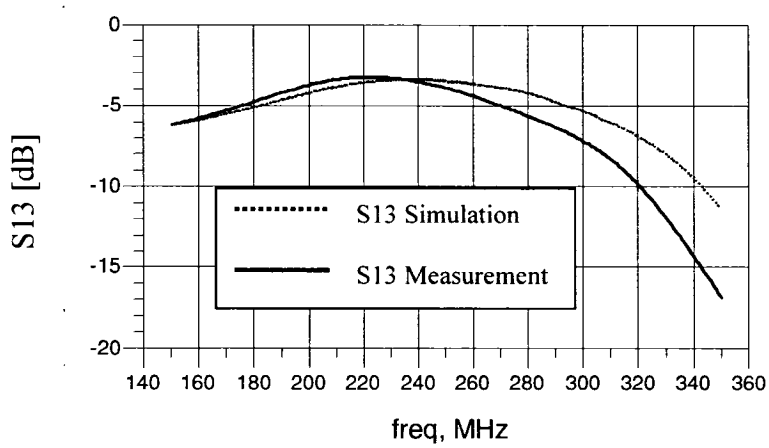

Figure 3-15 Insertion loss between port 1 and port 3

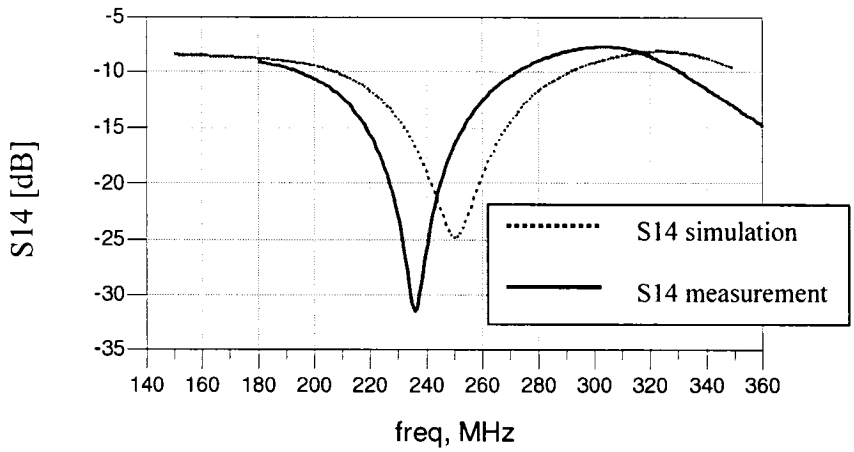

Figure 3-16 Isolation simulation between Port 1 and Port 4

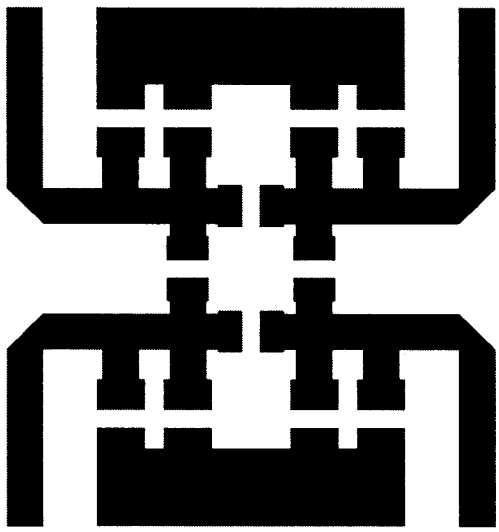

Figure 3-17 Layout of lumped-element coupler

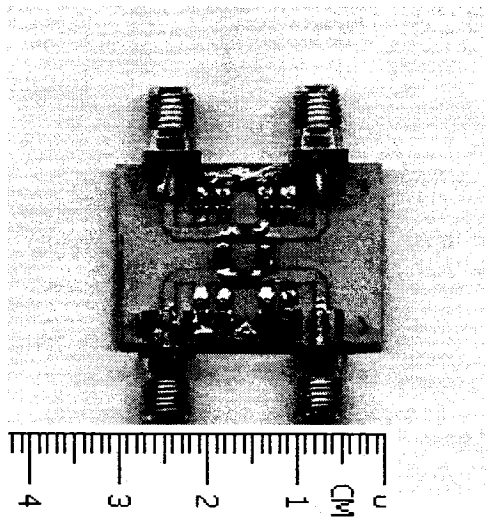

Figure 3-18 Fabricated lumped-element coupler

3.3.3 The design of Wilkinson power divider

Lumped-element Wilkinson power divider can be used to replace the conventional microstrip realization at frequencies from RF to several GHz, where quarterwave line segments become large. By employing low cost SMD passive components in VHF band, the circuits can be made compact, allowing reduced circuit dimensions. It also exhibits low pass behavior (not repeated at odd multiples of the center frequency), filtering the harmonic components of the input signal.

The element values are given in the following equations [7]:

$$L = \frac{Z_0\sqrt{2}}{\omega}$$
$$C = \frac{1}{\omega Z_0\sqrt{2}} \tag{3.2}$$

This network is only valid at the center frequency f_0 = 250 MHz. In our simulation and experiment results, we obtain a 25% bandwidth at -15dB return loss.

At 250 MHz, the calculation values for the inductor and capacitor using (3.2) were obtained, which were C = 9 pF and L = 45 nH, respectively. At port 1 we choose an 18 pF capacitor, and the balancing resistor is 100Ω. In Wilkinson power divider design, standard low-cost 0805 SMD components are used, featuring 5 percent tolerance. In order to realize proximity calculation values of SMD components, two parallel components were employed as shown in Table 3.1.

Table 3-1 Inductor and Capacitor values of coupler and power divider

	C1	C2	L1	L2
Coupler	27pF	2.2pF	30nH	22nH
Wilkinson Power Divider	9pF		68nH	82nH

3.3.4 The simulation and measurement of the Wilkinson power divider

The simulation schematic is shown in figure 3-19. Measurement results are presented in figures 3-20 to 3-21, which show insertion loss at the center frequency a value of about 3.3 dB, return losses result 14 dB at port 1, 16 dB at ports 2 and 3, and isolation between output ports reaches 20dB. As we can see that the proposed lumped-element power divider provides excellent performance with large bandwidth. The circuit board layout and the picture are depicted in figure 3-24. The sizes are less than two square centimeter.

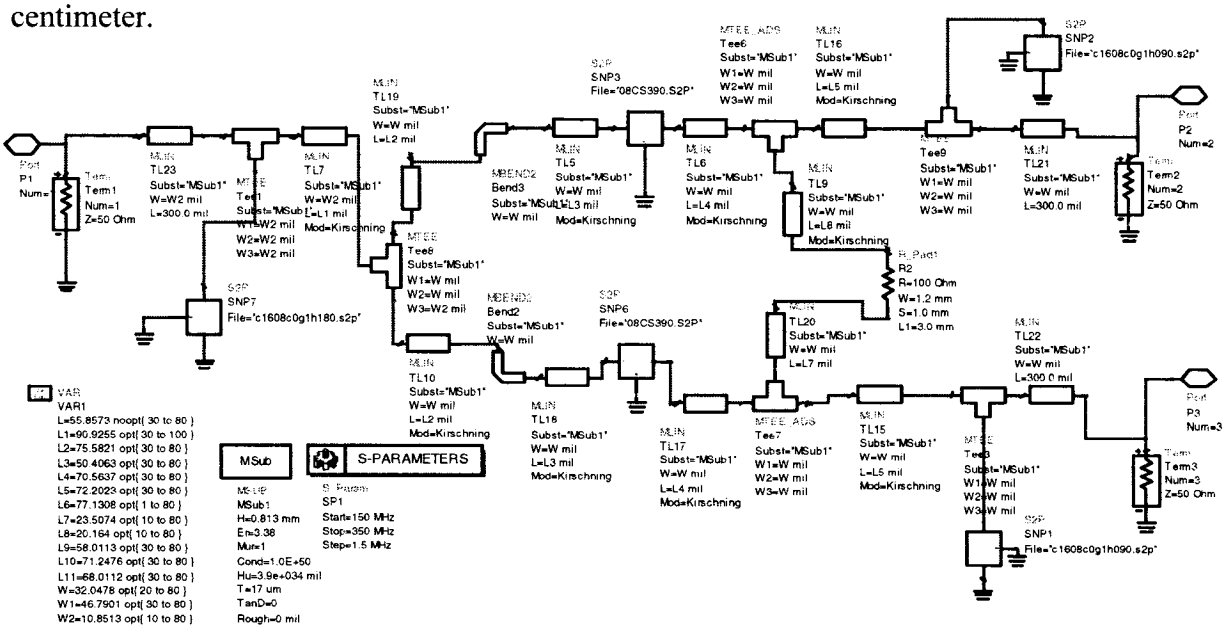

Figure 3-19 simulation schematic of the Wilkinson power divider

The actual behavior at VHF band differs from the expectations because device parasitics and other factors were neglected in the simulations. We will discuss this issue later.

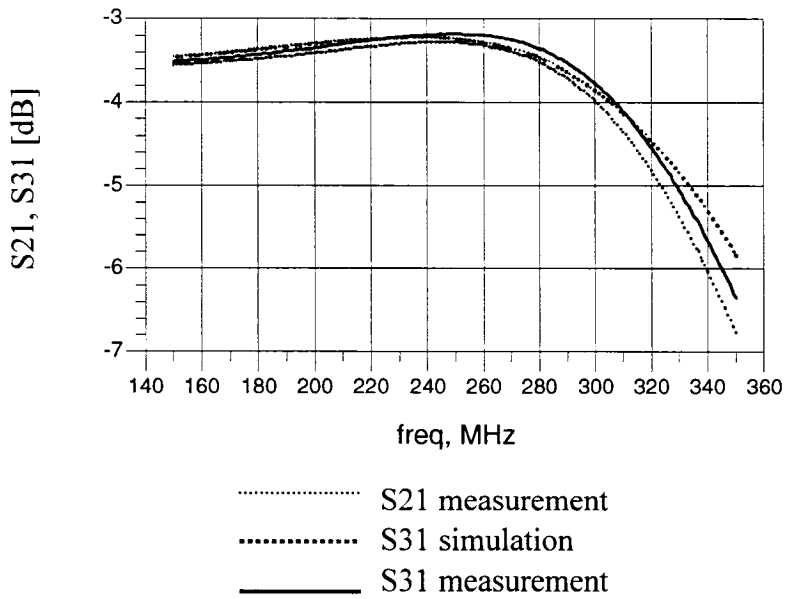

Figure 3-20 Measurements and simulation of S21 and S31 of the 250 MHz

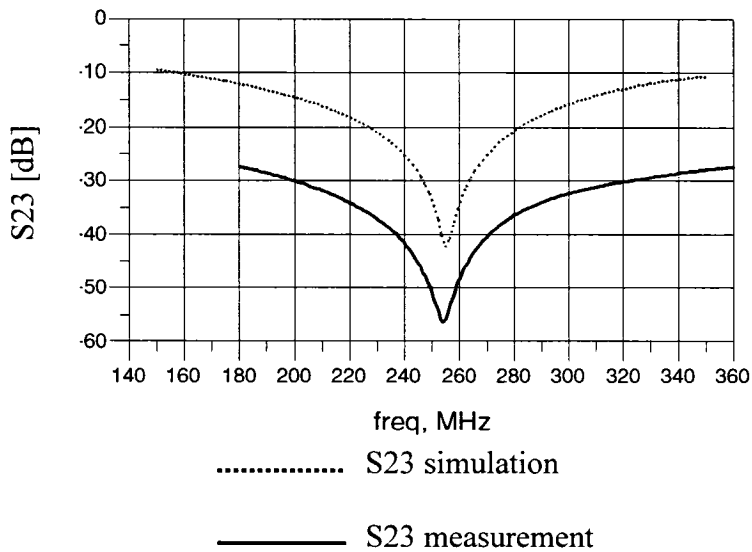

Figure 3-21 Isolation simulation of Lumped-element Wilkinson power divider

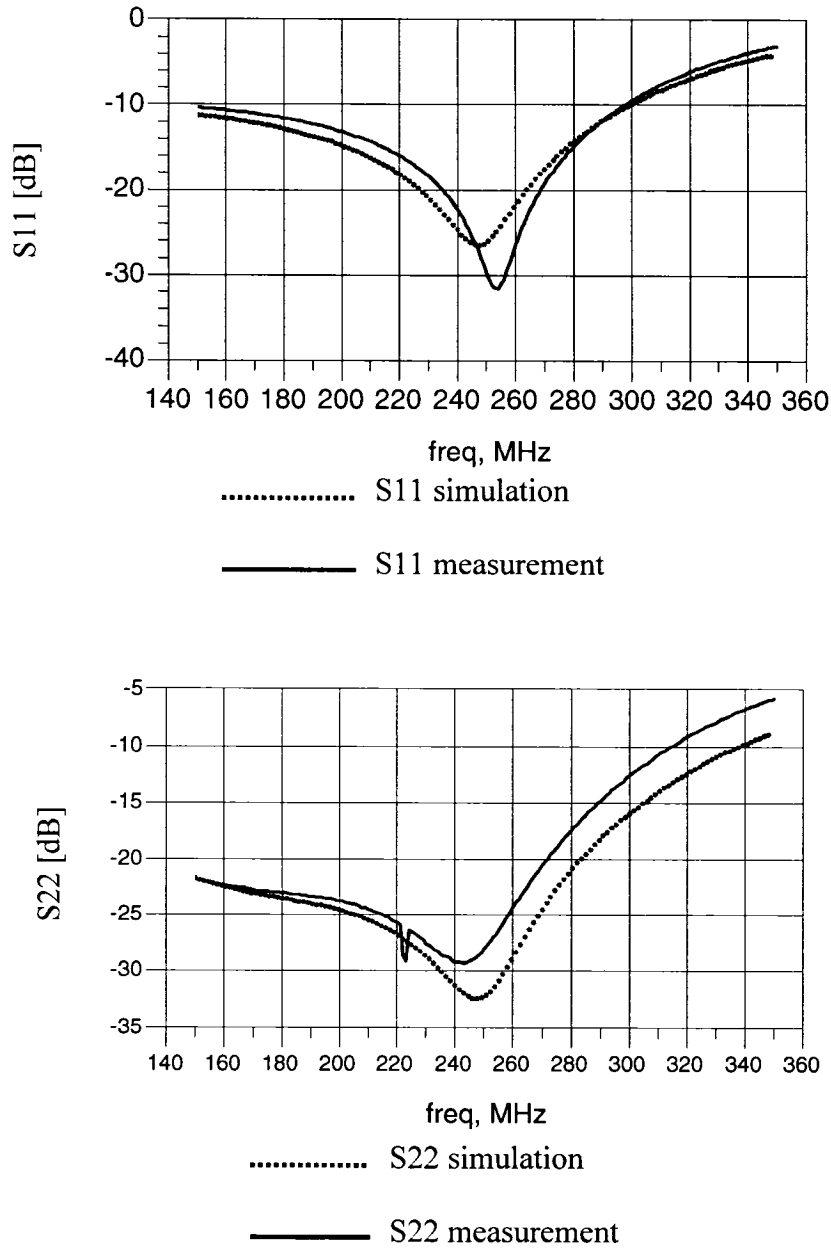

Figure 3-22 Return loss of port1 and port2 of Wilkinson power divider

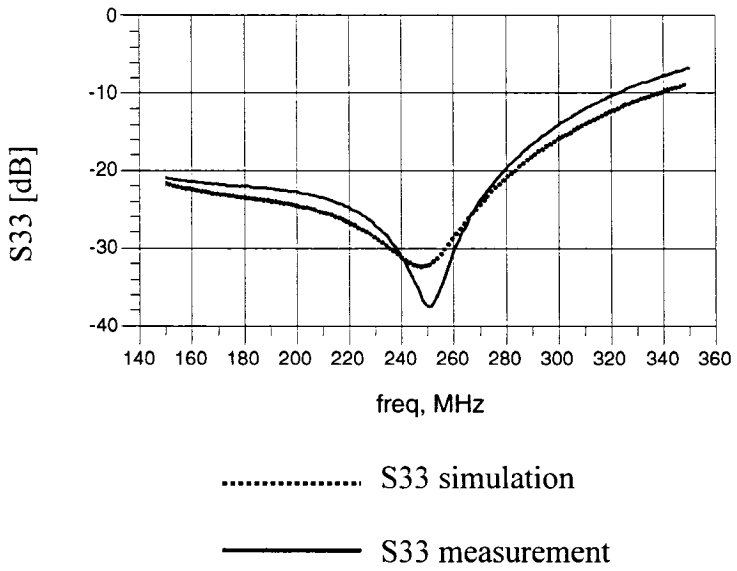

Figure 3-23 Return loss for port3 of Wilkinson power divider

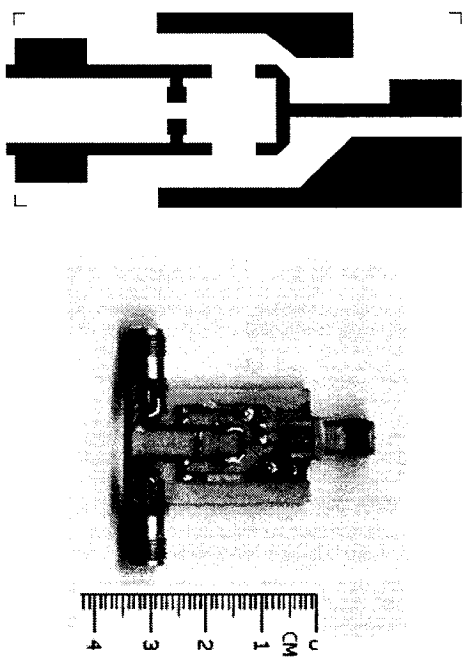

Figure 3-24 Layout (above) and photograph (bottom) of LE Wilkinson power divider

3.4 The system Implementation

Based on Agilent ADS, lumped-element Six-Port circuit board at VHF band is simulated. The schematic is shown in figures 3-25 and 3-26. The S-parameter simulation has been conducted to generate the S-parameters of the Six-Port. The simulation results are shown in figure 3-27.

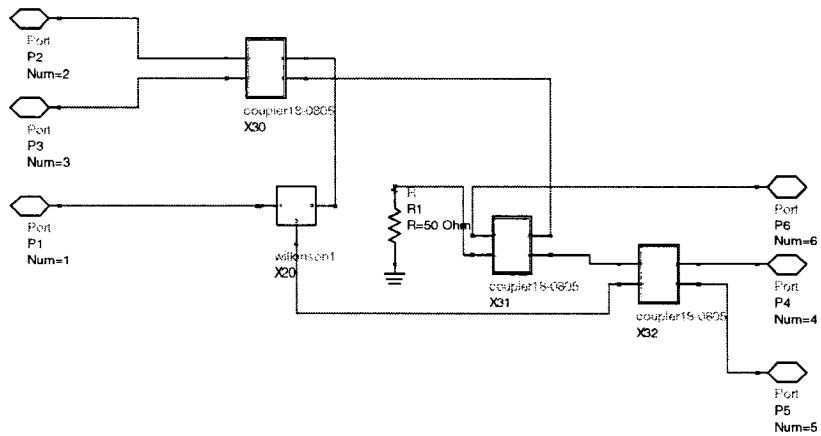

Figure 3-25 Six-Port schematic

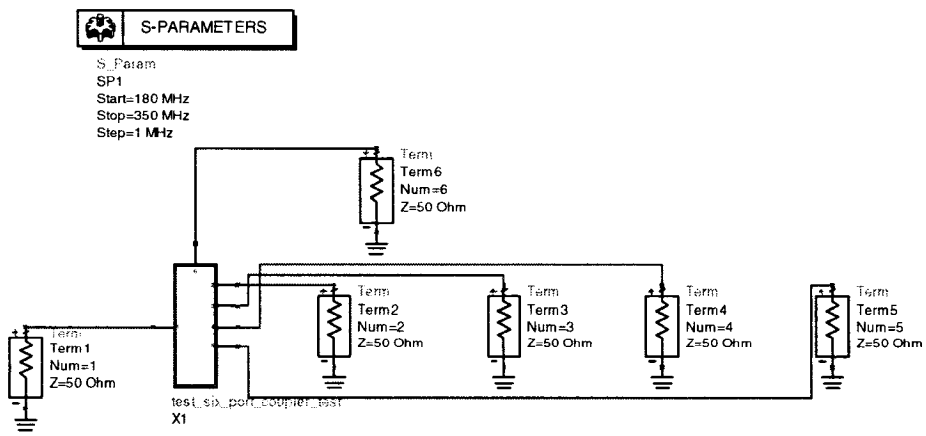

Figure 3-26 S-parameter simulation

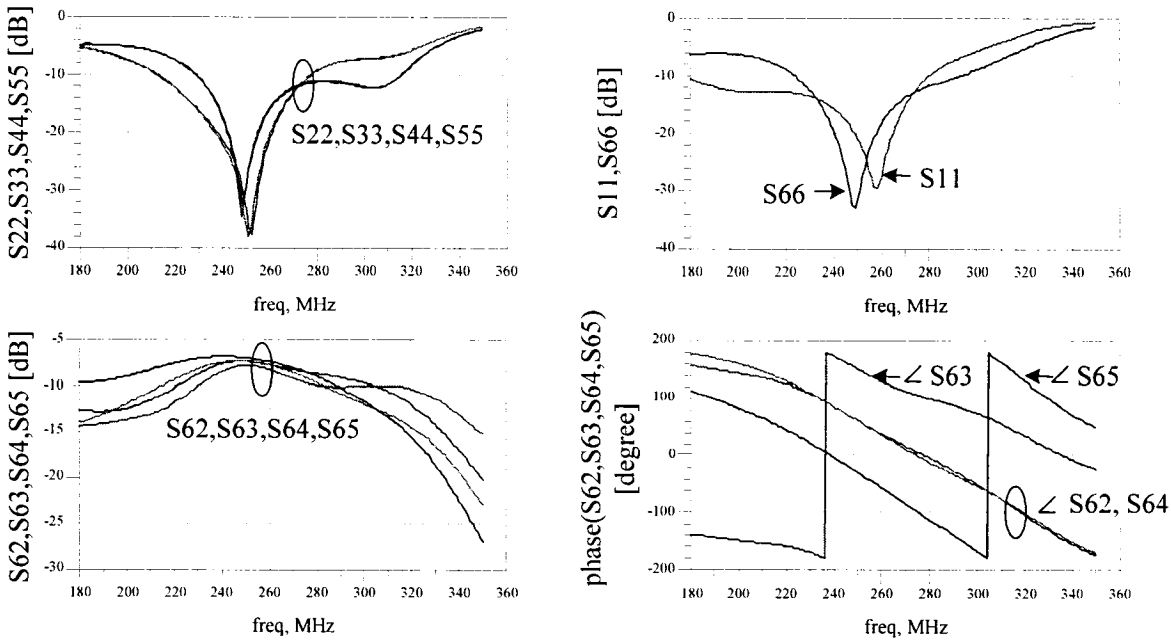

Figure 3-27 Six-Port simulation results

A harmonic balance simulation (figure 3-28) was performed using the ADS circuit model. Results are presented in figure 3-29, where the vertical is the DC voltage of the power detector diode, the horizontal is the phase difference between the RF input and the LO. We can see that at the lowest position of voltage, there is a 90 degree phase difference between the four outputs. Each position corresponds to a symbol in QPSK modulation. By measuring and comparing the four DC outputs, I and Q signals can be readily obtained.

The Six-Port PCB board was designed, fabricated in our lab using Rogers RO4003 material. The board layout and photograph are depicted in figures 3-30 and 3-31 respectively.

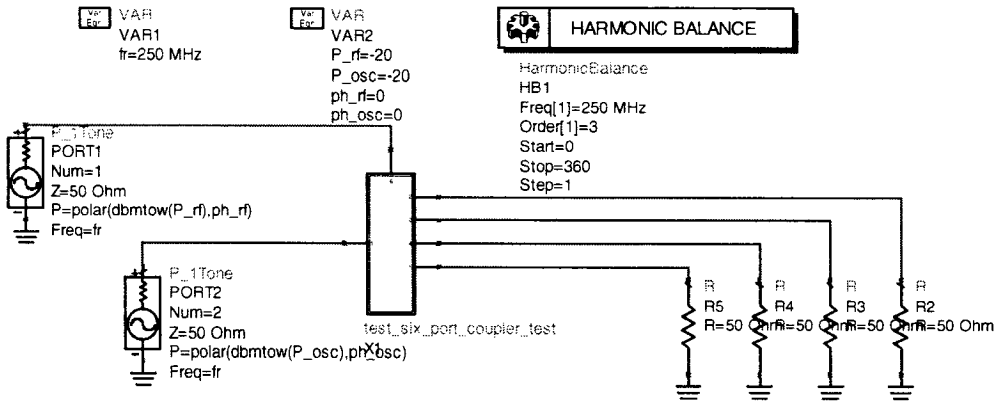

Figure 3-28 Harmonic balance simulation

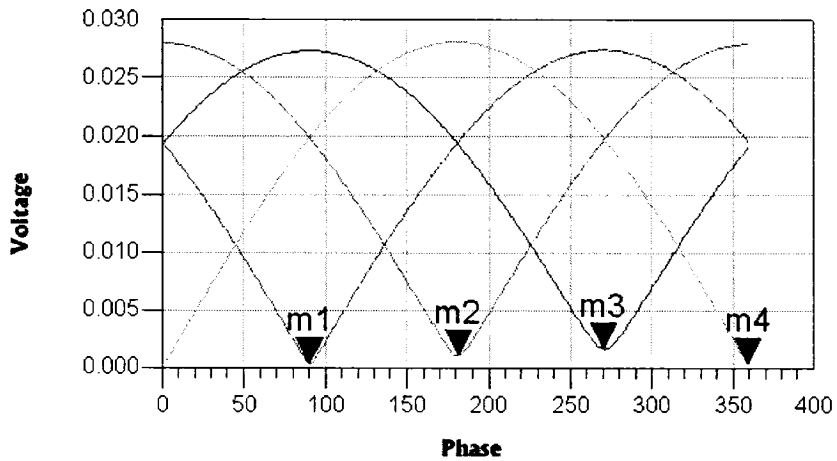

Figure 3-29 Harmonic balance Simulation of four outputs of power detectors

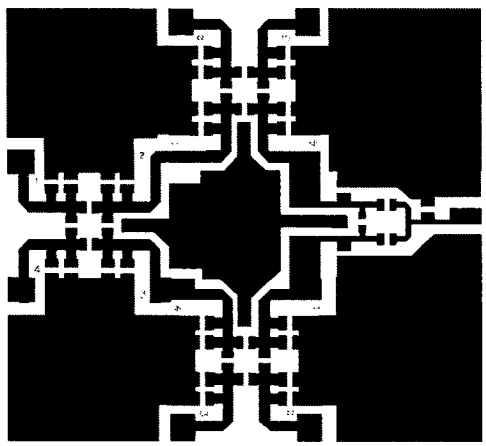

Figure 3-30 Layout of the Lumped-element Six-Port circuit

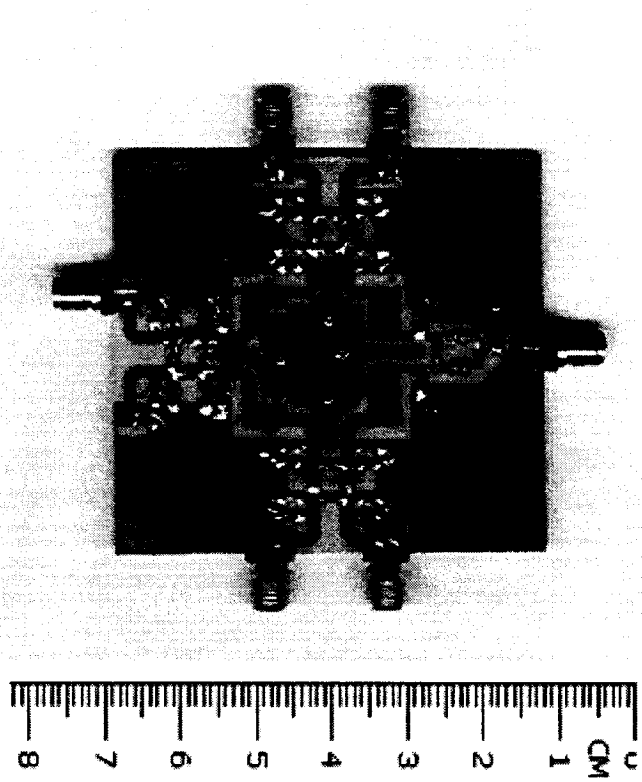

Figure 3-31 Photograph of the prototype circuit

3.5 Performance of Six-Port Hardware

Using HP8753D network analyzer, we have measured the S-parameters of the fabricated Six-Port. Measurement results are presented in figure3-32 to figure 3-34. They show that insertion loss at center frequency is about 6.8 dB, return losses result 20 dB at RF port, 30 dB at LO port, and isolation between LO and RF reaches 35 dB. The measurement results have an excellent agreement with simulation results.

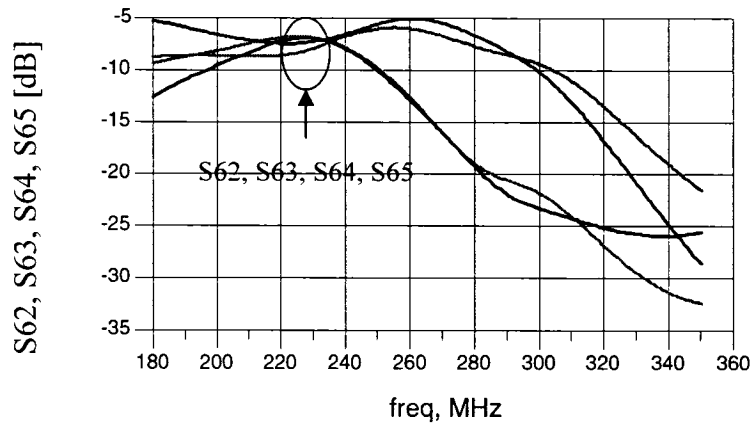

Figure 3-32 Insertion loss measurement results

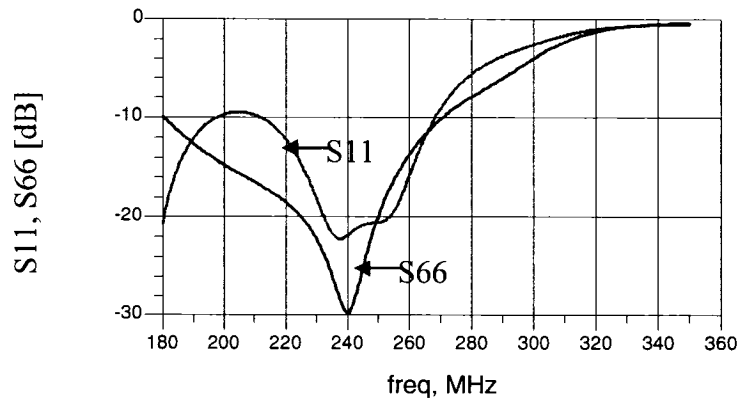

Figure 3-33 Return loss measurement results of RF Port and LO Port

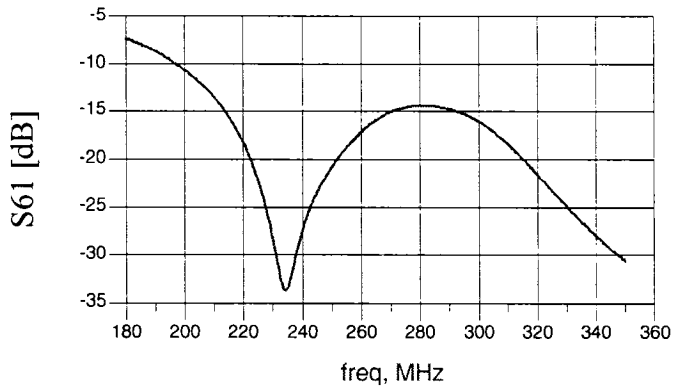

Figure 3-34 Isolation measurement results between RF and LO

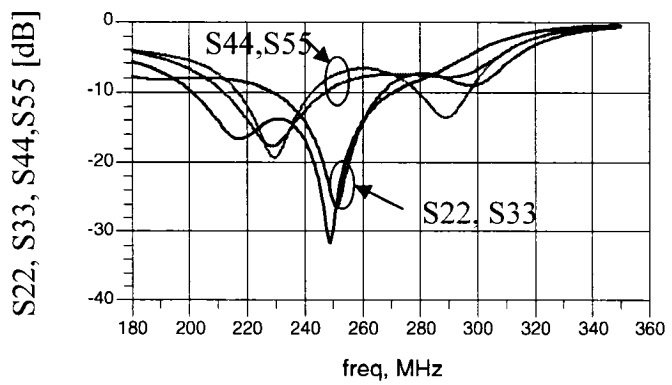

Figure 3-35 Return loss measurement results

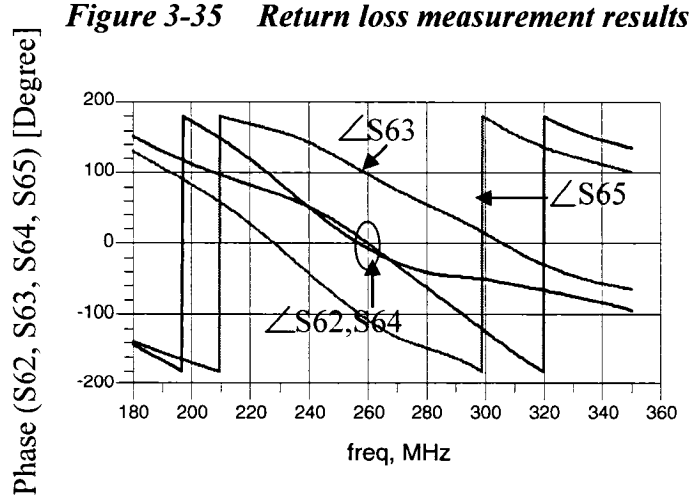

Figure 3-36 Phase measurement results

3.6 Frequency shift analysis

3.6.1 Coupler

Form the measurement results of the couplers, Wilkinson power divider and the Six-Port we can observe that there is a frequency shift phenomenon in the S-parameters results. Four major factors have impact on this phenomenon;

1. Via
2. Inductors tolerances
3. Capacitors tolerances
4. Extra transmission lines connecting the components

Inductors and capacitors manufactures measure S-parameter of these components using special fixtures which do not include via impact. Figure 3-37 demonstrate the schematic we will use to study the cause of the frequency shift. In this design, perfect components were used to generate the ideal results shown in figure 3-38.

From equation (3.1), we have frequency and inductors L value relationship as

$$f = \frac{Z_0}{2\pi Ls\sqrt{2}} \tag{3.3}$$

As L value goes high, f goes low.

Frequency and capacitor C value relationship from equation (3.1) is

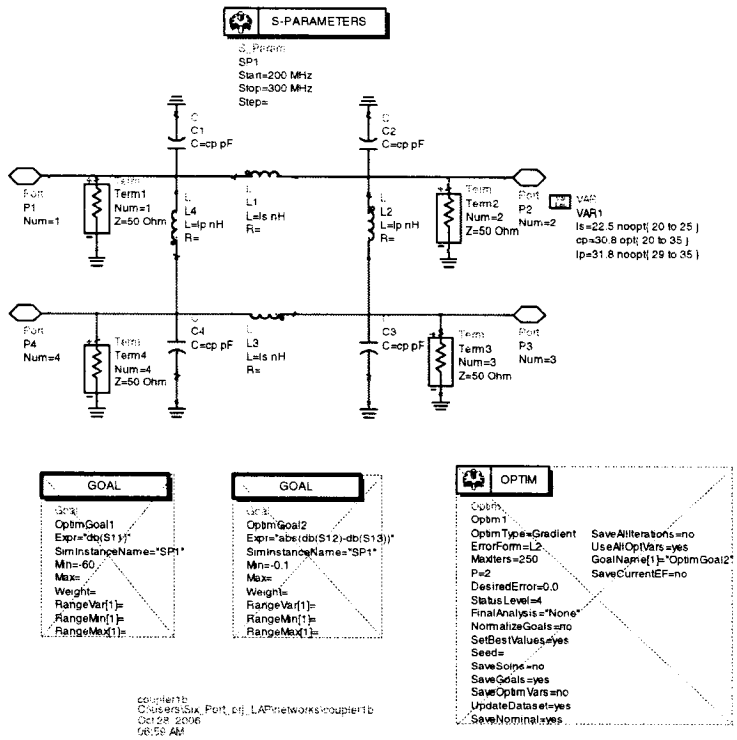

Figure 3-37 Schematic used to study the frequency shift in coupler

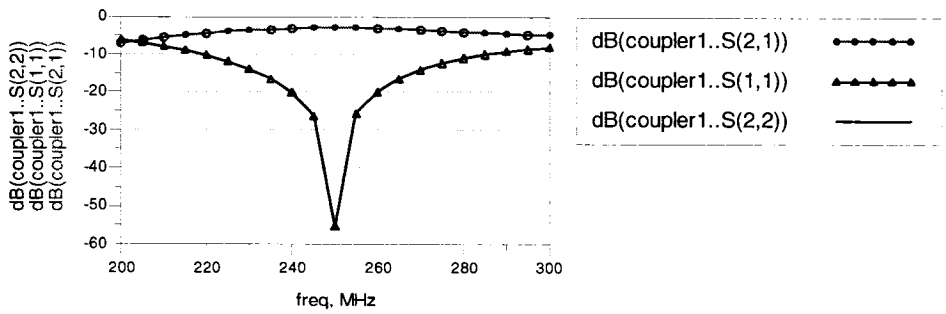

Figure 3-38 Ideal coupler components results

$$C = \frac{\sqrt{2}+1}{\sqrt{2}\omega^2 Ls} = \frac{\sqrt{2}+1}{\sqrt{2}(2\pi f)^2 Ls} = \frac{\sqrt{2}+1}{4\sqrt{2}\pi^2 f^2 Ls} \tag{3.5}$$

$$\begin{aligned} f &= \sqrt{\frac{\sqrt{2}+1}{4\sqrt{2}\pi^2 CLs}} \\ &= \frac{\sqrt{\sqrt{2}+1}}{2\pi\sqrt{\sqrt{2}CLs}} \end{aligned} \tag{3.6}$$

As square root of C goes high, the frequency goes high. Because frequency is proportional to the reciprocity of the square root of C, it has less impact to the frequency shift phenomenon. It seams that the inductor's tolerance can be a major error source of the frequency shift phenomenon.

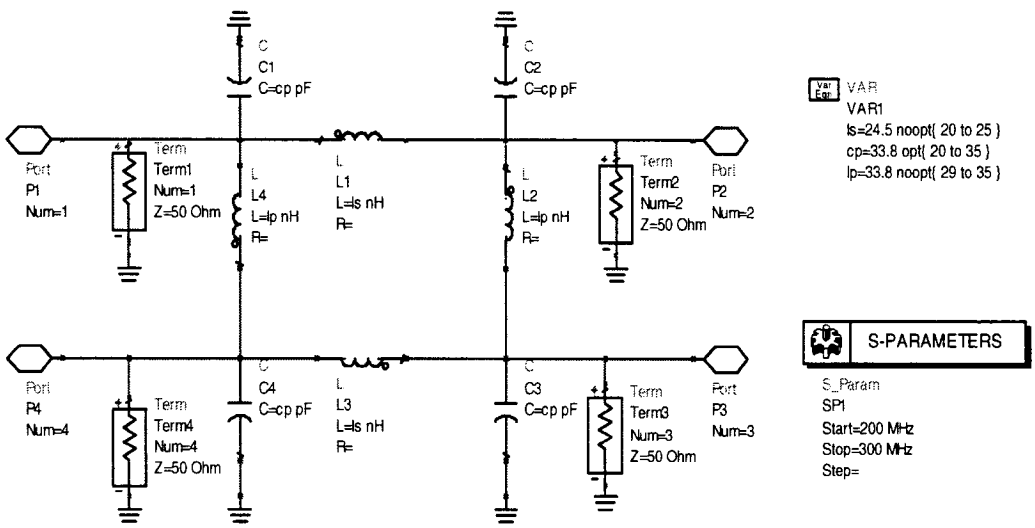

Figure 3-39 Inductor 10% higher than the reading value

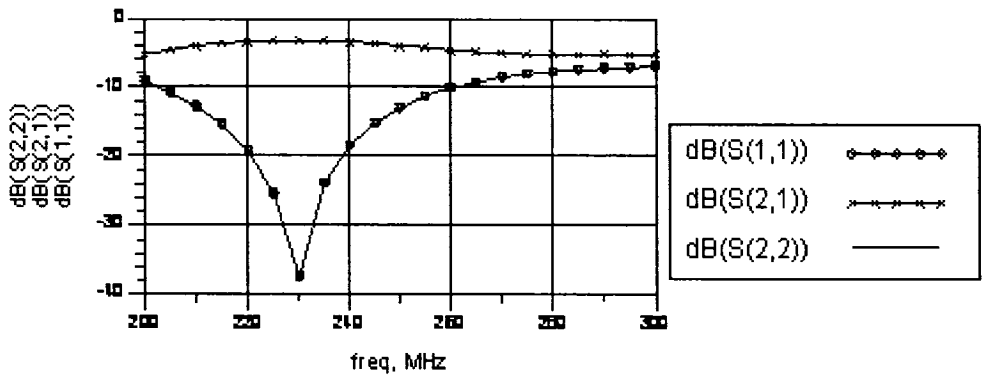

Figure 3-40 Frequency shift with inductor and capacitor value 10% higher

Assuming that the inductor has 10% tolerance, then another schematic (figure 3-39) was used to investigate the inductors impact. Figure 3-40 shows the familiar frequency shift down to 230MHz. But the inductors we used have only 5% tolerance according to the datasheets, the shift may not totally contribute to the 10% tolerance of the inductors. Thus we continue to investigate the other factor which is via. Figure 3-41 shows the schematic to investigate the via effect. Results from figure 3-42 show that via has little impact on the frequency shift.

Combining with 8% of tolerance in the inductors and capacitors and the via effect shown in the schematic in figure 3-43, we have the desired result which is shown in figure 3-44. The frequency is down shifted to 230MHz, which indicating that the biggest factor of the frequency is the tolerance in the inductors and capacitors.

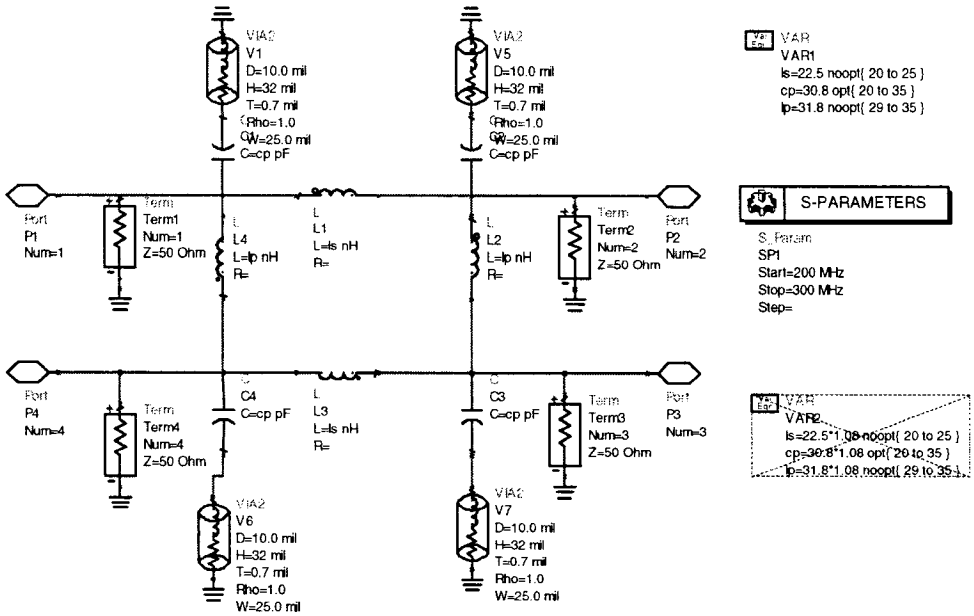

Figure 3-41 Schematic of frequency shift after Vias have been considered

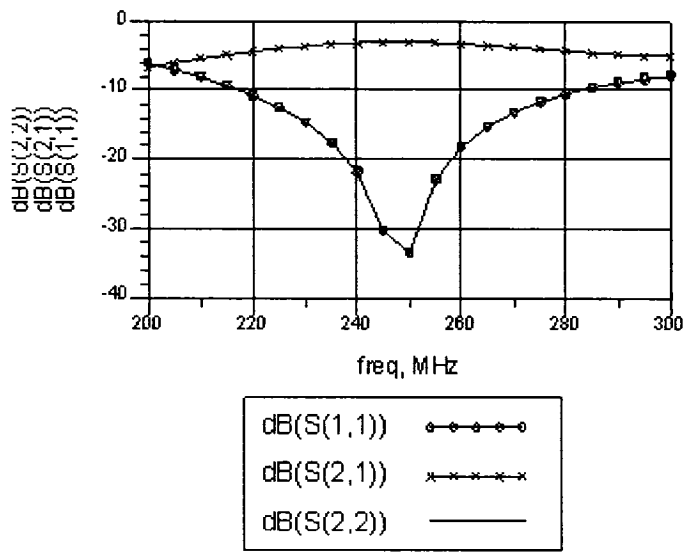

Figure 3-42 Frequency shift after Vias have been considered

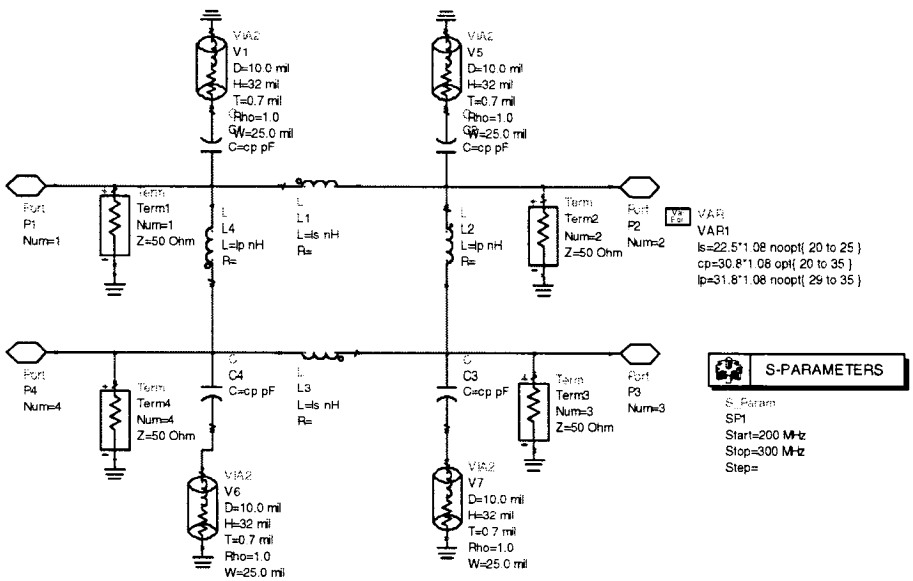

Figure 3-43 Schematic of investigating frequency shift with Vias and inductor and capacitor 8% higher than the reading value

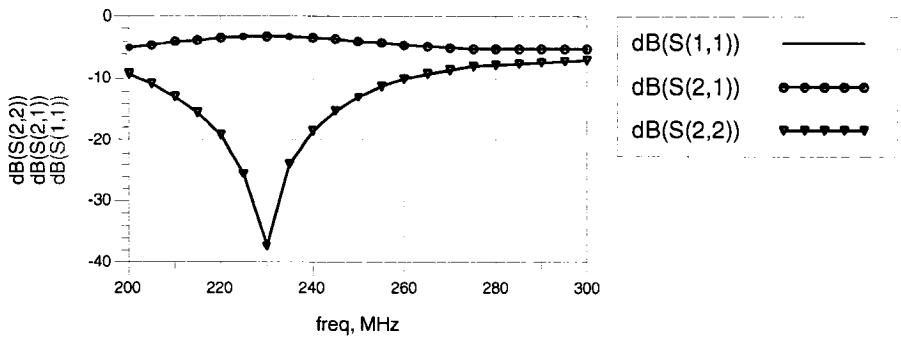

Figure 3-44 Frequency shift after inductor Vias and inductor and capacitor 8% higher than the reading value have been considered

Actually we can justify this point of view by a method called Balancing Circuit Concept [10].To know exact the value of the inductors, a circuit schematic is shown in figure 3-45. Ideally, Vout should be 0 Volt. From the optimized value of the schematic and the simulation results (figure 3-46) we can see that the actual inductance value for a reading 22 nH is 21.1995, that is 3.6% difference from the reading one, within the 5% tolerance range. We can also do the same estimate with capacitors.

A more accurate approach is using Agilent E4991A 3GHz impedance analyzer to evaluate passive component's characteristics.

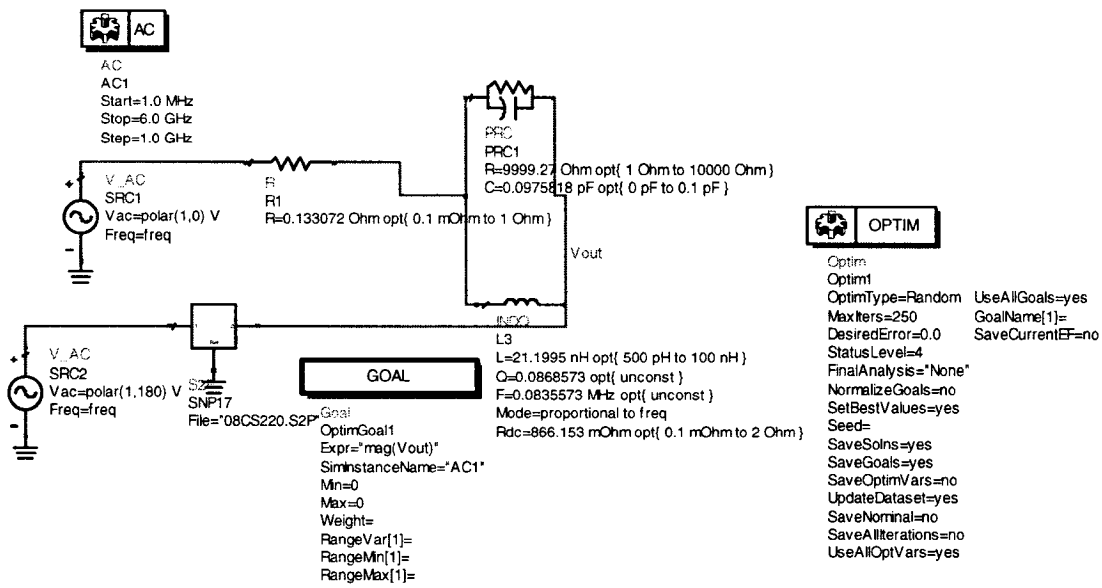

Figure 3-45 Schematic of Balancing Circuit Concept

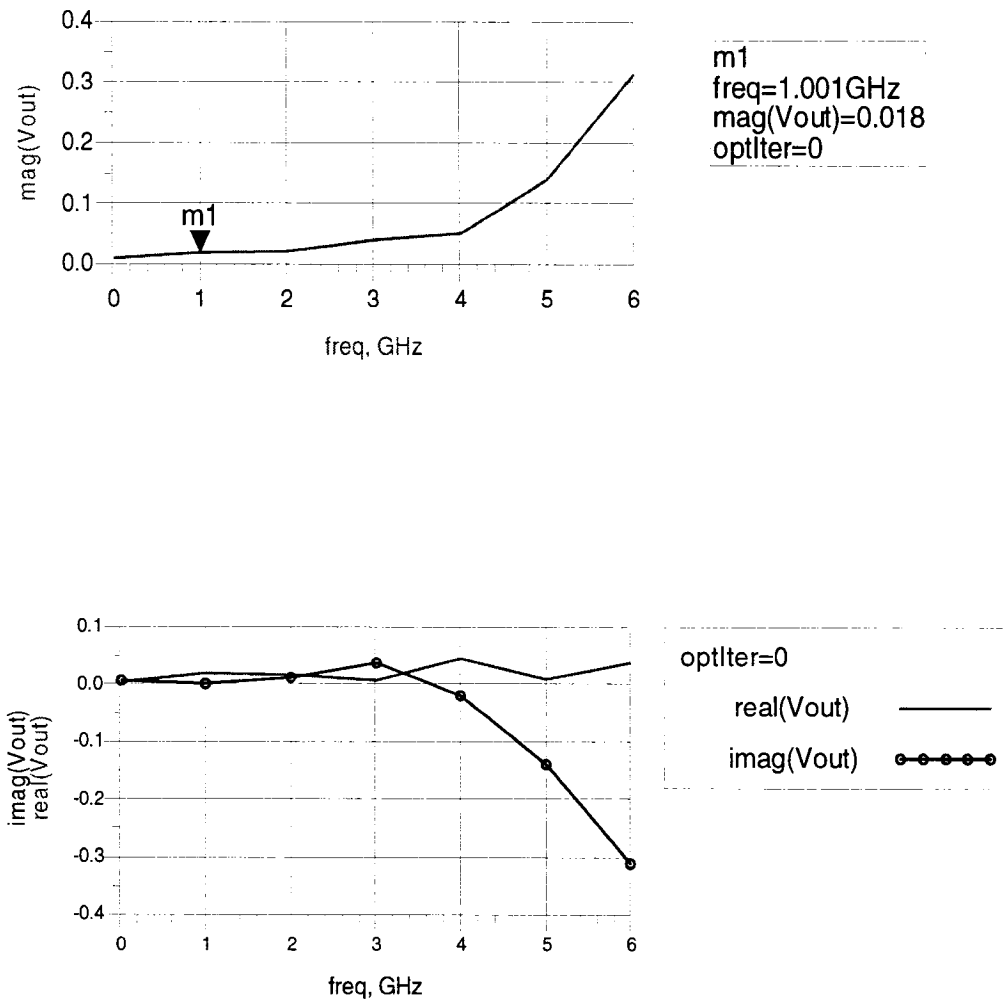

Figure 3-46 Balancing Circuit Concept results, Vout(above) and real, image value of Vout(bottom)

We did our coupler simulation without the transmission line effect. In reality, if we account for that effect, the proportion of the impact of the inductors and capacitors would be less than 8%. But we can still say that the 5% tolerance is the biggest factor to cause the frequency shift.

3.6.2 Wilkinson power divider

There is also a phase shift phenomenon associated with Wilkinson power divider. Same as in the case of the coupler, four major factors have impact on this phenomenon, Via, Inductors tolerances, Capacitors tolerances and transmission lines connecting the components. Here we evaluate the effect of the transmission lines first.

Showing in figure 3-47 are the schematics of the ideal components Wilkinson power divider without transmission lines Figure 3-47 (a) and with transmission lines Figure 3-47 (b). The simulation results are shown in figure 3-48. We can clearly see that the one with transmission lines (bottom) is shifted to the low end. Combining with the effect of components tolerance, the shift would go further down to the low end. To combat those effects, we chose to lower the value of the inductor which is about 37 nH (68nH||82nH) in order to bring the center frequency up to 250 MHz (Figure 3-49).

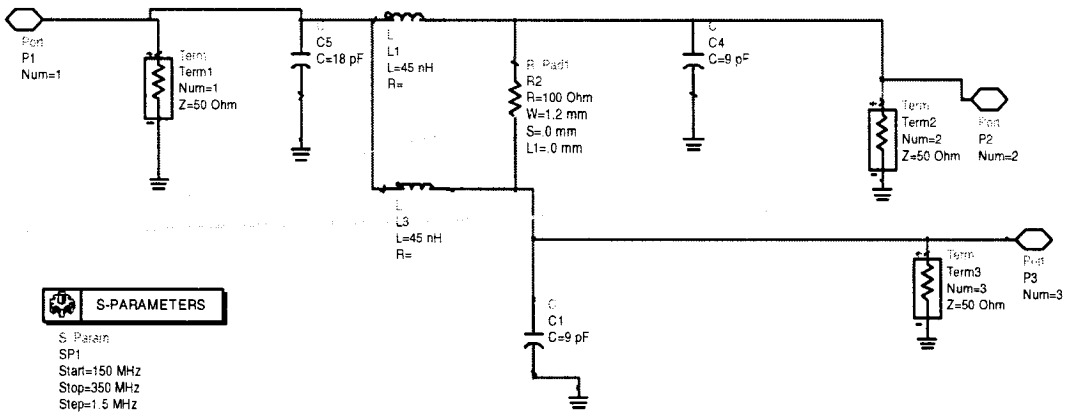

(a)

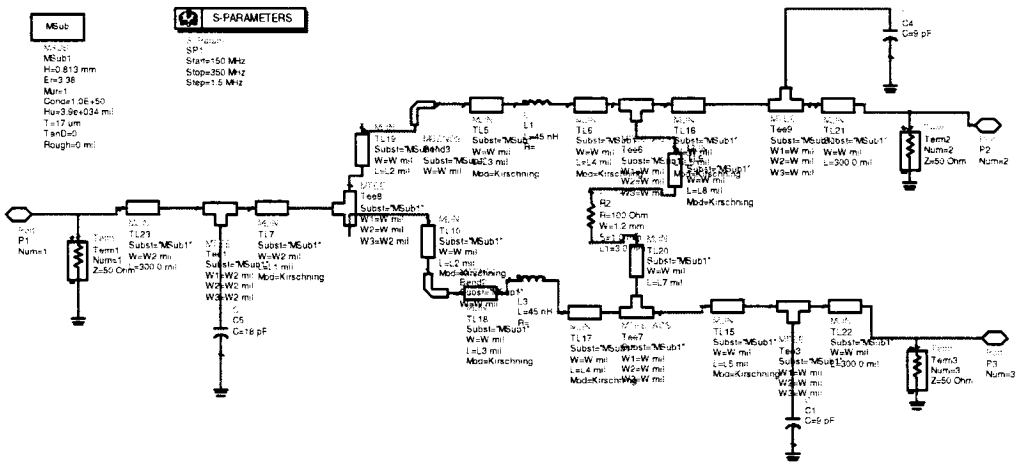

(b)

Figure 3-47 Schematics of the ideal components Wilkinson power divider without transmission lines (a) with transmission lines (b).

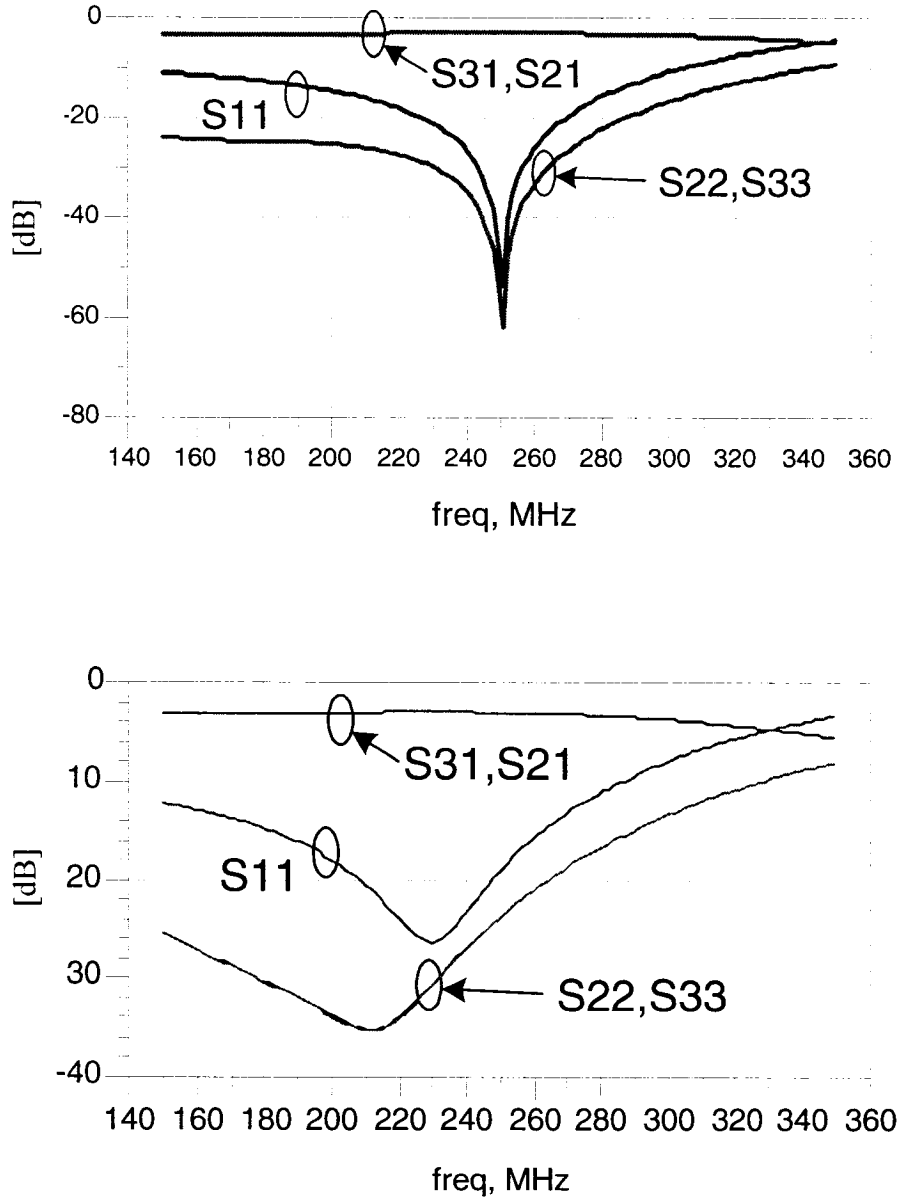

Figure 3-48 Frequency shift of Wilkinson power divider without transmission lines (above) with transmission lines (bottom)

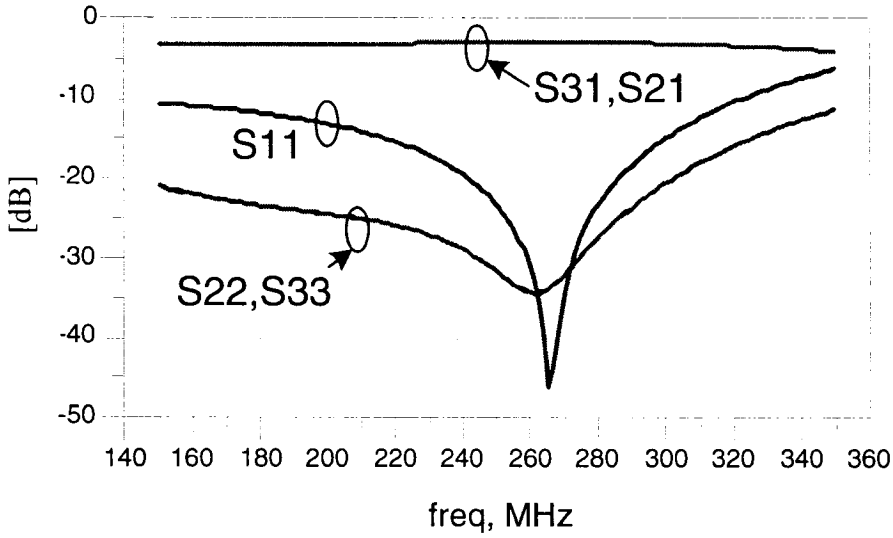

Figure 3-49 Frequency response after using 37nH inductors

Chapter 4

Lumped-element Six-Port Direct QPSK Demodulator

4.1 Introduction

Six-Port demodulation theory has been introduced in Chapter2 briefly. The principle is that, by reading the power of the four outputs of Six-Ports, the phase difference between RF and LO can be determined. Therefore in Six-Port QPSK demodulation, power detectors are the most crucial components. Theoretically, square law for the four power detectors is assumed. In this work, we use four square law power detectors from Wiltron to translate RF power to DC voltage. Hence, the design of lumped-element Six-Port direct QPSK demodulator subsystem is focused on modeling the Wiltron power detector or building power detectors from scratch. At first we review some basic knowledge of square law diode detectors, a model based on the measurement data has been derived, then simulations and measurements to validate the theory have been conducted. Finally BER measurement is done to demonstrate the demodulation system performance.

4.2 Power detector theory

The nonlinear function that represent the detector diode (Schottky diode) current I and voltage V characteristic can be expressed as [20]

$$I(V) = I_{SAT}(e^{\frac{qV}{\eta KT}} - 1) \tag{1}$$

Where q is the electron charge, K is Boltzmann's constant, 1.37 x 10^{-23} J/K, T is the absolute temperature. η is the ideality factor, a value between 1 and 1.2, which is used to account for the unavoidable imperfection in the junction. I_{sat} is the reverse saturation current. V is the voltage across the diode junction.

We can rewrite (1) in general form as

$$I = f(V) \tag{2}$$

Assuming we have a DC bias at V_0, and a small AC voltage $v(t)$ as input of detector diode, using Taylor theory to expand (2), we have

$$I(I_0 + i(t)) = f(V_0 + v(t)) \approx f(V_0) + v(t)f'(V_0) + v(t)^2 \frac{f''(V_0)}{2!} + ... + v(t)^n \frac{f^n(V_0)}{n!} \tag{3}$$

Assuming $v(t) << V_0$, then the small current $i(t)$ is

$$i(t) = f(V_0 + v(t)) - f(V_0) = v(t)f'(V_0) + v(t)^2 \frac{f''(V_0)}{2!} + ... + v(t)^n \frac{f^n(V_0)}{n!} \tag{4}$$

Let $v(t) = V\cos(\omega t)$, and ignore the terms above second order, we have

$$
\begin{aligned}
i(t) &= v(t)f'(V_0) + v(t)^2 \frac{f''(V_0)}{2!} \\
&= V\cos(\omega t)f'(V_0) + V^2\cos^2(\omega t)\frac{f''(V_0)}{2} \\
&= V\cos(\omega t)f'(V_0) + V^2(1+\cos(2\omega t))\frac{f''(V_0)}{4} \\
&= V\cos(\omega t)f'(V_0) + \frac{V^2}{4}f''(V_0) + \frac{V^2}{4}\cos(2\omega t))f''(V_0)
\end{aligned} \tag{5}
$$

The second term of (5) represents the DC component of the current, it comes from the second order and other even order terms, and has the relationship with the square of the magnitude of the input AC voltage $v(t)$ as

$$i(DC) \quad \propto \quad V^2 \tag{6}$$

Please note at zero bias point which is the case of Wiltron power detector, formula (5) is still valid for small current input $i(t)$ of RF signal, because our concern is the AC input, not the DC bias point.

4.3 Square law diode detectors

From (6) we have the definition of the square law detection. Square law detection simply means that the DC component of diode output is proportional to the square of the RF input voltage.

$$V_{out}(DC) \quad \propto \quad V^2{}_{in} \tag{7}$$

In other words, it means that output DC voltage is proportional to RF power delivered to the 50 ohm input terminating resistor. For example, if you apply ten times as much RF

input, you get 100 times as much DC output, if input power is increased from -30dbm to -20dbm, V_{out} will be increased from 10 mV to 100 mV. A 3dB increase of input results in twice as much output voltage.

The advantage for using Schottky diodes as detectors is its excellent sensitivity and noise characteristics with a modest, but sufficient square law range to make a fairly accurate power detector. The drawback is its temperature dependence. If you want to measure absolute RF input power, you'd have to know the diode's temperature, and do some non-linear corrections of the DC output[22].

4.4 Wiltron power detector

Wiltron power detectors are square law zero bias Schottky diode detectors. Zero bias means that the nonlinear function curve of the detector crosses or is very close to the zero point at I/V diagram. Zero bias detectors usually have lower sensitivity at lower input level because the junction resistance across the diode is much higher than the load resistance, hence, very little detected voltage appears across the load resistance. At higher input levels, the junction resistance is reduced by rectified current. Thus for a good detection using zero bias detector, an adequate power and a large load resistance are needed.

A model is needed to do the simulation of the power detectors and the Six-Port demodulation. Before doing the modeling of the power detector, a measurement is required to characterize the power detectors.

.

4.4.1 Measurement results and analysis of the Wiltron power detector

The encapsulated microwave diode detectors (former Wilitron now Anritsu 75KC50) with frequency range from 0Hz to 40GHz have been used as the power detectors for the Six-Port QPSK demodulator. The output impedance of the encapsulated microwave diode detectors usually is 1.5K Ohm; the input impedance of OPA (OPA2850) is 550K Ohm. To measure the sensitivity of the Wilitron power detector in order to make sure it works in the VHF frequency, we use the 330K Ohm as the load of the detector to do the measurement. A digital multimeter was used to measure the DC output of the Wiltron power detector.

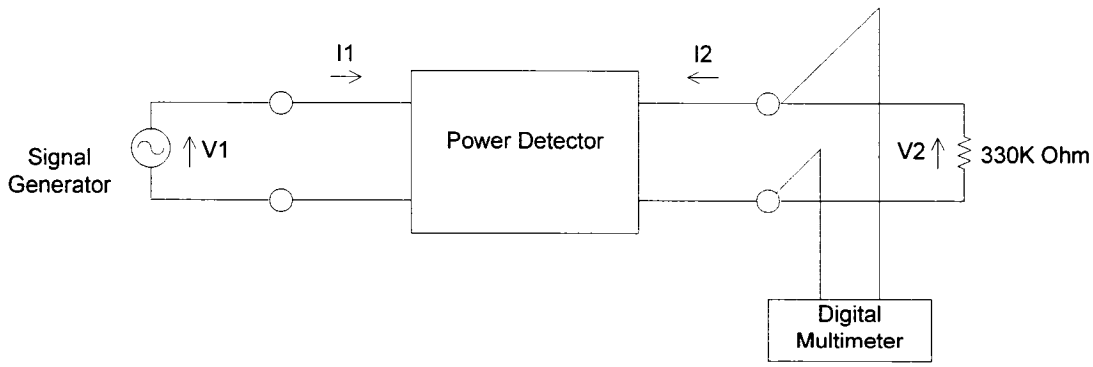

Figure 4-1 Test setup for Power Detector measurement

Figure 4-1 shows experimental setup for the response of Wiltron 75KC50 power detector. Three different loads, OPEN, 11K ohm load, and 330k ohm load, were used to evaluate the effect of the load to the power detector's sensitivity.

The results are shown in Figure 4-2. We can see that in region between -30 dBm to -10 dBm, the response varies from a higher law to square law. It also can be seen from the diagram that the best fit is the 330K load, which the square law range is from -10 dBm to - 25 dBm. The 11Kohm load has better fit below -15 dBm range. For the open load, the performance begins to deteriorate below -25 dBm.

4.4.2 Modeling the Wiltron power detector

In order to generate the model to simulate Wiltron 75KC50 power detector circuits in ADS, data from above measurement and Matlab from Mathwork as curve fitting tool were used, and we have the following fitted equation

$$y = 880x^5 - 2400x^4 + 2500x^3 - 1300x^2 + 550x + 1.1 \tag{8}$$

After lowpass filter, we only concern the fundamental item, which is

$$V_2 = 550P + 1.1 \tag{9}$$

Then we have

$$P = V_1 I_1 / 2 = V_1^2 / 100 \tag{10}$$

$$I_2 = -V_2 / 330000 \tag{11}$$

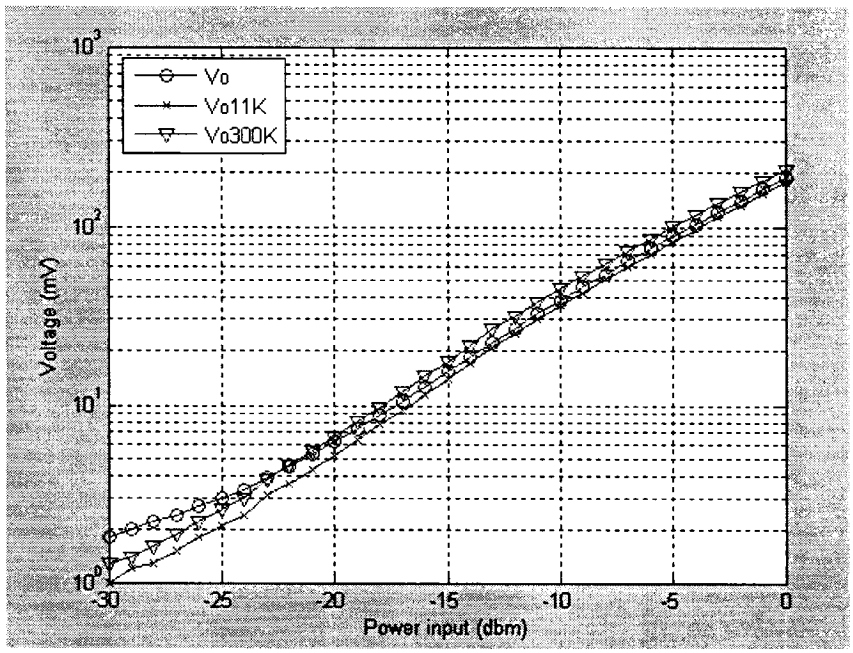

Figure 4-2 Wiltron 75KC50 power detector load sensitivity test

The simulation schematic is as Figure 4-3.

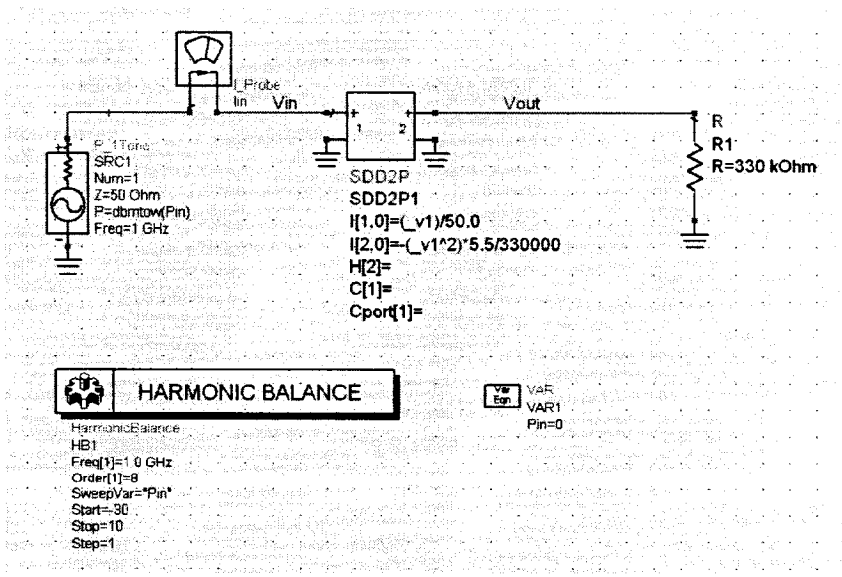

Figure 4-3 Simulation schematic of power detector

4.5 Discrete power detector simulation and measurements

A measurement has been conducted to measure the DC outputs of the four power detectors as the RF input phase changes according to LO phase. The result is shown in figure 4-4. We recall the simulation of the four power detectors from Chapter 3 which is shown in figure 4-5. As we see at each 90 degree phase difference between RF an LO, one of the four detector has the maximum DC voltage output. Thus we can use this feature to compare four different phase states using the following comparison stage of circuits.

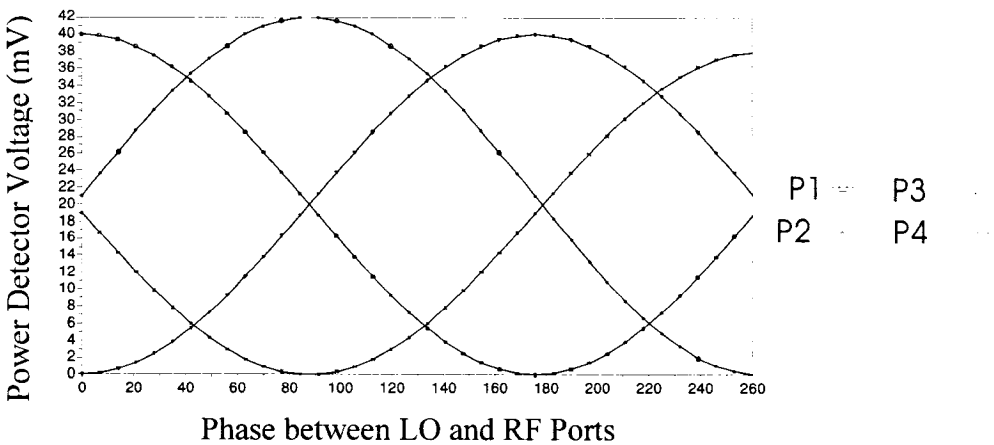

Figure 4-4 Measurement four outputs of the power detectors

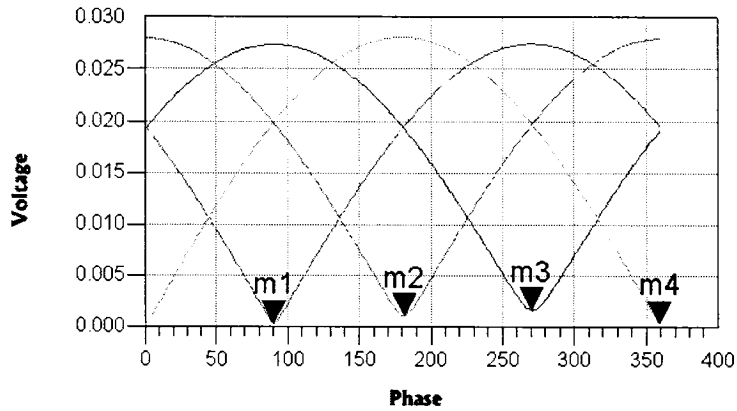

Figure 4-5 Simulated four outputs of the power detectors

4.6 DC offset in Six-Port QPSK demodulator

As we mentioned before that the I/V characteristic of square law Schottky diode detectors are temperature dependent, because its performance is heavily dependent upon its saturation current, which is a strong function of temperature. Every time the ambient temperature changed, the characteristic of the diode also changed, consequently the DC output level changed. Therefore a constant DC level adjustment is needed in order to make following stages in the circuit working, if we do not keep a constant ambient temperature.

4.7 Four Channels amplifier design

The output voltages of four power detectors are very low, usually of the order of 30 mV. Thus four channels amplifier was used to amplify the DC outputs of the power

detectors in order to make a good BER measurement. Two stages of operational amplifier OPA2658 from TI is cascaded to get 20dB gain. The OPA2658 is a dual, ultra-wideband (800 MHz), low power current feedback video operational amplifier featuring high slew rate and low differential gain/phase error.

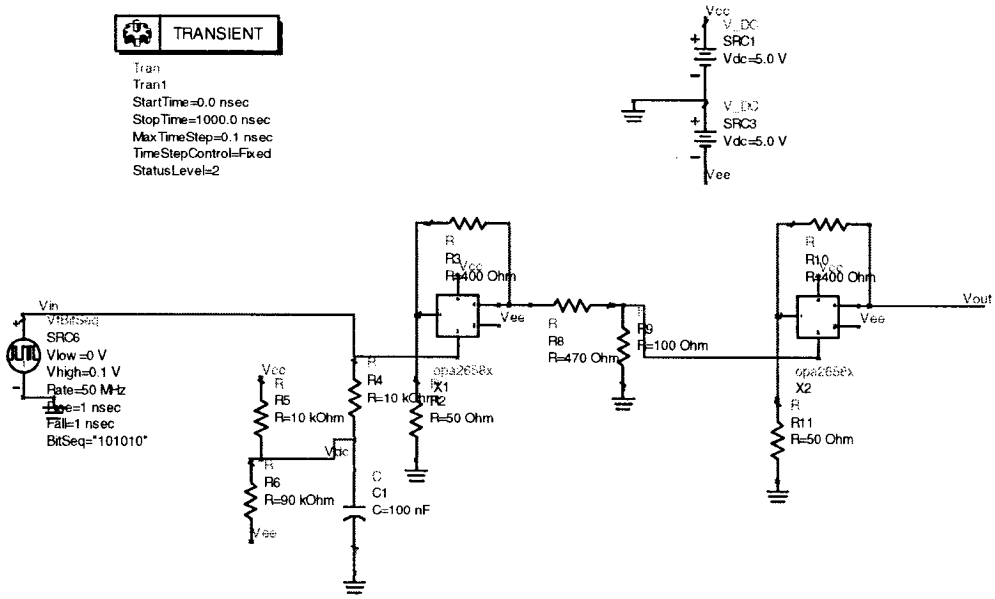

Figure 4-6 Two stages of operational amplifier OPA2658

TI provide the Spice model for this device which is used to model the OPA2658 in the ADS simulation. The schematic of two stages of operational amplifier is shown in figure 4-6. A transient simulation was conducted and the input and output waveforms are shown in figure 4-7. We can see that the gain is about 20dB (100 times amplifying).

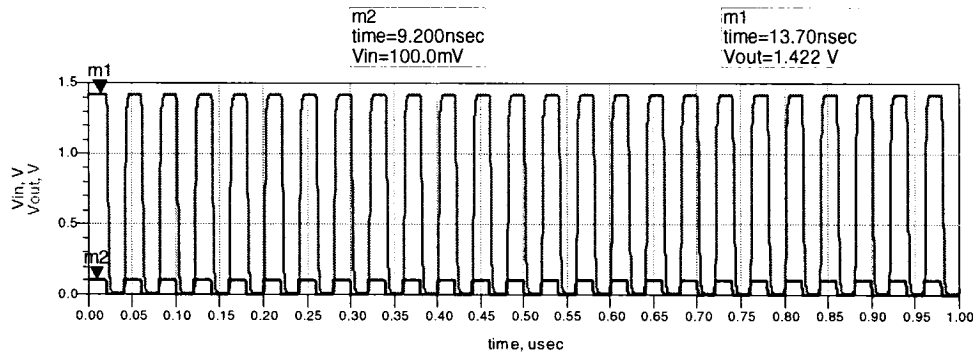

Figure 4-7 Input and output waveform of two stages OPA2658

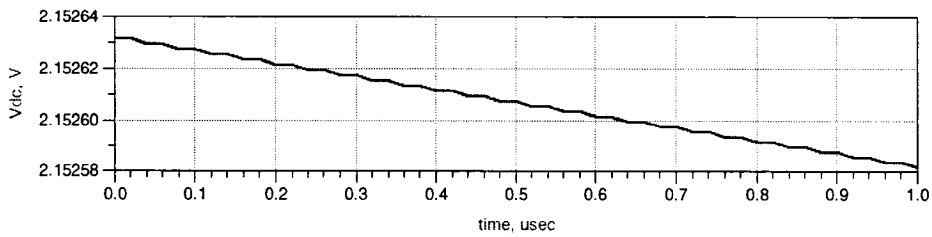

Figure 4-8 Tuning voltage to combat DC offset of Six-Port

4.8 Decoder design

We borrow the work of decoder design from another master project [13], fabricated by Dr. Serioja [21] which is a perfect decoder for our project.

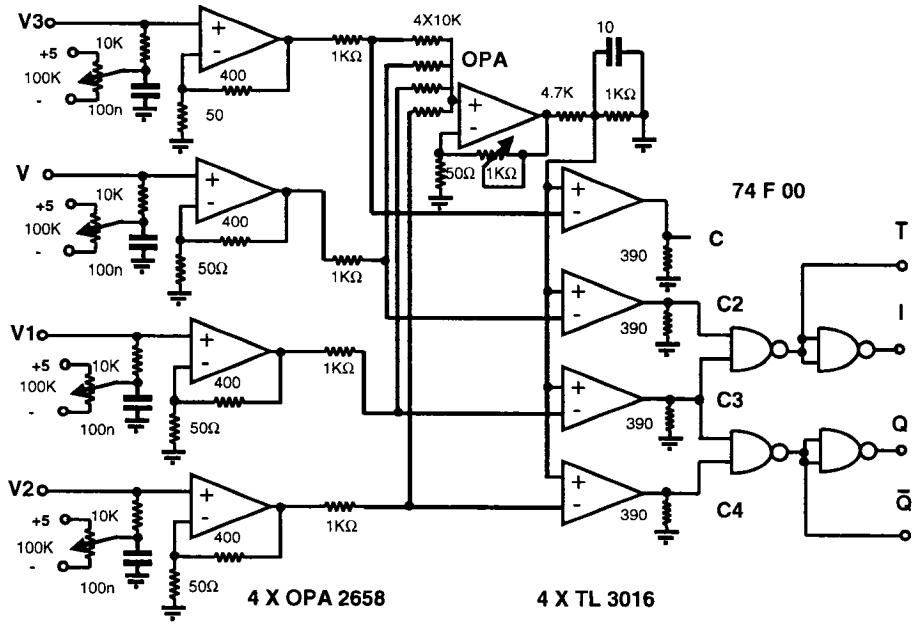

Figure 4-9 Decoder from *[19] [13]*

The TL3016 is used for the comparators. It is an ultrafast comparator designed to interface directly to TTL logic.

4.9 Design and the implementation of the QPSK demodulator

Figure 4-10 shows the diagram of the Six-Port as a QPSK demodulator. Figure 4-11 shows the actual connection of the Six-Port. Following the four outputs of the Six-Port are four Wiltron power detectors which have DC outputs. Four variable resistors were used to adjust the DC offset in the power detector's DC outputs. Following the four channels amplifiers and low pass filters, the decoder generates I and Q outputs, one of

which is used to make the BER test.

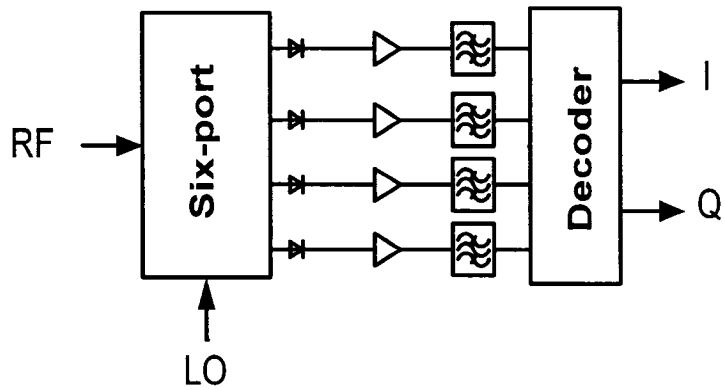

Figure 4-10 Six-Port QPSK demodulator

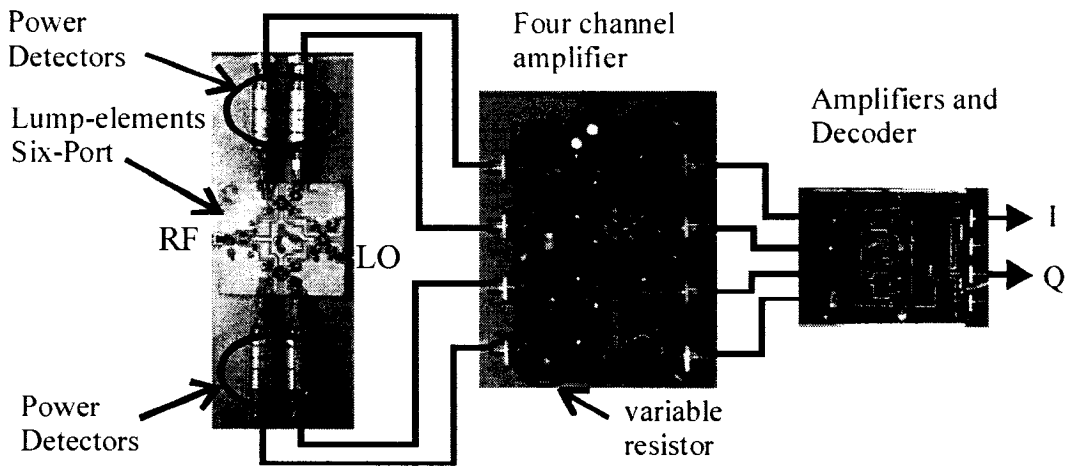

Figure 4-11 Six-Port QPSK demodulator assembly

4.10 Measurement results and analysis of the QPSK demodulator

After we have the test bench setup and have perfect output waveforms of I and Q data, the next step is to do the BER test. But first, let us review the relationship between S/N and Eb/N_0.

4.10.1 Eb/N0 to S/N relationship

S/N refers to signal to noise ratio, Eb/N_0 stands for bit energy to noise power spectrum density (noise power per Hz bandwidth) ratio.

The relationship between Eb/N_0 and S/N [12]

$$S/N = E_b/N_0 * R_b/W \tag{13}$$

Where

S= signal power

N=white noise power

R_b=bit rate of bit stream.

W= receiver noise bandwidth

For QPSK with Nyquist channel [12],

$$E_b/N_0(dB) = S/N(dB) - 3dB \tag{14}$$

The bandwidth may require some further analysis based on the modulation scheme and data rate being used. We use a bandwidth W equal to the symbol rate, and R_b=2*W in

QPSK modulation. One way to determine the W is to observe the spectrum of the modulator on a spectrum analyzer [15]. The measurement results show that Rs=1 M Symbol /s, the 3db W=0.5 MHz.

In our measurement, the data output from Anritsu ME522A BER measuring system actually is the symbol input of the Six-Port. Therefore, the BER measurement is actually SER(symbol error rate) measurement. We have this relationship

$$\frac{S}{N} = \frac{Es}{N_0} * \frac{R_b}{W} = \frac{Es/T_b}{N_0} * \frac{1}{W} = \frac{E_b \log_2(M)}{N_0} * \frac{R_b}{W}$$

Here Es is the symbol energy, $T_b=1/R_b$, $M=2^k$ is the size of the symbol set, for QPSK modulation, k=2. For convenience, we still call our symbol error rate as bit error rate.

4.10.2 The test bench setup for BER measurement

The setup for the BER measurement is shown in figure 4-12. For the test of BER, first an oscilloscope was used to check the waveform of the four outputs of the power detectors by putting the data pattern of ME522A with 10101010 patterns. In this way, the waveform of the power detectors becomes a square wave which is easy to be identified using oscilloscope. Then, the amplifier was connected to further check the function of the decoder. Care must been taken with the DC offset. We can change the

DC level of the power detectors outputs by adjusting the variable resistors, in order to make them be compared to the reference level. The reference leave can also be adjusted to accommodate the DC level change. Finally pseudo-random binary sequence (PRBS) data of PBRS=2^{23}-1 was setup to make the BER test.

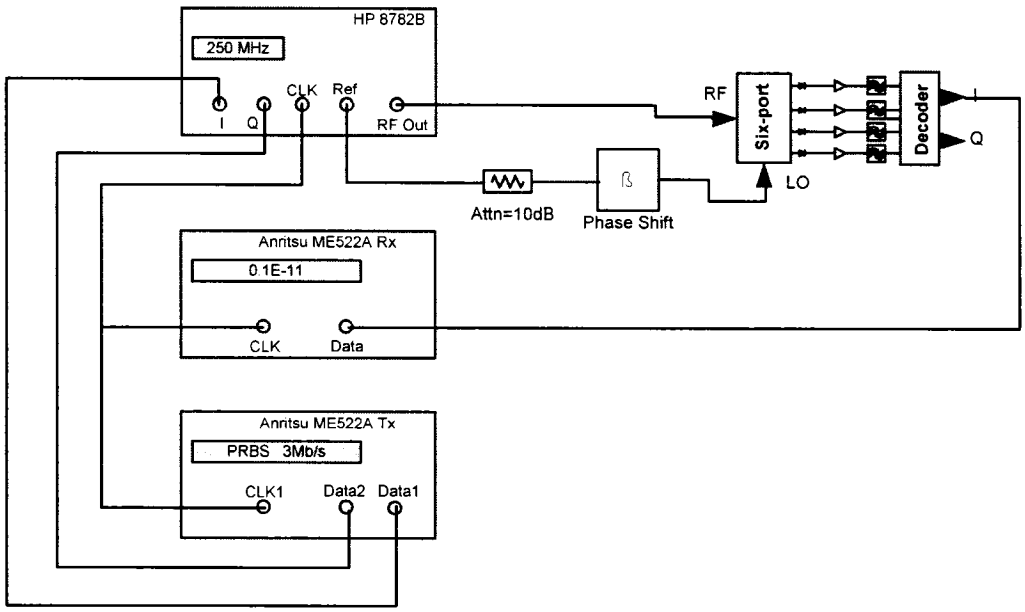

Figure 4-12 Test bench setup for BER measurement

4.10.3 BER measurement

Two methods have been proposed to measure the BER. Method one is to utilize a noise source which combine with input RF signal to provide needed SNR (signal to noise ratio). Method two is to utilize the system noise itself and by adjusting the level of output RF signal to achieve desired SNR.

Method one has been tried but failed. Because the noise level from noise source is so low (about -144 dBm/Hz), a few of amplifiers which provide huge gain (about 120 dB) are needed. It is impractical in our situation. Method two was used and another issue has arisen. The dynamic range of the detector did not meet our requirement.

In BER measurement, the dynamic range of the Six-Port is a major issue. To generate the required Eb/N_0 ranging from 7 dB to 20 dB, the RF power needed from HP8782B vector signal generator for QPSK modulation is measured through Agilent VSA 89600 main frame and software, and presented in Table 4-1

Table 4-1 *RF power from HP8782B needed to get desired* E_b/N_0

RF power (dBm)	SNR measured from VSA89600 (dB)	E_b/N_0 (dB)
-5	23.5	20.5
-10	22	19
-15	19	16
-18	16.5	13.5
-20	14.5	11.5
-21	13.6	10.6
-22	13	10
-23	12	9
-25	10	7

Note: PBRS=2^{23}-1, Rs=1M/s, f=230 MHz

The Six-Port QPSK demodulator dynamic range problem stems from the power detector square law range. When the RF signal goes below -15 dBm, the Six-Port can not demodulate the QPSK signal correctly, since it falls out of the power detector square law range. It can be seen from Figure 4-2 that the square law ranges from 0.2 mW (-25 dBm) to 1 mW(-10 dBm). Since the 6 dB loss of the couplers, in order to drive power detectors, the input RF power has to be 6 dB more than the dynamic range of the power detectors. However, the actual dynamic range is lower than that value because the parallel variable resistor has decreased the load resistor of the power detectors. Therefore through measurement, the real dynamic range is from 0.2 mW (-7 dBm) to 1 mW(0 dBm), hence the previous 10 dB amplifier obtained with the analogue decoder is insufficient.

Measurements have also shown that at -10 dBm level of input power, the detected voltage is only 5mv, too low to make it detectable, causing the BER measurement setup synchronization problem.

The solution of the aforementioned the problem is either to put additional amplifier stage after the power detector in order to increase the DC level or to make a better power detector by linearizing the diodes in order to extend the dynamic range beyond -15 dBm. The goal is to detect -40 dBm signal and to calculate the power of the signal at

comparator as -40 -6(Six-Port insertion loss) +30 =-16 dBm (36mV), enough power to drive the comparator.

The BER simulation has been conducted using ADS with schematic shown in figure 4-13. The measurement was performed using Anritsu ME522A bit error test instruments. The measurement result is shown in figure 4-14 with the following parameters: RF frequency = 230 MHz, LO frequency = 230 MHz, RF power= -10 dBm, LO power = -10 dBm, R_S=2MHz. Simulation result has a very little difference of 2.5 dB with measurement one at 10^{-3} BER. It should be note that our BER measurement is actually symbol error rate measurement, which is 3 dB higher than the BER result.

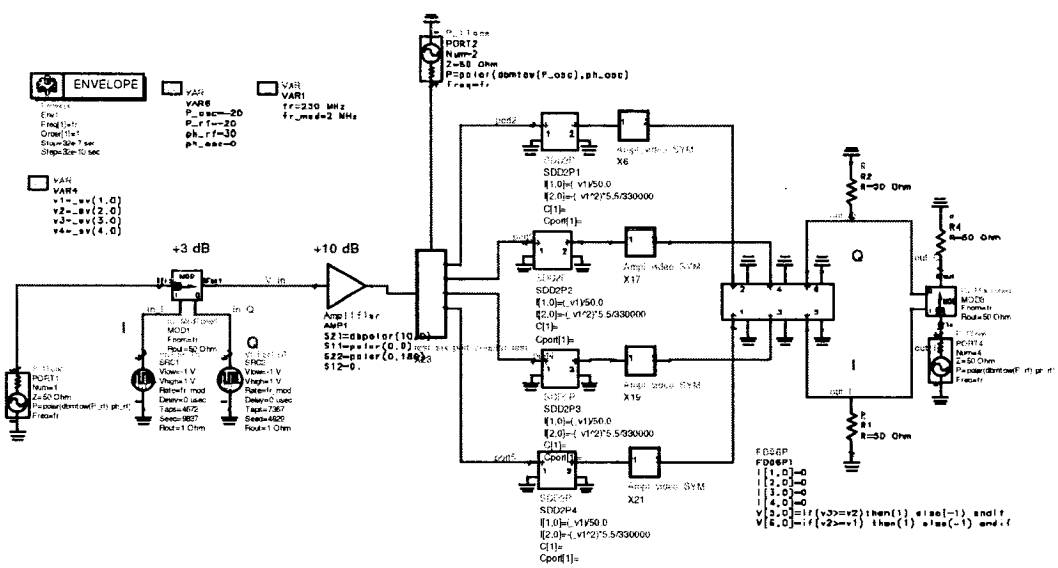

Figure 4-13 BER simulation schematic

Figure 4-15 shows the BER performance with phase variation between input RF carrier and LO signal with the following parameters: RF frequency= 230 MHz, RF power= -10 dBm, LO power = -10 dBm, R_s=2MHz. It can be seen that even though the carrier phase has changed by 46 degrees relative to the LO signal, we can still get good BER result of 10^{-9}. This means that the tolerance for the phase change in RF or LO signal is excellent. When coherent detection is used, which usually tracks the phase of the RF carrier to do the carrier recovery, the specification for PLL can be loosed, or using non-PLL oscillator such as DRO as LO. Figure 4-16 shows BER performance with RF frequency variation and other parameters given by: LO frequency= 230 MHz, RF power= -10 dBm, LO power = -10 dBm, R_s=2MHz. We can see that the bandwidth of demodulation can be 34 MHz, about 14.78%, which means that the proposed Six-Port is suitable for the wideband application.

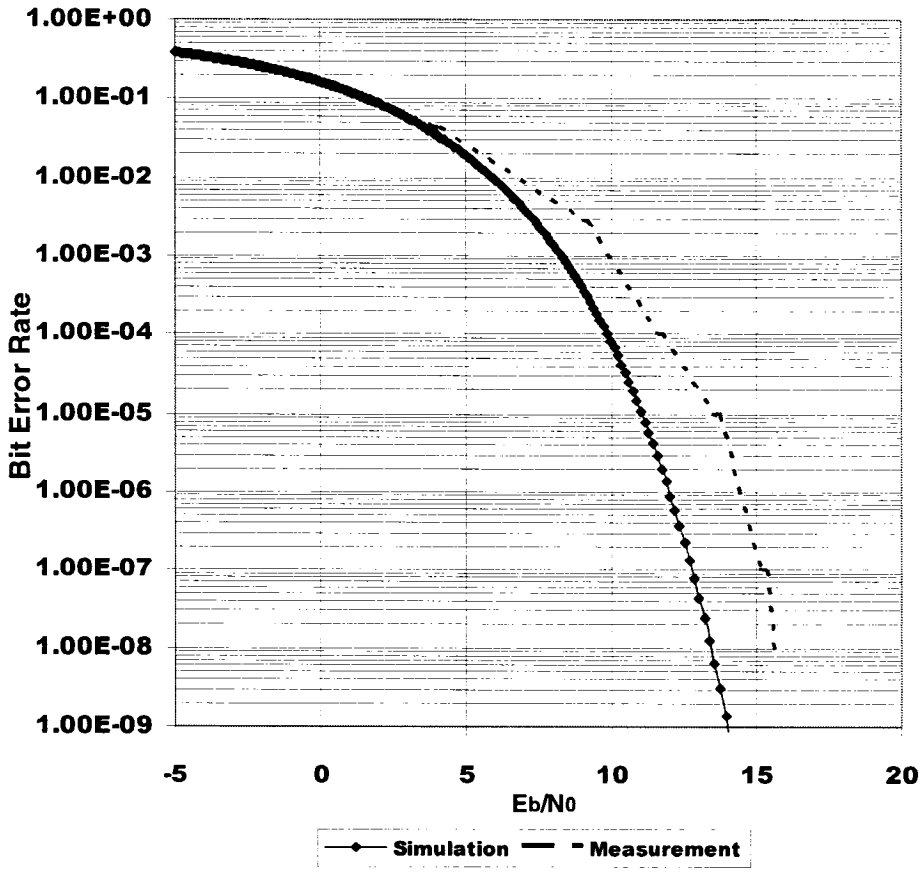

Figure 4-14 BER measurement results

(RF frequency = 230 MHz, LO frequency = 230 MHz RF power= -10 dBm, LO power = -10 dBm, R_s=2MHz)

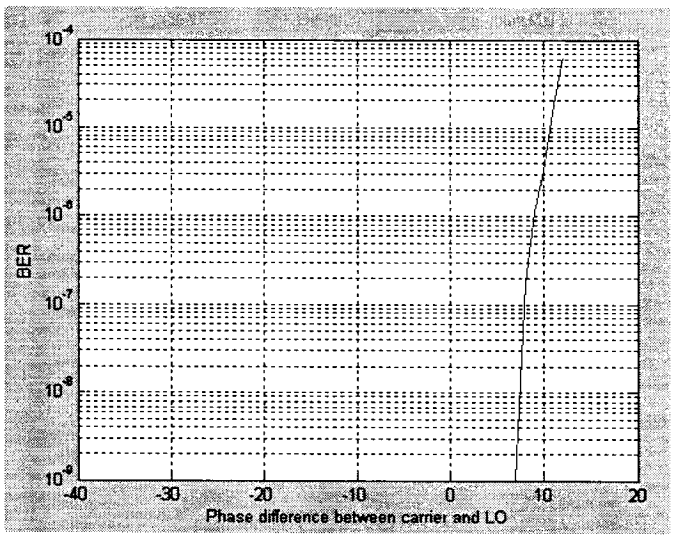

Figure 4-15 Phase difference between LO and carrier

(RF frequency = 230 MHz, RF power= -10 dBm, LO power = -10 dBm, R_s=2MHz)

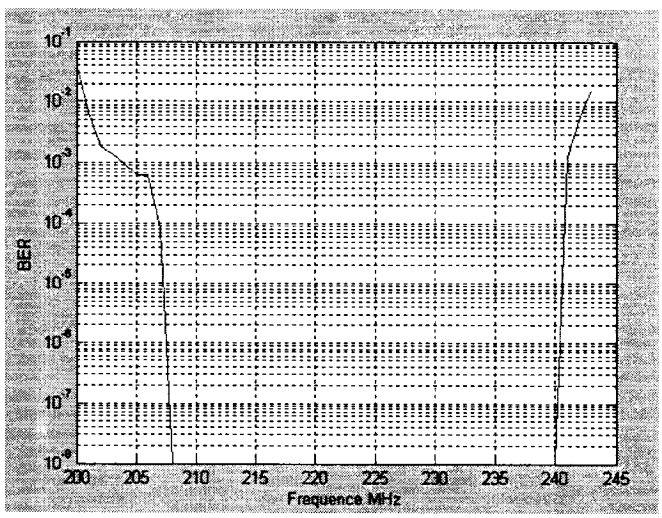

Figure 4-16 BER result with RF frequency variation

(LO frequency= 230 MHz, RF power= -10 dBm, LO power = -10 dBm, R_s=2MHz)

Chapter 5

Lumped-element Six-Port Direct QPSK Modulator

5.1 Introduction

In chapter 2, we briefly introduced the principle of the theory of Six-Port Direct QPSK Modulation. The mechanism of the Six-Port direct QPSK modulation is that, by applying I/Q data signals to the switches control ports to make switches either short to ground or open terminal. In this way, the value of -1 or +1 which is the reflection coefficient of the two ports among the Six-Port can be obtained simultaneously as illustrated in figure 5.1. Therefore the phase of the incoming RF signal can be direct manipulated to form the modulated QPSK signal. In our design, four switches are employed.

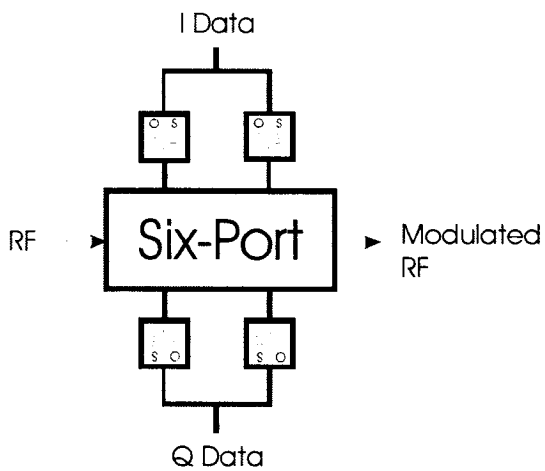

Figure 5-1 Block diagram of Six-Port QPSK modulator

In this chapter we conduct first the system design; next the design of the switch is introduced, then the measurement of the system, finally the QPSK modulator system test results are given.

5.2 QPSK Modulator design and simulation using ADS

In order to evaluation the performance, we begin the system level design of the Six-Port QPSK modulator. Figure 5.2 shows a schematic diagram of the proposed Six-Port Modulator. It consists of a discrete component Six-Port at 250MHz model, four ideal switches. I and Q random symbol data are employed as inputs of the switched control signals.

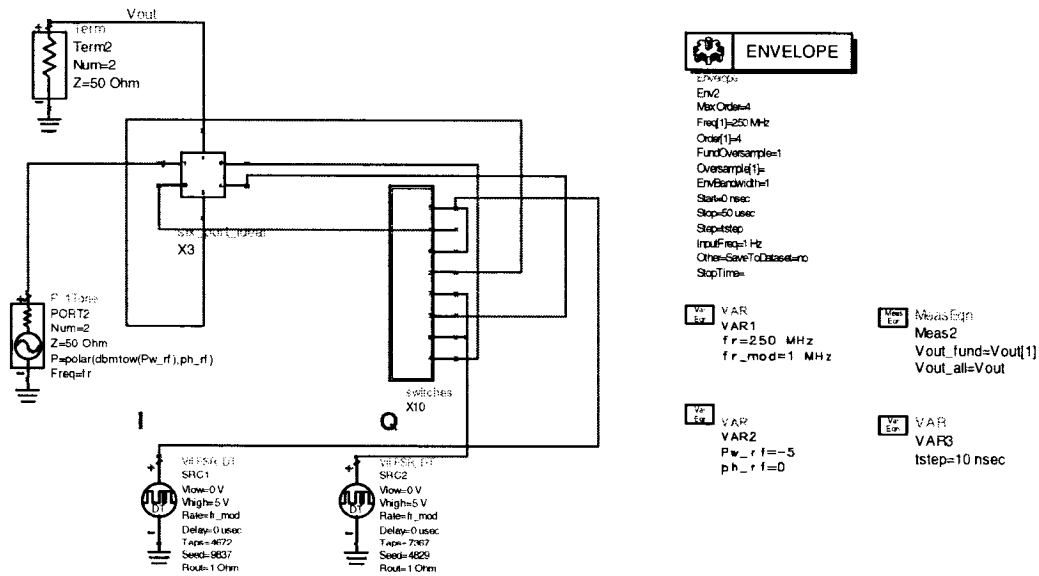

Figure 5-2 QPSK modulator system simulation schematic

A system level simulation has been conducted as shown in figure 5-2 using ADS with four ideal switches with promising results. Then ideal switches were replaced by measurement S1P S-parameter data file for open and short of RF2436 switches as shown in Figure 5-3. The data was taken using HP8753D network analyzer. Envelope simulation in ADS was conducted to check the constellation diagram and power spectrum diagram of the Six-Port QPSK modulator. The results are shown in figure 5-4 and figure 5-5, respectively.

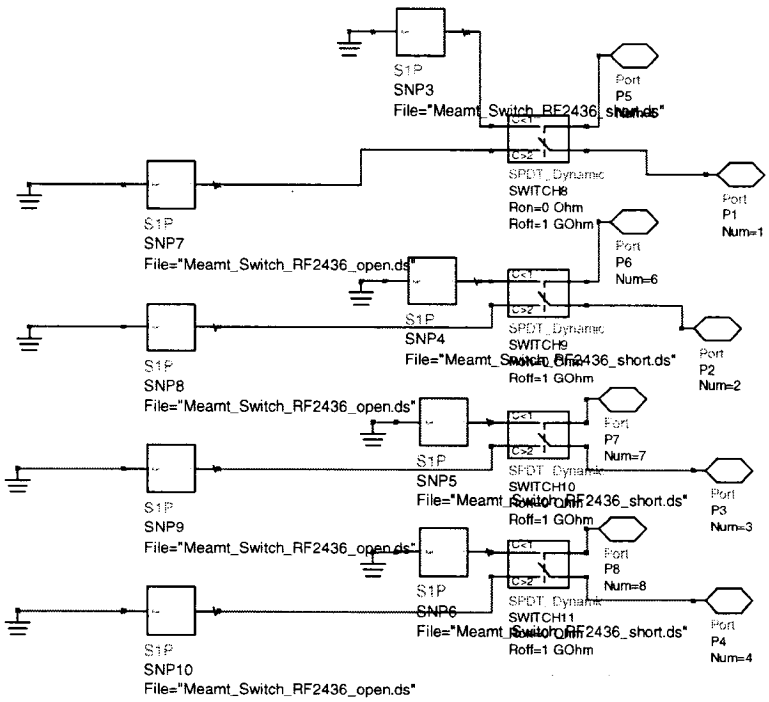

Figure 5-3 Schematic of RF2436 switches

A printed circuit board which is shown in figure 5-6 was built in our lab using Rogers RO4003C material with Er=3.38 and 32 mil of thickness.

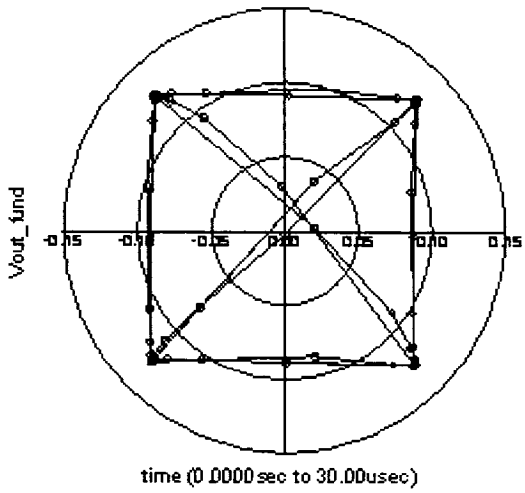

Figure 5-4 Constellation diagram for QPSK Modulator

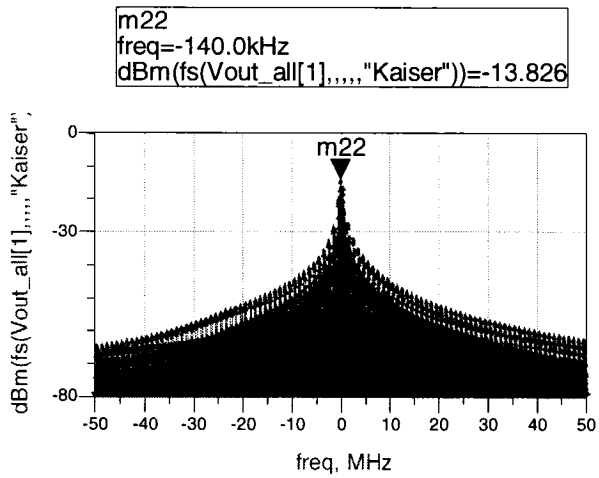

Figure 5-5 Spectrum for QPSK Modulator with RF2436 switches (Rs=1M, Prf=-5 dbm, f=250MHz)

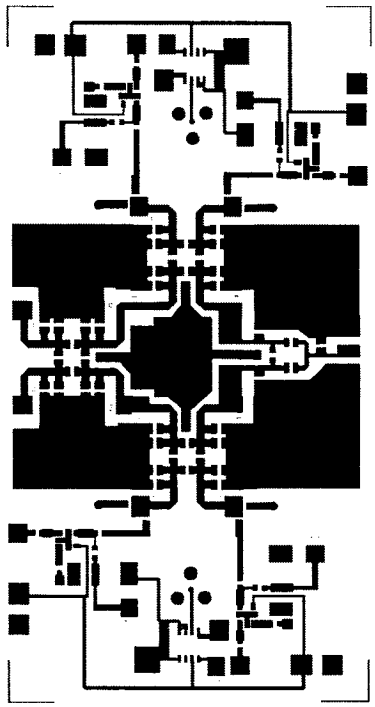

Figure 5-6 PCB layout of QPSK modulator

5.3 Switch Design

In Six-Port Direct QPSK Modulator design, successful realization of the switches forms the major parts of the overall QPSK modulator project. Therefore, to complete the design of the modulator, all that required is the realization of the switches. A good matched switch gives a good short reflection (Γ = -1) and open refection (Γ = +1). Reflected in constellation diagram, there should be no phase and amplitude imbalance. Switches should also have good switching speed and good isolation between input port, output port and control port.

Switches usually made from PIN diodes since they have good V-I characteristic. When reverse biased, a small series junction capacitance leads to relatively high diode impedance, while a forward bias current removes the junction capacitance and leaves the diode in a low impedance state.

A single pole double throw (SPDT) switch is required in our project. There are two types of SPDT switches. Series PIN SPDT Switch (see figure5-7) and shunt PIN SPDT Switch (see figure 5-8).

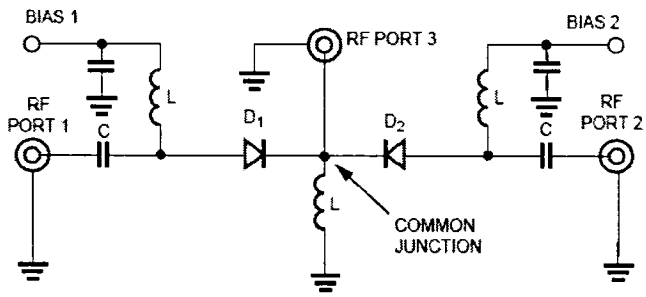

Figure 5-7 Series PIN SPDT Switch. [1]

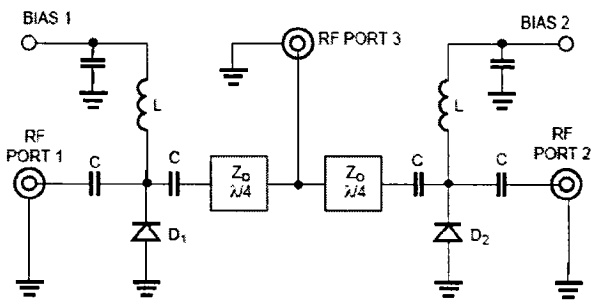

Figure 5-8 Shunt PIN SPDT Switch. [1]

Series PIN SPDT Switch also called absorption type because the incoming RF wave sees a 50 ohm termination when it is in off state; likewise Shunt PIN SPDT Switch is called reflection type because the incoming RF wave is reflected by a shorted PIN diode when it is in off status.

5.3.1 Switch implementation

A commercial switch RF2436 from RF Micro Devices was chosen, which is a low-cost transmit/receive GaAs MESFET switch originally designed for cordless phones RX/TX application. The device can handle power levels as high as +28dBm. The switch will operate from power supply voltages as low as 1.5V and as high as 6V with a CMOS logic driver for the control input. No negative voltage is required, and current consumption is very low. The operating frequency range is from DC to 2500MHz. The matrix for RF2436 is shown in Table 5-1

Table 5-1 *Matrix for RF2436*

Parameter	Specification (Typical)	Unit	Test Condition (T=25 °C, VDD=3.0V, Freq=900MHz)
Insertion Loss	1	dB	
Isolation	22	dB	Receive mode
	24	dB	Transmit mode

5.3.2 Switching Speed Test

There is no switching speed data in the datasheet. To test the switching speed of the switch, a circuit was built and a setup was made for the test as shown in Figure 5.9. We use TTL signal with data rate of 1MHz as input control signal. Form the previous chapter regarding Six-Port we understand that the mid band operating frequency for the Six-Port is 230MHz, thus the RF frequency was set to 230MHz. The test result showed that the rising time of the switch is about 10 ns, equals frequency of 100MHz, indicating that the switch is suitable for our application.

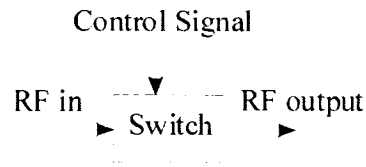

Figure 5-9 Switching speed test setup

5.3.3 Matching of the switch

The schematic of RF 2436 is shown in figure 5-10, following is the layout of the circuit and the photograph in figures 5-12 and 5-12, respectively.

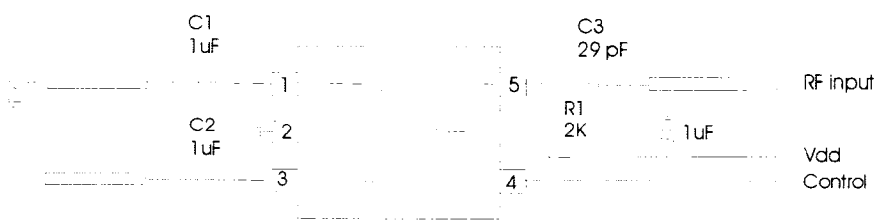

Figure 5-10 Schematic of RF 2436

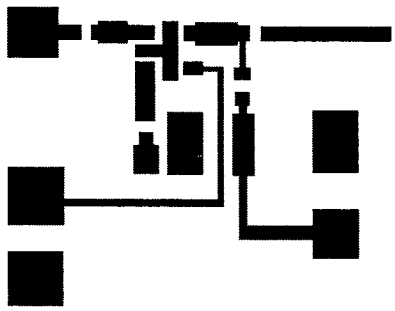

Figure 5-11 Layout of the circuit of RF2436

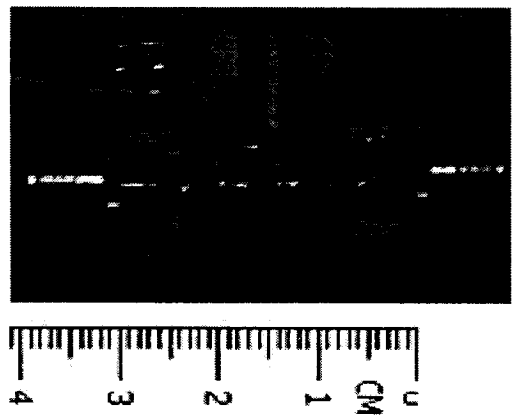

Figure 5-12 Photograph of the circuit of RF2436

Measurements of the OPEN/SHORT S-parameter of RF2436 have been done by applying high (+3.3V) and low level DC voltage (0 V) on the control port (pin 4) of RF2436 switch respectively. Using HP 8753D network analyzer as measurement instrument, the reflection S-parameter (S11) at RF port of RF2436 has been obtained. The results are shown in figure 5-13. As we can see, the open circuit S11 at 230MHz is close to ideal open, but the short circuit S11 at 230 MHz is far away from the ideal short. A matching for the short is needed in order to bring the short to the ideal one.

At f=230MHz, the RL=6.95+j24.05 and the software winSMITH from eagleware has been used as matching tool (Figure 5-14) to do the matching. A serial capacitor of 29nF has been added between the RF input port and the input port of RF2436 (pin 5) for the good matching.

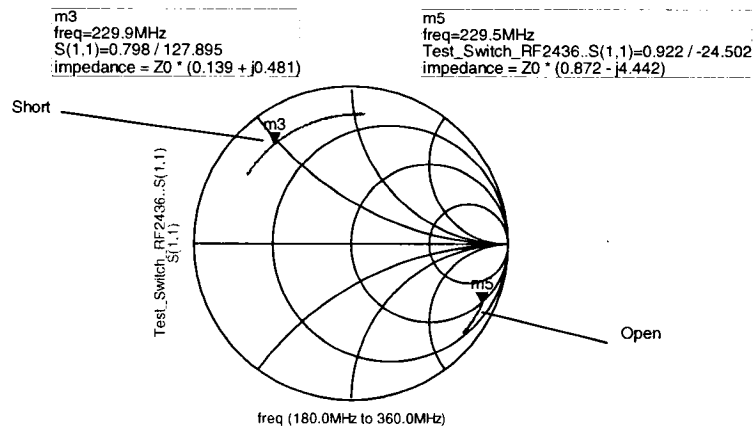

Figure 5-13 S11 at RF port of RF2436 before matching

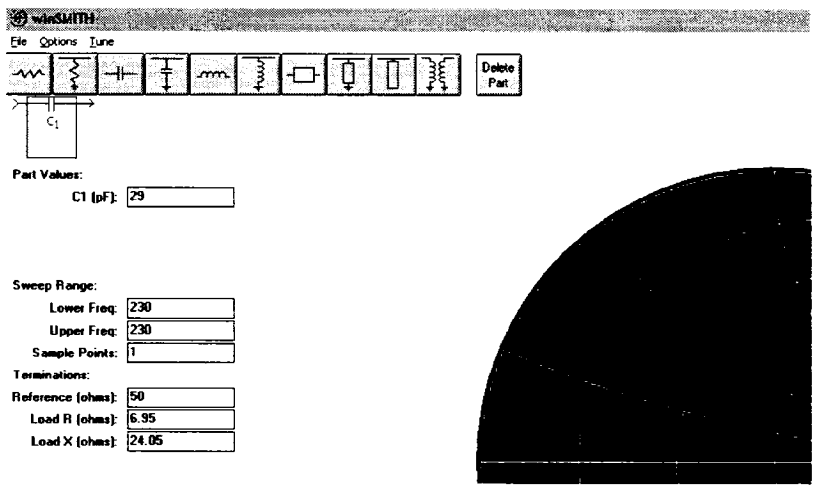

Figure 5-14 Figure winSMITH from Eagleware as matching tool

After doing the matching with winSMITH using a series 29nF capacitor, SHORT S-parameters gave a better performance as shown in figure 5-15.

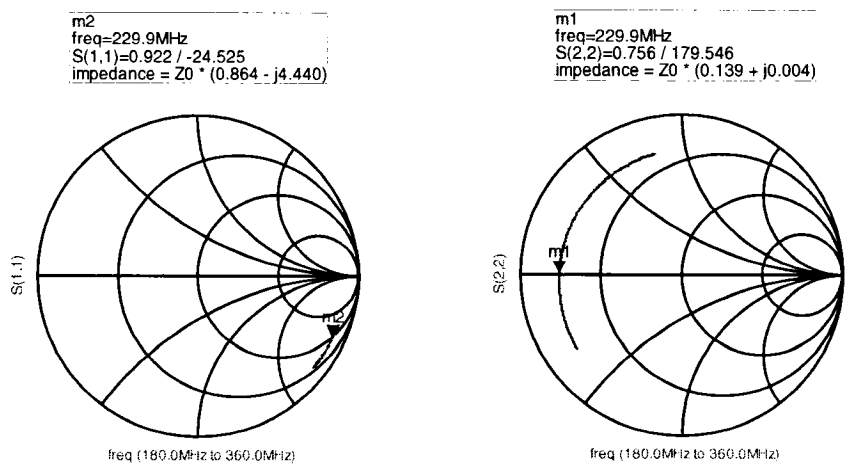

Figure 5-15 OPEN /SHORT measurement S-parameter of RF2436 after matching

5.3.4 Phase and amplitude test of Six-Port with the switches

In order to validate the feasibility of using RF2436 as switches, a phase and amplitude tests of Six-Port with the four switches have been conducted. The process is to apply low and high voltage to the four switches control ports to generate four constellation states at the four RF reflecting ports. The result is shown in figure 5-16 and 5-17. As

we can see, the phase differences between RF input and RF output for the four different switching states are equal to 90°, and the amplitude differences for the four states are within 5 dB at 215 MHz to 240 MHz range indicating that the switch is suitable for our modulation application.

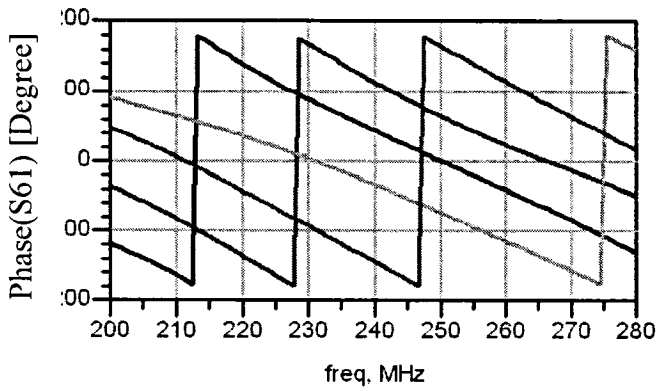

Figure 5-16 Phase measurements of Six-Port with four RF2436

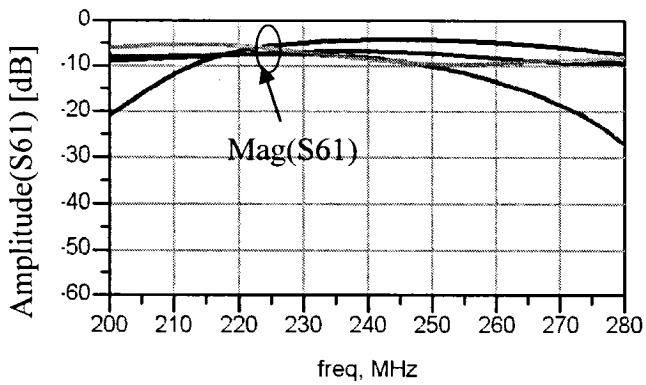

Figure 5-17 Amplitude measurement of Six-Port with four RF2436

5.3.5 ECL to TTL converter design

ECL level stands for Emitter Coupled Logic. TTL stands for Transistor-Transistor Logic. The logic level for both ECL and TTL is shown in Table 5-2

Table 5-2 *ECL and TTL logic*

	V_{OH}	V_{OL}
ECL	-0.8 V	-1.6 V
TTL	3.3 V	0 V

Since the BER measurement instrument ME522a from Anritsu can only output ECL data, and RF2436 switch control can only accept TTL logic, an ECL to TTL logic translation interface was needed. ECL to TTL converter MC10ELT25 from On Semiconductor was used. The MC10ELT/100ELT25 is a differential ECL to TTL translator. It Features 2.6 ns typical propagation delay and 100 MHz maximum toggle frequency. Because ECL levels are used, a +5 V, −5.2 V (or −4.5 V) and ground are required.

5.4 The implementation of the QPSK modulator using switches

The measurement setup is shown is figure 5-18. An Agilent VSA 89600 vector signal analyzer was employed as a receiver to demodulate the QPSK signal from Six-Port QPSK modulator. Agilent 89600 vector signal analyzer VSA is a powerful analysis instrument which comes with 89600 vector signal analyzer software and mainframe

hardware. It offers RF spectrum displays, baseband (I/Q) analysis such EVM and eye diagram, signal capture, a wide variety of analog and digital demodulators, and an extensive set of time, frequency and modulation analysis tools. These capabilities make 89600 VSA ideal for evaluating digital communication signals. Because the model we used has only IF input (36 MHz), therefore a mixer from HP was used to translate the 230 MHz RF signal to 36 MHz IF signal for the input of VSA 89600 vector signal analyzer.

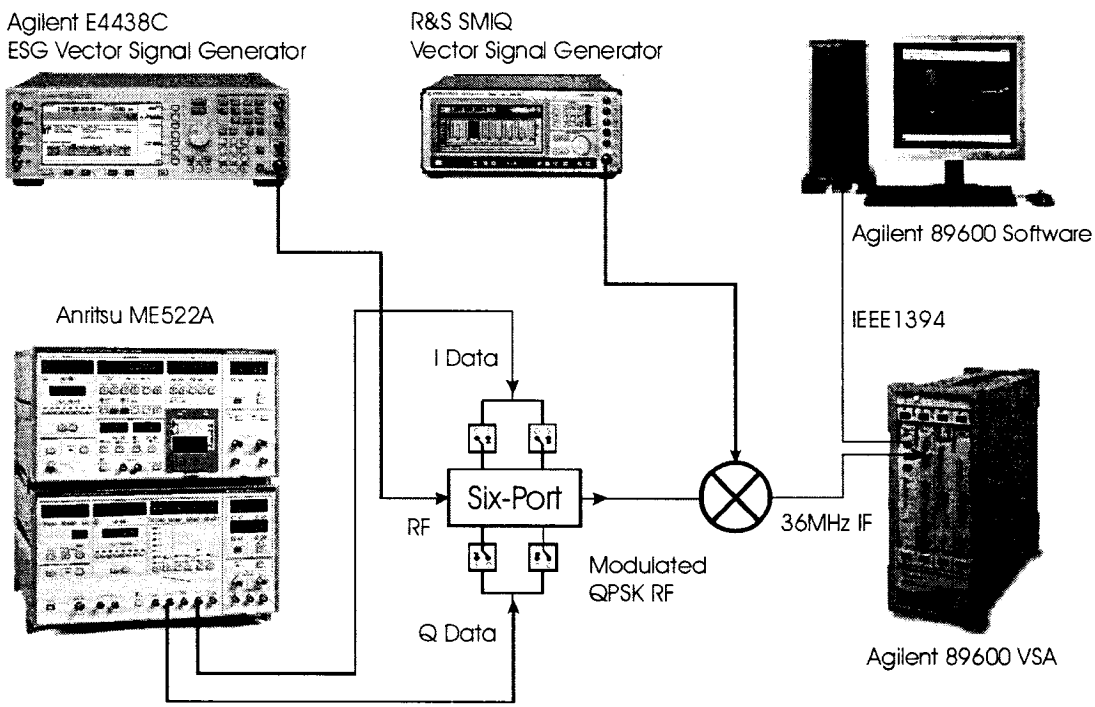

Figure 5-18 QPSK Modulator Measurement Setup

5.5 Measurements and results analysis of the QPSK modulator

The measurements for spectrum, constellation, EVM and diagram were made at RF power level from -15 dBm to 13 dBm respectively. The data rate is 1 MHz, f_{RF}= 230MHz fixed. Measurement results and performances of the Six-Port QPSK modulator are shown in figure 5-19 to figure 5-23. As we can see from the measurement results that the best case (figure 5-19) is that S/N= 21.79 dB and RF power equals 13dBm which is the maximum output power from the signal generator. The EVM(rms) is 8.13%. The worst case is shown in figure 5-23 with S/N= 14.67 dB, RF power equals -15dBm and EVM(rms) is 29.56%. If RF power is lowered below -15dBm, there was no demodulation obtained with VSA 89600.

We then conclude our measurement results as:

- Constellation diagram shows four dots inside the circle at S/N bigger than 20dB.
- Eye diagram is clear and wide open even at S/N equals 14dB.
- EVM is 29.56% at worst case which is good compared with the EVM specification of IEEE 802.15.4(ZigBee) which is 35%.
- Spectrum is comparable with ideal QPSK Modulator.
- The Spectrum efficiency of Six-Port QPSK Modulator needs to be improved because there is no pulse shaping available for the baseband data wave form in Six-Port QPSK modulation.

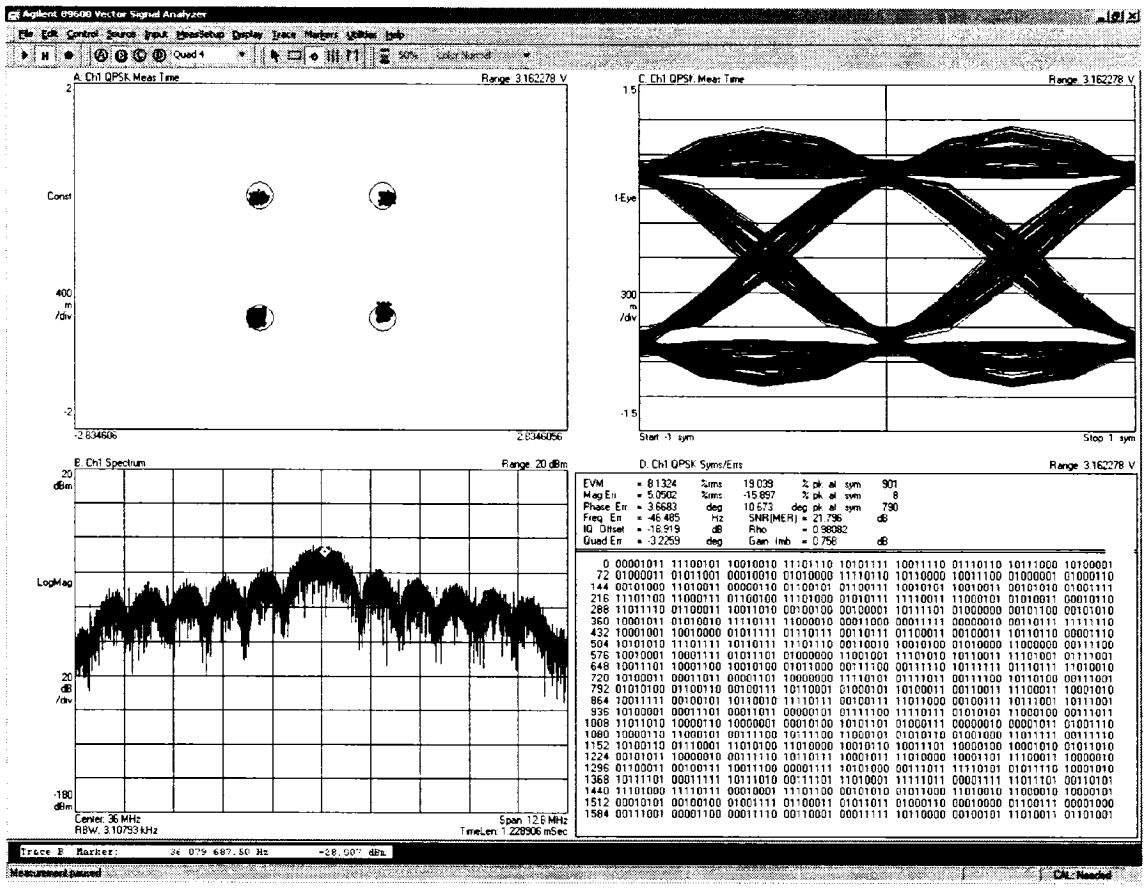

Figure 5-19 Measurement Results and performances of the Six-Port QPSK modulator, R_s=1 MHz, f_{RF}= 230MHz, RF Power=13 dBm

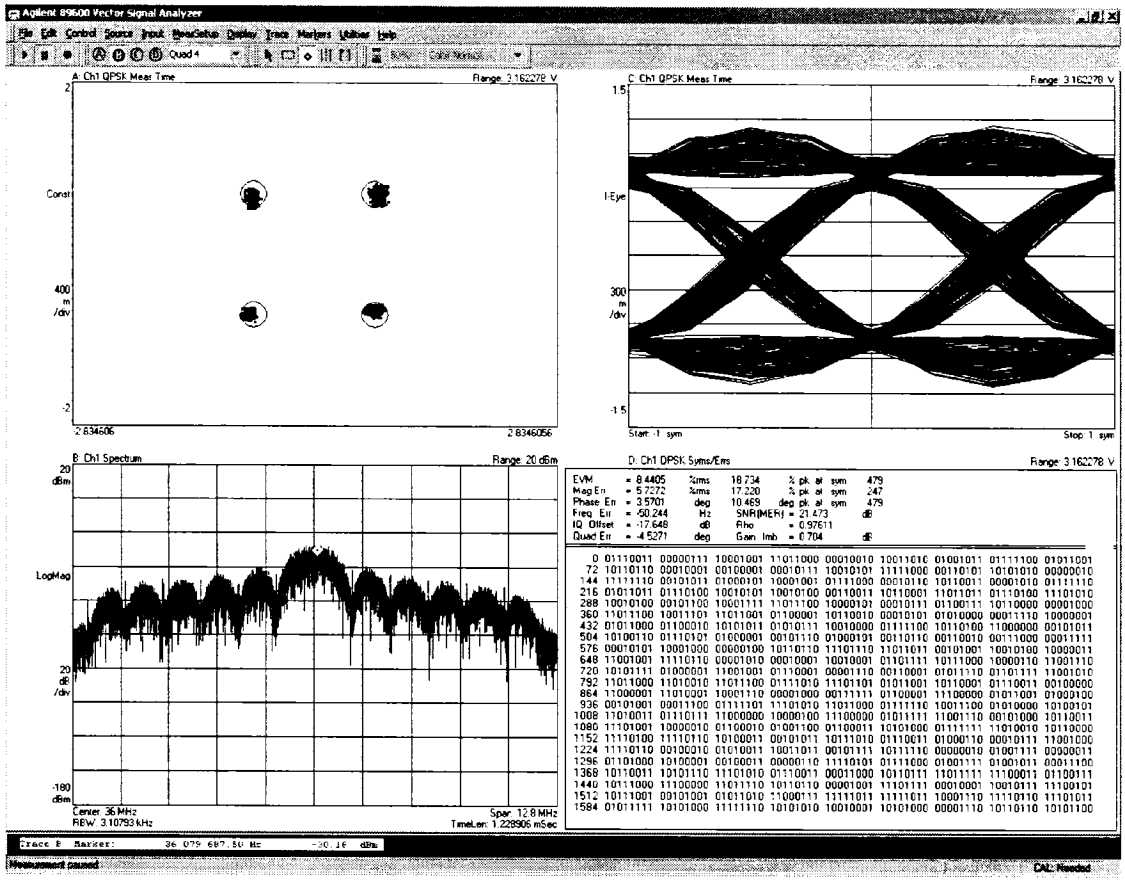

Figure 5-20 Measurement Results and performances of the Six-Port QPSK modulator, R_s=1 MHz, f_{RF}= 230MHz, RF Power=10 dBm

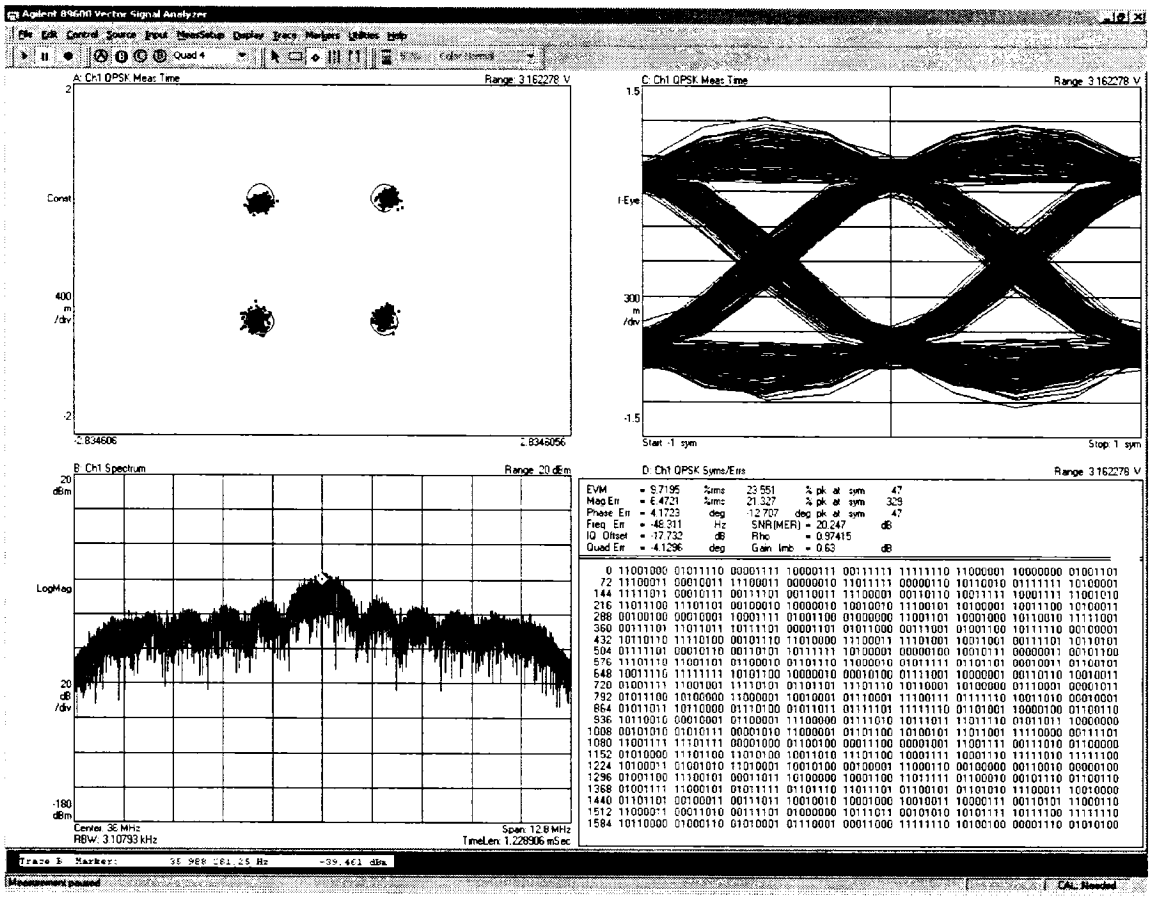

Figure 5-21 Measurement Results and performances of the Six-Port QPSK modulator, R_s=1 MHz, f_{RF}= 230MHz, RF Power=0 dBm

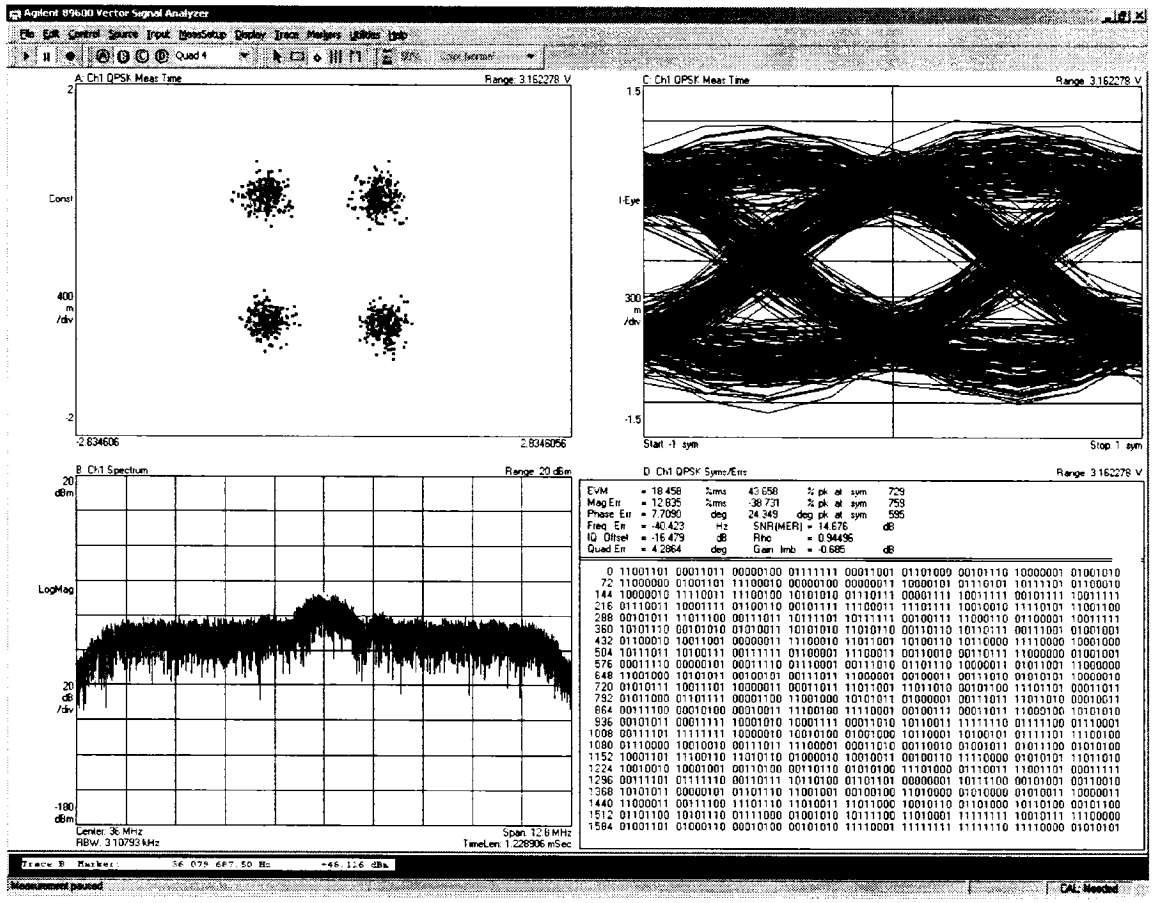

Figure 5-22 Measurement Results and performances of the Six-Port QPSK modulator, R_s=1 MHz, f_{RF}= 230MHz, RF Power=-10 dBm

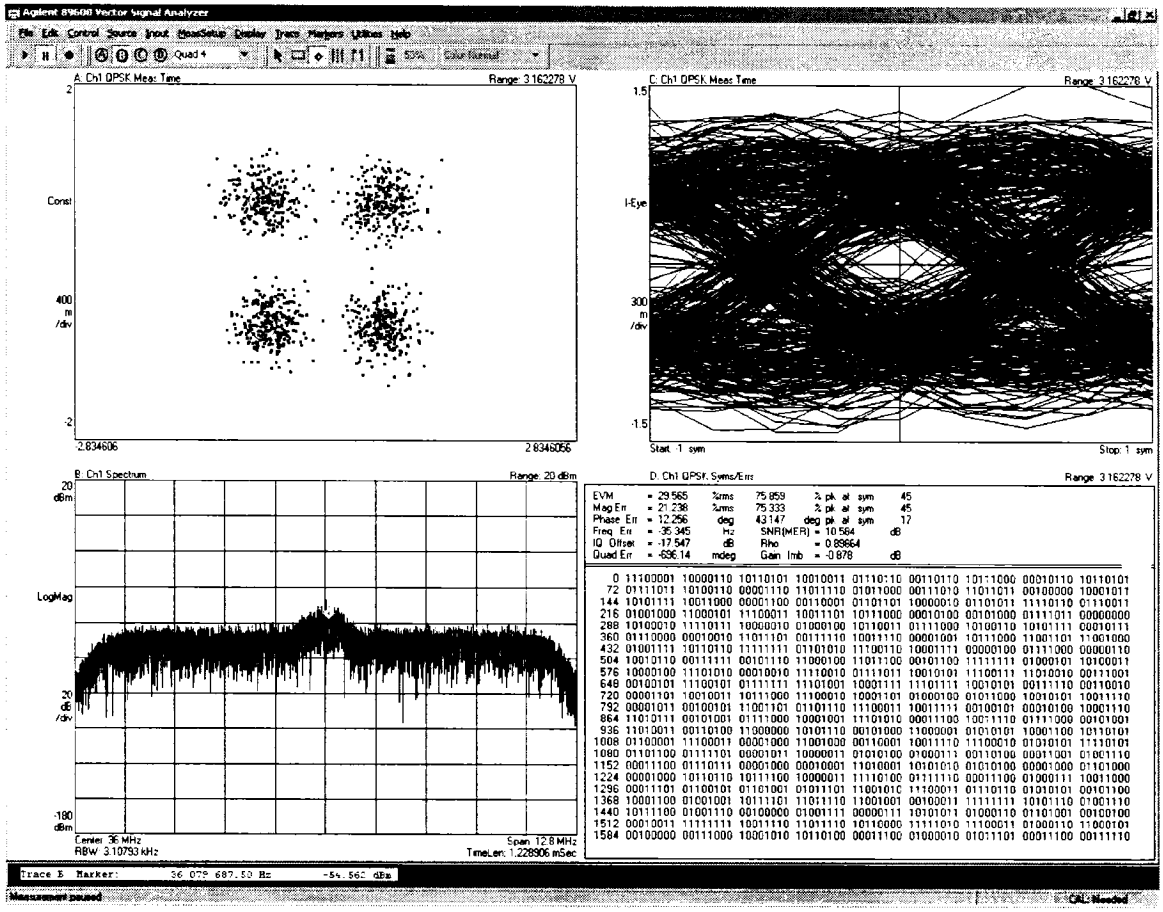

Figure 5-23 Measurement Results and performances of the Six-Port QPSK modulator, R_s=1 MHz, f_{RF}= 230MHz, RF Power=-15 dBm

5.5.1 Spectrum analysis

Since the spectrum of the QPSK modulation is a very important parameter, we make a further discussion for this specification.

- HP8563 spectrum analyzer was used to measure the spectrum of the Six-Port QPSK modulator at different RF power levels which are shown in figure 5-24 to figure 5-25. We can see that at RF = 0 dBm, the conversion loss is 10 dB. Compared to the spectrums taken from VSA 89600, the conversion loss is about 40 dB. The reason for the different measurement result is the mixer we used to do the down-conversion which causes such a big loss. The spectrum taken from HP8563 spectrum analyzer is accurate; the one from VSA 89600 is just for reference.

- Compared to the spectrum taken from a commercial QPSK Modulator such as vector signal generator Agilent 4438C, the spectrum from Six-Port QPSK Modulator is wider and occupied more adjacent bandwidth, and needs to be improved. The reason is due to the lack of the pulse shaping mechanism for the data waveforms in Six-Port QPSK Modulator.

- In the following session, we propose a theory which will improve the spectrum shape by using half wavelength transmission line loads.

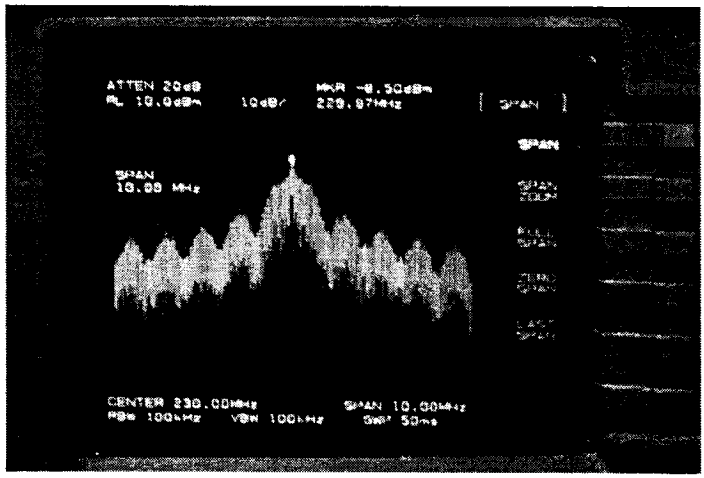

Figure 5-24 Measurement Results and performances of the Six-Port QPSK modulator, R_s=1 MHz, f_{RF}= 230MHz, RF Power=0 dBm

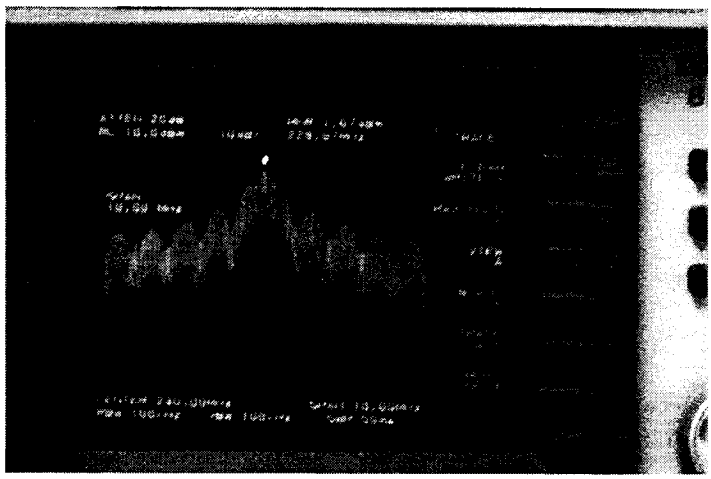

Figure 5-25 Measurement Results and performances of the Six-Port QPSK modulator, R_s=1MHz, f_{RF}= 230MHz, RF Power=10 dBm

5.6 Spectrum shape improvement by transmission line load

The reason of the wider spectrum spread for the Six-Port QPSK modulator is the abrupt changes between symbol states which correspond to the short and open in the Six-port modulator. We propose a transmission line load approach that uses four $\frac{\lambda}{2}$ transmission line loads which are inserted between the Six-port four output ports and the switches connecting to Short or Open loads. The proposed transmission line diagram is shown in figure 5-26. The transmission line loads slow the changes between symbols, avoiding the sudden phase change of the Six-port QPSK modulator. Ideally, a linear change happens in a symbol time.

Simulations using Agilent ADS were done and the spectrum results are shown in figure 5-27. From the simulated spectrums we can see that a 10 dB outside band reduction has been realized with the proposed transmission line method.

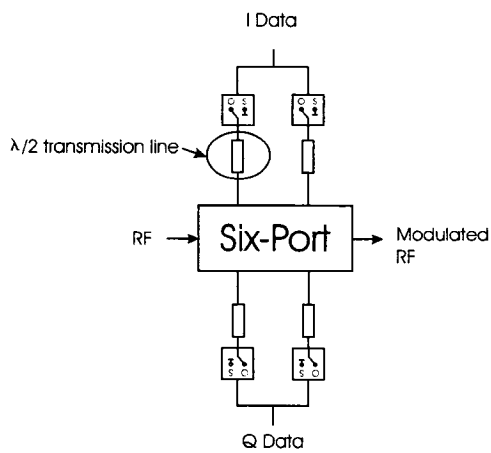

Figure 5-26 Proposed transmission line to shaping the spectrum

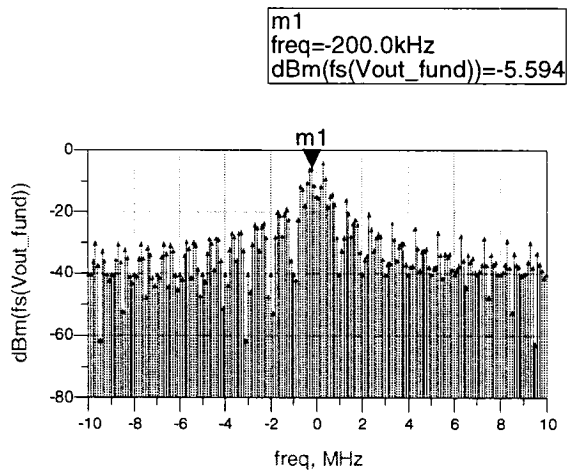

(a) Without λ/2 transmission line.

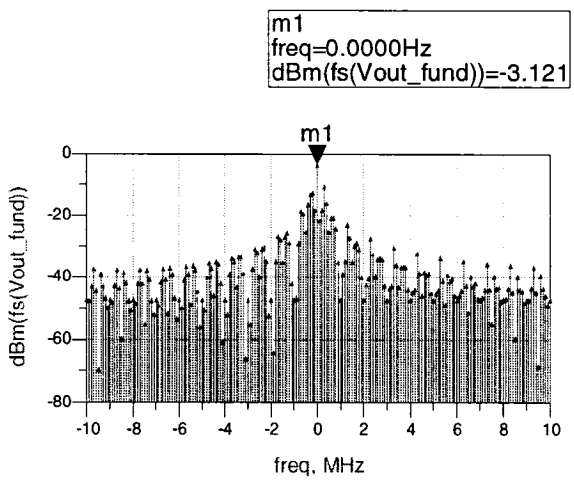

(b) With λ/2 transmission line.

Figure 5-27 Spectrum shaping simulation for the QPSK Six-Port modulator (a) without λ/2 transmission line (b) improve shape using λ/2 transmission line

Chapter 6

Conclusions and future works

6.1 Conclusions

The research for this thesis was focused on demonstrating the Six-port technology in the digital modem operating at VHF frequencies. This involved the use of simulations and physical implementation of a QPSK modulator and demodulator in hardware. For the QPSK demodulation, the BER performance is the most important parameter which must be maintained. For the QPSK modulator, the constellation and the shaping of the spectrum are the critical ones.

The theory of the Six-Port radio was given in Chapter 2. It was shown that simply combining passive components such as couplers, power divider and diode power detectors, the Six-Port can realize the phase discrimination of the input modulated RF signal. By connecting the short and open load using switches, the Six-Port can also be a QPSK modulator.

For illustrating proof of concepts, a Six-Port using discrete components was implemented at VHF band. Different simulations and measurement results show that the proposed Six-Port has functioned properly. A discussion of the results which focused on

the frequency shift has been given to show the components tolerance and the transmission lines effect on the S-parameter performance. As we have already seen even at low frequency as VHF band, the transmission line effect which cause the frequency shift can not be overlooked.

The implementation of the QPSK demodulator was performed in two steps and is presented in Chapter 4. As Wiltron power detectors were used, to characterize those devices, a proper modeling is necessary and has been done by measuring the input and output power of the detectors. BER performance is the critical criteria for the QPSK demodulator. In order to make the proper BER measurement, a four channel amplifier has been fabricated to address the issue related to the dynamic range of the Six-Port receiver. To save our time, a decoder from previous work has been adopted in our BER measurement setup.

Finally a Six-Port QPSK modulator at VHF band was described, designed and implemented in chapter 5. Commercial switches were used to realize the short and open loads. To reduce the outside band interference, a good modulator should have a proper spectrum shaping. As there is no baseband pulse shaping available for Six-Port QPSK modulator, a transmission line load approach was proposed to improve the spectrum shape of the Six-Port QPSK modulator.

The Six-Port QPSK modem implemented in this thesis has achieved simultaneously the highest data rate, the best BER performance and the excellent modulation constellation at VHF band. This was also done with significantly lower system implementation cost.

6.2 Future works

As the time is running out at this moment, there are many unfinished works need to be continued. Firstly, a recommendation is given for the transmitter and receiver BER measurement by integrating the antennas, LNA, power amplifier into a whole radio system.

For further circuit simplicity and cost effectiveness of the demodulator, the next recommendation is to use SMD power detectors instead of the costly Walton power detectors in the Six-Port QPSK demodulator.

The third task for the future work is the modulator spectrum shaping implementation by future simulating the different loads and building the circuits to test the theory.

This work in concentrated on QPSK modulation and demodulation. But the potential of the Six-Port radio is enormous. Other modulation schemes such as QAM and M-ary phase demodulation using Six-Port have been reported. Therefore the forth

recommendation is the implementation of those modulation schemes at VHF frequencies with Six-Port. This will dedicate the Digital Signal Processing (DSP) to perform the necessary signal processing for the complex modulation schemes.

References

[1] Application Note 957-1: *Broadbanding the Shunt PIN Diode SPDT Switch.* Agilent technologies.

[2] Coilcraft. www.coilcraft.com.

[3] David M. Pozar. *Microwave Engineering, 2nd Edition*, John Wiley & Sons Ltd., 1997.

[4] Department of Defense Interface Standard, MIL-STD-188-181A, Interoperability Standard for Single-Access 5-khz and 25-khz UHF Satellite Communications Channels, Mar 31, 1997.

[5] E. Marsan, J.C. Schiel, G. Brehm, K. Wu, and R.G. Bosisio, High-speed carrier recovery circuit suitable for direct digital QPSK transceivers, *Proc. IEEE Radio and Wireless Conference (Rawcon), Boston, MA., USA, Aug. 2002, pp. 103-110.*

[6] E. Moldovan, S.O. Tatu, T. Gaman, K. Wu, and R.G. Bosisio, A new 94 GHz six-port collision avoidance radar sensor *IEEE Trans. Microwave Theory Tech.*, vol. 52, no. 3, pp 751-759, March 2004.

[7] Eric Marsan, *Intégration d'une jonction six-port en technologie MMIC et son utilisation pour la conception d'un récepteur QPSK.* École Polytechnique de

Montréal, Master thesis, 2003.

[8] Eric Marsan, Gailon Brehm, Ke Wu, Renato G. Bosisio, C-BAND DIRECT DIGITAL RECEIVER MMIC *Conf. Proc. ANTEM'2002, pp. 421-424, St-Hubert, Quebec, Canada, July 31-August 2.*

[9] R.J.R.H. Frank Carden . *Telemetry Systems Engineering*, Artech House Publishers, 2002.

[10] Gregory L. AMORESE , Developing sophisticated models for capacitors, inductors and other passive components. *Microwave journal*, vol. 46, no3, pp. 120-125, Mar., 2003.

[11] Gagné, J. F. Gauthier, J. and R.G. Bosisio, High speed low cost architecture of direct conversion digital receiver. *International Microwave Symposium*, Phoenix, AZ, USA, May 2001.

[12] Kamilo Feher. *Digital communications: satellite/earth station engineering,* Englewood Cliffs, N.J: Prentice-Hall, 1983.

[13] Lainé, F., Étude d'une jonction six-port et conception du décodeur d'un récepteur homodyne. Projet de fin d'étude ele4196 et ele4199, Ecole Polytechnique de Montréal, (2002 hiver)

[14] Li, J., Bosisio, R. G., and Wu, K., A six-port direct digital millimeter wave

receiver. *Microwave Symposium Digest, 1994., IEEE MTT-S International*, vol.3, pp. Page(s):1659-1662, May 23, 1994-May 27, 1994.

[15] Application Note 701: Maximizing E_b/N_o (C/N) Accuracy. Micronetics

[16] Naishadham, K., Experimental equivalent-circuit modeling of SMD inductors for printed circuit applications. *IEEE Transactions on Electromagnetic Compatibility, v 43, n 4, November, 2001, p 557-565.*

[17] Ryszard W. Vogel, *S. M.* I., Analysis and Design of Lumped- and Lumped-Distributed-Element Directional Couplers for MIC and MMIC Applications, *IEEE Transactions on Microwave Theory and Techniques, vol. 40, no. 2, February 1992*

[18] S.H. Li and R.G. Bosisio, The automatic measurement of N-port microwave junctions by means of the six-port technique. *IEEE Trans. Instrum. Meas*, vol. 31, no. 1, pp. 40-43, 1982.

[19] S.O. Tatu, E. Moldovan, K. Wu, and R.G. Bosisio, A new direct millimeter wave six-port receiver. *IEEE Trans. Microwave Theory Tech. Special Issue,* vol. 49, no.12, pp. 2517-2522, 2001.

[20] Stephen A. Mass. *Nonlinear Microwave Circuits*, Artech House, 1998.

[21] S.O. Tatu. *Nouveau récepteur six-port en ondes millimétriques. Thčse de*

doctorat, École polytechnique de Montréal, Département de génie électrique , 2004.

[22] Zhaowu, C. and Binchun, X., Linearization of Diode Detector Characteristics. *MTT-S International Microwave Symposium Digest, Vol. I, pp 265-267*, 1987